FABRICATION AND MECHANICAL PROPERTIES OF METAL MATRIX SYNTACTIC FOAMS

Thesis submitted in accordance with the requirements of the University of Liverpool for the Doctor degree of Philosophy

by

Xingfu Tao

May 2010

ABSTRACT

Metal matrix syntactic foams are composite materials consisting of cellular ceramic spheres embedded in a continuous metal matrix. They have attracted many researchers' interest due to higher energy absorption capacity, specific stiffness and strength compared with metal foams or polymeric syntactic foams. They are promising candidate materials for energy absorption applications, e.g. lightweight panels, packing materials, safety devices and automobile bumpers.

The present study focuses on the fabrication techniques and compression properties of Al matrix syntactic foams. Ceramic microspheres (CMs) with two different inner structures, either porous or hollow, and four different particle size ranges were used. Two fabrication processes, pressure infiltration casting and liquid sintering, were used to fabricate syntactic foams with different microstructures and varying Al/CM volume ratios. The density and microstructure of the as-fabricated syntactic foams were evaluated.

Indentation tests were conducted on syntactic foams with different structured CMs. The indentation collapse load of the syntactic foam was proportional to the compressive strength of the syntactic foam, which in turn depended on the strength of the CMs. Syntactic foams with hollow CMs were brittle, while those with porous CMs were ductile.

Static compression tests were performed on all the as-fabricated syntactic foams. The compressive strength of the syntactic foams increased with the increase in the strength of Al and CMs and also with increasing volume fraction of Al in the low to medium Al volume fraction regions. Both ductile and brittle failure modes were present in the deformation of the syntactic foams. Three failure criteria, collapse, Griffith and Coulomb, were developed to explain the conditions under which the different failure modes occur.

The capability of energy absorption of the different types of syntactic foams was compared. The energy absorption was mainly determined by plateau strength and onset strain of densification. The syntactic foams fabricated by Al particle toughening had a good balance of the two factors and therefore had the highest capability of energy absorption.

Low speed impact tests were conducted on a few syntactic foam samples. Both maximum stress and energy absorption were found to increase with impact speed. The failure mode was found to be similar to that in static compression.

Tensile and shear tests were also performed on a few syntactic foam samples. The samples all failed by brittle fracture. For a fixed Al/CM ratio, the tensile and shear strengths were mainly determined by the matrix, largely independent of the type of the CMs embedded in the syntactic foam.

Contents

LIST OF FIGURES

LIST OF TABLES

PUBLICATIONS

[1] Tao X.F. & Zhao Y.Y. (2007), "Mechanical Response of Porous Copper Manufactured by Lost Carbonate Sintering Process", *Journal of Materials Science Forum 539-543, 1863-1867.*

[2] Zhao Y.Y., Tao X.F. & Xue X.B. (2008), "Manufacture and Mechanical Properties of Metal Matrix Syntactic Foams", P*roceedings of Material Science and Technology 2008,* Printing House, Inc., Pittsburgh, PA, pp. 2607–2615.

[3] Tao X.F, Zhang L.P. & Zhao Y.Y. (2008), "Compressive Response of Al Matrix Syntactic Foam Manufactured by Liquid Sintering", *Proceedings of Material Science and Technology 2008*, Printing House, Inc., Pittsburgh, PA, pp. 2587–2594.

[4] Tao X.F, Zhang L.P. & Y.Y. Zhao (2009), "Al Matrix Syntactic Foam Fabricated with Bimodal Ceramic Microspheres", *Materials & Design*, 30(7), 2732-2736.

[5] Tao X.F., Schleyer G. K. and Zhao Y. Y. (2009), "Indentation Tests on Al Matrix Syntactic Foams", in: Han Zhao and N. A. Fleck (eds.), *Proceedings of the IUTAM Symposium on Mechanical Properties of Cellular Materials 2007*, LMT-Cachan, Cachan, France, IUTAM Bookseries Volume 12, Springer Netherlands, pp. 97-104.

[6] Tao X.F. & Zhao Y.Y. (2009), "Compressive Behavior of Al Matrix Syntactic Foams Toughened with Al Particles", *Scripta Materialia* 61(5), 461-464.

[7] Zhao Y.Y. & Tao X.F., " Fabrication and Compressive Behaviour of Metal Matrix Syntactic Foams", Accepted by Materials Science and Technology (MS&T) 2009 Conference and Exhibition, October 25-29,Pittsburgh Pennsylvania, pp. 1785-1994

[8] Zhao Y.Y. & Tao X.F., " Compressive Failure of Al Matrix Syntactic Foams Manufactured By Melt Infiltration" to be submitted to *Composite Science and Technology.*

ACKNOWLEDGEMENT

This thesis could not be finished without the help and support of many people who are gratefully acknowledged here.

At the very first, I must express my deepest gratitude to my dedicated supervisor, Dr. Yuyuan Zhao, who is the most conscientious, patient, tolerant and kindest supervisor I ever know. Without his conscientiousness, I could not learn the way to do research; without his patience many interaction of revisions, I could not complete my thesis and any publications; without his tolerance, I could have lost courage to fight against my negligent and blundering temperament; without his kindness, I would not have had so many opportunities to discuss with him. With his superb guidance, I could have worked out this thesis.

I am also extremely grateful to Dr. Liping Zhang, who helped me in fabricating hundreds of samples in a very tough condition, and nicely it taught me so much about local culture and society, which is indeed very helpful for me to adapt myself quickly to a new environment.

In addition, I wish to extend my thanks to three technicians Mr Stephen Pennington, Mr Jijimon Mathew and Mr Dave Atkinson, for their great help in sample preparations and mechanical tests. Thanks are also due to Prof. Cantwell and Mr Fanjin Yang for their great help in low speed impact tests. I am also indebted to Prof. Zhou Li for his enlightenment in sample fabrication.

Thanks also go to those friends I met during my postgraduate study: Dr Zhen Yang, Mr Yue Tao, Mr Yujia Zhuai, Mr Yuanyuan Qi, Miss Yang Yang, Miss Jiehui Chen, Mr Mengqi Zhang, Miss Lu Liu, Miss Ningning Li, Mr Jun Wang, Dr Chen Ma, Mr Wei Zhang, Mr Yang Liu, Mr Jie Hu, Miss Qian Wang, Mr Lei Wang, Mr Xiaobing Xue, Mr Miao Lu, Mr Zhu Xiao, Mr Chen Wu, Mr Yixuan Peng. With your care and friendship, I never feel lonely in Liverpool.

At last but not least, I would like to thank my family for their consistent support and encouragement during my last four years postgraduate studying, which is the greatest power for me to move on.

CHAPTER 1 INTRODUCTION

1.1 Motivation behind the research

Metallic syntactic foams are composite materials consisting of a continuous metal matrix embedded with hollow or porous ceramic particles. In comparison with polymeric syntactic foams, they have higher strength and can be used at higher temperatures and in more harsh environments. In comparison with metal foams or porous metals, although they usually have higher density, they have higher compressive yield strength and better energy-absorbing capacity, due to extensive strain accumulation at relatively high plateau stresses. Therefore, metallic syntactic foams have many potential applications in lightweight structures and in impact energy absorption; examples include lightweight panels, packing materials, safety devices and automobile bumpers.

The syntactic foams in the prior existing studies were mainly fabricated with pressure infiltration method, where molten metal or their alloys was infiltrated with packed ceramic particles of monomodal size. The advantages of this method are easy process control, good reproducibility, uniform distribution of ceramic particles and good interfacial bonding between the metal matrix and the ceramic

particles. The main disadvantage is that the volume percentage of the ceramic particles in the syntactic foam is largely fixed, around 63% (Hartmann *et al.* 1999) when the particles have a similar size and are randomly packed. The effect of different volume ratios of metal matrix/ceramic particles on the structural or mechanical properties of syntactic foams has not been studied yet.

It is also interesting to find that different failure modes operate in the compression of metallic syntactic foams due to their complicated structure. The failure modes can be either ductile, as in metal foams, or brittle mode, as in polymeric syntactic foams. However, no criteria have been developed so far to explain these different failure modes.

The capability of energy absorption of syntactic foams is usually much higher than that of metal foams, although the former has a higher density (Balch *et al.* 2005). However, there has been little research up to date on the effects of processing conditions and structural properties on the energy absorption of metallic syntactic foams.

1.2 Objectives of the study

The primary objective of this study is to fabricate Al matrix syntactic foams with different structures and to study their mechanical properties. This is achieved by

systematic studies on the fabrication methods, composition, structure, mechanical properties and failure mechanisms as detailed below.

1.2.1 Development of fabrication processes for different types of syntactic foams

Al syntactic foams with monomodal sized ceramic particles will be fabricated by the melt pressure infiltration method. Al syntactic foams with bimodal sized ceramic particles will be fabricated by the melt pressure infiltration method with an aim to increase the volume percentage of ceramic particles. Al syntactic foams will be fabricated by mixing Al and ceramic particles followed by melt infiltration, with an aim to increase the volume percentage of Al. Moreover, Al syntactic foams will also be fabricated by liquid sintering of Al and ceramic particles with an aim to achieve variable Al/ceramic particle volume ratios. The fabrication conditions, such as infiltration pressure and heating temperature, will be optimised to fabricate syntactic foams with a uniform distribution of ceramic particles and a good bonding between the Al matrix and the ceramic particles.

1.2.2 Investigation into the mechanical properties of the as-fabricated syntactic foams

The compressive behaviour of all the syntactic foams fabricated will be studied. The main factors affecting the compressive strength and deformation behaviour of the syntactic foams will be studied. Indentation, tensile, shear and low speed

impact tests will also be performed on selected syntactic foams to investigate their behaviour under different loading conditions.

1.2.3 Investigation into the failure mechanisms of syntactic foams in compression

The failure modes of syntactic foams in compression will be studied both qualitatively and quantitatively. The factors that may affect the failure mode, such as strength of the Al matrix, strength of the ceramic particles and volume ratio between the Al matrix and the ceramic particles, will be considered.

1.3 Structure of the thesis

A total of six chapters are included in this thesis. Chapter 2 evaluates the literature that is relevant to the work presented. The manufacture methods and mechanical properties of polymeric and metallic syntactic foams are first reviewed. The compressive behaviours of cellular materials and particulate reinforced metal matrix composites are then introduced.

Chapter 3 gives a detailed explanation of each of the experimental procedures used in this work, including different fabrication procedures used to manufacture different types of syntactic foams, the characterization techniques for structural analysis, and the mechanical test methods for characterising the syntactic foam samples.

Chapter 4 presents the detailed results from the structural analysis and mechanical tests. The microstructures of the raw materials and the syntactic foam samples are displayed. The measured and calculated values of density and porosity of the syntactic foam samples are also presented. The results of the mechanical tests, including indentation, static compression, tensile, shear and low speed impact, are also presented.

Chapter 5 presents a detailed analysis of the results shown in Chapter 4. The process parameters affecting the fabrication processes and their effects on the structural properties of the syntactic foams are analysed and discussed. In particular, the key factors influencing the mechanical properties of the syntactic foams in compression, such as strength, failure mode and energy absorption, are discussed. Moreover, three criteria of compressive failure are developed based on the different failure mechanisms and modes found in the metal matrix syntactic foams.

Chapter 6 summarises the conclusions drawn from this study and three possible areas for future work. The three areas are the study on manufacturing syntactic foams with bimodal CMs to obtain maximum porosity, the optimization of the fabrication conditions for liquid sintering and the work on the mechanical properties and energy absorption of syntactic foams impact of much higher speed.

CHAPTER 2 LITERATURE REVIEW

2.1 Compressive behaviour of cellular materials

The majority of the research on the mechanical properties of cellular materials is to study their compressive behaviour. The compressive behaviour of cellular materials is quite different from that of solid material due to different structures. This section introduces the general compressive properties of cellular materials and the relevant concepts and terms.

2.1.1 Compressive stress-strain curves of cellular materials

The stress-strain curve in the compression of a cellular material is normally divided into three regimes, which are named linear elastic, plateau and densification (Andrews, Sanders & Gibson 1999, Banhart & Brinkers 1999, Ashby *et al.* 2000). The cellular material undergoes elastic deformation in the linear elastic region, as in the compression of a solid material. The plateau region is a process of pore collapse, buckling and cell wall fracture for cellular materials (Ashby *et al.* 2000). When the cells have almost completely collapsed opposing cell walls touch and further strain compresses the solid itself, leading to a final region of rapidly increasing stress.

Gibson and Ashby (1999) illustrated the compressive stress-strain curves for elastomeric foam, elastic-plastic foam and elastic-brittle foam, respectively, as shown in Figure 2.1. The stress-strain curves of these three cellular materials have no marked differences in linear elastic and densification regimes. However, these three foams have different behaviour in the plateau regime in their compressive stress-strain curves. It is because the compressive deformation of foam in plateau is associated with collapse of the cells — by elastic buckling in elastomeric foams (rubbers, for example); by the formation of plastic hinges in a foam which yields (such as metal); and by brittle crushing in a brittle foam (such as ceramic) (Gibson & Ashby 1999).

2.1.2 Energy absorption

Foams are ideal options for packaging and protection due to their good capability of energy absorption in compression. Energy absorbers for packaging and protection are chosen so that the plateau stress is just below that which will cause damage to the packaged object. The best choice is then the one which has the longest plateau, and therefore absorbs the most energy. Solid sections do not perform well in this role (Ashby *et al.* 2000). Figure 2.2 shows the comparison of energy-absorbing capacity between a solid and a foam made from the same solid. For the same amount of energy-absorption, the foam always generates a lower peak force. Energy is absorbed in foams as the cell walls bend plastically, or buckle, or fracture, depending on the material of which the foam is made. The

stress is limited by the long, flat plateau of the stress-strain curve (Gibson & Ashby 1999).

When a foam is loaded, work is done by the force applied to it. The work per unit volume in deforming the foam to a strain ϵ is simply the area under the stress-strain curve up to the strain ϵ, as shown in Figure 2.2. Very little energy is absorbed in the short, linear-elastic regime. The stress is increasing rapidly in the densification regime and might cause damage to the packaged object. Therefore, the energy absorbed in the densification regime is often not useful. As a consequence, the energy-absorbing capacity of a foam is mainly determined by the energy absorbed in the plateau regime, which is determined by the plateau stress and the onset strain of densification, i.e., the strain where the foam enters the densification regime (Avalle, Belingardi & Montanini 2001, Li, Magkiriadis & Harrigan 2006).

2.2 Introduction to syntactic foams

Syntactic foam is a particular class of materials with a foam structure. It consists of cellular spheres embedded in a continuous matrix, as shown in Figure 2.3. The matrix is usually either a polymer, or a light metal or alloy, such as Al, Ti and Mg. The cellular spheres are usually ceramic particles with either porous or hollow structure. Hollow metal spheres are also used occasionally. With the different porosity levels provided by different volume percentages or structures of the embedded cellular spheres, syntactic foam can have different porosities. Therefore,

syntactic foam has some physical and mechanical properties unique to cellular materials, including honeycomb structures, polymer foams (Ouellet *et al.* 2006, Voit *et al.* 2007), and metal foams (Davies & Zhen 1983, Sugimura *et al.* 1997, Hall *et al.* 2000). With the reinforcement of the polymer or metal matrix by ceramic particles, syntactic foam generally has much higher strength and capability of energy absorption than other foam structures.

Syntactic foams have current and potential applications in many areas due to their special physical and mechanical properties. Syntactic foams can be used in underwater buoyancy for their low density and low moisture absorption (Watkins 1988, Seamark 1991, Hinves *et al.* 1993). When syntactic foams are used as core materials for sandwich composites, they contribute to increased specific stiffness of the composites (Tsai & Hahn 1980, Jize *et al.* 1996, Cvitkovich & Jackson 1999). Syntactic foams are also attractive materials for structural components in the automotive, locomotive, aerospace, naval and other industries where weight reduction and improvement in comfort are needed (Banhart 2001). Because of their good capability of energy absorption, syntactic foams can be used for protective structural components, where they prevent or reduce the failure of other components by inducing their own failure; examples include lightweight panels, packing materials, safety devices and automobile bumpers (Hiel *et al.* 1993, Kim & Plubrai 2004, Zhang & Zhao 2007).

Syntactic foams are primarily fabricated with polymeric matrices and only recently metal matrices have been applied. Polymeric syntactic foams have the advantages of low density, good flexibility to design and low cost. Metal matrix syntactic foams have higher strength, better capability of energy absorption and higher temperature capability. The fabrication methods and mechanical properties for both types of syntactic foams will be reviewed in the following two sections.

2. 3 Polymeric syntactic foams

2.3.1 Fabrication process

The three primary constituents used in the fabrication of polymeric syntactic foams are (i) the matrix material (epoxy resin), (ii) the porosity provider material and (iii) the curing agent to cure the matrix material. A fourth constituent, a diluent which helps in lowering the viscosity of the resin, is sometimes used (Kim & Plubrai 2004, Woldesenbet *et al.*2005).

Different types of resins have been used in fabricating syntactic foams. Bunn and Mottram (1993) used the cold-setting thermoset epoxy binder comprised of three components. Part one was "Araldite", which is a mineral filled epoxy paste which increases the viscosity of the base resin and is an inexpensive way to increase the strength. The other two parts were also different forms of araldite used to enhance properties such as reduction in viscosity and curing time.

There have been studies on syntactic foams using polystyrene. In these, a small amount of polystyrene was mixed with glass bubbles and spread onto a fluoro-carbon coated pan that was exposed to 200 °C for 2 minutes. This was done until the beads were fused. This beads mixture was then mixed in an epoxy resin (Schott & Bhatacharjee 1993). These foams exhibited mechanical properties similar to conventional foams.

Most of the studies used epoxy resin D.E.R-334, which is manufactured by Dow Chemical Company. This epoxy was hardened with a tetraethylene pentamine curing agent and was diluted with a reactive diluent (Gupta *et al.* 2004, D'Almeida 1999). The other types of resins used were modified epoxies, phenolics, polyurethanes, urethane acrylates, and polyester and vinyl ester resins.

Hollow glass microspheres, which are made of borosilicate glass, are usually used as the porosity provider (Gupta *et al.* 2004, Karthikeyan *et al.* 2000, Kim & Oh 2000). This filler material has been chosen as it has very low densities ranging from 0.22 to 0.5 g/cm^3. Microspheres come in different diameters and are chosen depending on the strength desired. Studies have been done using industrial waste as reinforcement in epoxy composites. The porosity provider material used in these studies was particulate powder obtained after drying the mud retained on the final sieving operation of a hydrometallurgical zinc plant. Using industrial wastes as filler materials saves the cost of their treatment and disposal (Rodelheimer & D'Almeida 2001).

In a general fabrication procedure, the resin is diluted with the diluent to reduce viscosity. The hardener (curing agent) is later added by stirring the mixture slowly. The porosity provider is added at last. The fabrication is completed after a casting process of the mixture slurry.

Although this process is easy to operate, a few issues should be considered. Bunn and Mottram (1992) proposed that three methods should be used in the casting process according to the different viscosities caused by different volume fractions of the ceramic microspheres (CMs). For the syntactic foams with a low volume fraction of CMs, the mixture slurry has low viscosity and is directly poured into the mould. When the volume fraction of CMs is over 15%, the mould has to be filled by extrusion due to the increased viscosity of the slurry. For volume fractions of CMs high than 50%, the slurry is too dry to extrude and high pressure moulding is used to produce the sample. Gupta *et al.* (2006) mentioned that the stirrer should be wooden or made of other soft material to prevent the breakage of CMs duirng the stir process.

2.3.2 Microstructure

The scanning elctron micrograph of a polymeric syntaic foam is shown in Figure 2.4 (Gupta *et al.* 2006). The polymeric syntactic foam was made by mixing resin and CMs by stirring followed by casting. Air voids were observed in the microstructure of the as-fabricated syntactic foam (Gupta *et al.* 2004). Gupta and Woldesenbet (2002) stated that it is difficult to avoid entrapement of air in the

material system while mixing the consitudents, though it can be minimized and mainteined at nearly the same level among different specimens by careful processing. Gupta *et al.* (2006) used the following equation to calculate the volume percentage of voids :

$$V_v = \frac{\rho_{th} - \rho_m}{\rho_{th}} \quad (2.1)$$

where ρ_{th} and ρ_m are the theoretical and measured densities of the syntactic foam, respevtively.

2.3.3 Mechanical properties of polymeric syntactic foams

2.3.3.1 Compressive properties

Early results on compressive strength were reported by Bunn and Mottram (1993). They tested foams having volume fractions of microballoons between 0% and 53%. The maximum amount of microballoons in this case was 53% by volume. As the volume fraction of the microballoons decreased from 53% to 0% it was found that the bulk density increased from 0.78 g/cm^3 to 1.5 g/cm^3. A linear relation was observed between the filler content and the bulk density. Compressive tests showed that the lowest strength was for foams having the highest microballoon concentration. This indicates that the addition of microballoons reduced the compressive strength (Bunn & Mottram 1993).

Palumbo *et al.* (1996) conducted compression tests on polymeric syntactic foams with different weight percentages of microballoons. It was observed that the

compressive strength decreased from 70 MPa to 50 MPa as the weight fraction of the microballoons increased from 15% to 35%. Micrographic analysis of the fracture surface indicated that the failure occurred due to extensive debonding between the resin and the microballoons. SEM analysis also showed that some microballoons might have broken during the mechanical mixing process when the foam was being fabricated. They conducted an analytical analysis and compared this with the experimental results. The difference in strength between the two was attributed to the mechanical damage of the microballoons which occurred in the course of composite preparation or occurred due to residual thermal stresses around the glass spheres as a consequence of the inevitable mismatch between the coefficients of thermal expansion of the resin and the microballoons (Palumbo *et al.* 1996).

D'Almedia (1999) studied the effect of changing the diameters of the glass microballoons on the mechanical properties. These studies showed that as the volume fraction of the microballoons increased, the compressive strength and elastic modulus decreased. The microballoons act as pores inside bulk resin matrix. At a fixed volume fraction, the compressive strength and elastic modulus were higher for composites fabricated with microballoons of smaller diameters (greater relative wall thickness). This means that smaller microballoons result in better resistance to crack propagation. In other words, the use of microballoons with selected diameters permits one to maximize the use of these composites (D'Almedia 1999).

Gupta *et al.* (1999) correlated the raw materials used in processing and void content. The microballoons used in the fabrication process had a density of 0.25 g/cm^3 and the diameter was varied in the range of 10-100 μm. The void fraction was estimated to be greater than 10% and it was attributed to bubble formation and entrapment while the mixture was being stirred during fabrication. These bubbles formed as voids in the final composite structure. The other reason for void formation was attributed to the incomplete wetting of the microballoons. During mixing, a film of resin might have enclosed a cluster of microballoons. This can happen when microballoons are of small size or when the viscosity of the resin is high. To avoid the formation of voids, the authors used fibres along with microballoons and this reduced the void content to below 4%. Their compressive tests showed that the compressive strength increased as the void content in the foam was reduced from 10% to 4% (Gupta *et al.* 1999). At a constant volume fraction of microballons at 67.8%, shearing and wedge shaped cracks were observed in the specimens under compression. SEM micrographs showed the formation of debris, which indicates that the specimens have a combination of both compression and shear failure components. (Gupta *et al.* 2001).

Karthikeyan *et al.* (2000) studied the compressive strengths of syntactic foams with and without fibrous reinforcements. They found that besides physical features like voids, microstructural variations had a significant influence on the compressive behaviour. The addition of fibres in low proportions of around 2% did not increase the compressive strength, whereas the addition of fibres in high proportions, around 6%, increased the compressive strength significantly. High magnification micrographs of the compressive fracture surfaces revealed the

presence of plastic deformation marks that were in the form of steps. These marks cannot be generated if the matrix fractures in compression, but are possible in only shear type of failure. The banded structure appeared due to the frequent change in the localized plane of crack propagation in a specific direction. Undamaged microballoons were seen all over the structure with a few broken fragments. In foams with fibre reinforcements, it was observed that there exists a preferred orientation of the fibres (Gupta *et al.* 2002).

Gupta *et al.* (2004) studied the effects of microballoon radius ratio and specimen aspect ratio (width/thickness) on the compressive properties. Radius ratio is the ratio of the inner diameter to the outer diameter of the microballoon. Changing radius ratio changes the mechanical properties, such as compressive strength and fracture properties, but does not change any other parameters, such as surface area of microballoons and microballoon/matrix interfacial strength. Specimens tested in edgewise orientation have lower values of compressive modulus compared to that of flat wise orientation because of lateral expansion. Peak compressive strength in edgewise orientation showed dependence on crack propagation. Compression tests carried out with slabs with microballons of different radius ratios showed that the peak compressive strength and modulus increase with decrease in radius ratio. The strain at the peak compressive stress does not depend on the radius ratio and is a property that comes from the matrix resin (Gupta *et al.* 2004). Surface analysis after compressive testing indicated a sequential fracture pattern. When compressive load is initially applied the microballoons in the top and bottom layers resist deformation and the load is transferred to the middle layer of microballoons. As more compressive load is applied the weakest microballoon

in the middle layer fractures forming void and debris. This results in neighbouring microballoons being damaged due to load transfer from the weakest microballoon. This slowly results in the whole of middle layer being crushed. This pattern of crushing transfers towards the top and bottom of the compressive test specimen and finally it fails. This mechanism of compressive fracture was framed from the microscopic studies of the fractured specimen and is termed as layered crushing. This occurs in the case of high density foams. The low density foams fail by a phenomenon called longitudinal splitting (Kim & Plubrai 2004).

Studies by Kim and Oh (2000) on the impact behaviour of syntactic foams showed that inclusion of hollow glass microballoons in resin reduced the maximum impact force/stress. The addition of microballoons from 0% to 65% in volume decreased the maximum impact force three times. Compression tests showed that the modulus of the foam was reduced by a factor of two from that of the pure resin. A scanning electron micrograph of the fractured compression test specimen showed broken microballoons. The broken specimens showed that the failure mode was by shear on planes inclined approximately 45° to the loading direction. It was concluded that impact performance of these composites as protective materials can be enhanced by increasing the microballoon content.

2.3.3.2 Tensile properties

Gupta and Nagorny (2005) studied the tensile behaviour of polymeric syntactic foams fabricated with glass microballoons with different volume fractions in the range of 30% to 60% and different wall-thickness-to-diameter ratios. They

reported that the tensile strength increased with a decrease in the volume fraction of microballoons. The tensile strengths of all the syntactic foams were found to be decreased by 60%-80% compared with that of neat resin. They also studied the effect of wall thickness to diameter ratio on tensile modulus. It was found that the foams containing low strength microballoons showed lower tensile modulus compared with the neat resin, but the presence of high strength microballoons led to an increase in the tensile modulus. Their study on the fracture surface by SEM showed that all the microballoons in the fracture surface were broken.

2.3.3.3 Flexural properties

Kim and Khamis (2001) studied the flexural characteristics of polymeric syntactic foams by varying the volume fraction of the microballoons. The specific flexural strength decreased as the volume fraction of microballoons increased. The specific fracture energy decreased with increase in the volume fraction of the microballoons. SEM analysis showed that microballoons on the top surface were crushed. This was observed for specimens having volume fraction of 65%. The fracture characteristics of the syntactic foams with high volume fractions of microballoons were dominated by microballoons and less affected by the matrix.

2.4 Metal matrix syntactic foams

2.4.1 Fabrication processes

Most metal matrix syntactic foams are based on light metals or alloys including aluminium and magnesium, although other metals, such as zinc, are also used (Daoud 2008). There are four different types of cellular spheres used in the past studies to fabricate metal matrix syntactic foams: CMs composed of crystalline mullite ($3Al_2O_3$-$2SiO_2$) and amorphous silica (SiO_2), Al_2O_3 spheres, steel spheres and fly ash. These spheres have either a hollow or a porous structure.

Metal matrix syntactic foams are usually fabricated by infiltration casting or stir casting. In infiltration casting (pressure infiltration, melt infiltration), the molten metal is pressed to infiltrate into the packed ceramic particles and solidifies to produce a metal matrix syntactic foam. The infiltration casting process can be conducted either by a gas pressure assisted infiltration (Balch *et al.* 2005), or by die casting (Rohatgi *et al.* 2009), by casting (Zhang *et al.* 2009). The reported infiltration pressure was in the range of 0.2—3.5 MPa depending on the matrix and spheres used in the fabrication process. Marchi and Mortensen (2002) suggested that the pressure required for full infiltration is related to the size and volume fraction of the spheres. Finer spheres and larger volume fractions of CMs require higher infiltration pressures. It is suggested that the heating temperature be about 100°C above the liquidus temperature of the metal matrix (Nadler *et al.* 1999). A temperature far higher than the melting point of the Al matrix could

accelerate the dissolution of the ceramic spheres used for fabricating the syntactic foam (Palmer *et al* 2007). In most cases, the packed spheres were randomly distributed and accounted for 63%, i.e., the voids between the packed spheres accounted for about 37%, when they had a similar size (Hartmann 1999). Syntactic foams were also fabricated by infiltrating molten Al into hexagonally close-packed alumina spheres with an average size of 2.8 mm, increasing the volume fraction of the spheres from 63% to 74% (Hartmann 1999).

In stir casting, the ceramic particles are mixed in the liquid metal and then cast to produce syntactic foams (Daoud 2007). This method is widely used in producing metal matrix composites; its advantages and limitations are well documented. The volume fraction of the ceramic particles can be easily adjusted and the production cost is low. However, this method has a few problems. The ceramic particles are normally not wetted by the molten metal and tend to cluster together. They also tend to float to the top of the melt because they are much lighter than the metal. Both of these problems lead to poor dispersion of the ceramic particles in the liquid metal and thus inhomogeneous structures of the syntactic foams.

The syntactic foams manufactured by these processes often have different microstructures, which can result in different structural properties, including denseness of the Al matrix, volume fraction of the ceramic particles, and homogeneity of ceramic particle distribution.

2.4.2 Microstructure

Metallic syntactic foams fabricated by different methods can have different microstructures, as shown in Figure 2.5. The syntactic foams fabricated by the infiltration casting method have a more uniform distribution of ceramic spheres and better bonding between metal matrix and ceramic spheres than those fabricated by the stir casting method. Some hollow spheres may be broken either when received or during packing and infiltration, and can be infiltrated with molten metal in both the foams fabricated by the infiltration method and by the stir casting method (Balch *et al.* 2005).

2.4.3 Porosity

In comparison to polymeric syntactic foams, the porosity of metallic syntactic foams is determined mainly by the porosity of the cellular spheres since there are normally no voids in the metal matrix. Kiser *et al.* (1999) produced a formula to calculate the porosity of syntactic foams with hollow spheres:

$$\varphi = f(1 - t/R)^3 \qquad (2.2)$$

where φ is the porosity of the syntactic foam, f is the volume percentage of the hollow spheres, and t and R are the shell thickness and radius of the hollow sphere. This equation is only suitable for syntactic foams containing hollow spheres with known thickness-to-radius ratio. Zhang and Zhao (2007) developed a formula to calculate the porosity of metallic syntactic foams suitable for all types of cellular spheres:

$$\varphi = \frac{\rho_m - \rho_f}{\rho_m - \rho_s}\left(1 - \frac{\rho_s}{\rho_0}\right) \quad (2.3)$$

where, ρ_m, ρ_f and ρ_o are the density of metal matrix, syntactic foam and solid part of the cellular spheres, respectively, and ρ_s is the effective density of the cellular spheres.

2.4.4 Static compressive properties

2.4.4.1 Factors affecting compressive strength

The compressive strength of metal matrix syntactic foams depends not only on the mechanical properties of the metal matrix and the ceramic particles but also on the volume fraction, structure and distribution of the ceramic particles. The interfacial bonding between the metal matrix and the ceramic particles and the amount of defects in the syntactic foams also affect the compressive strength.

The compressive strength of the syntactic foam is sensitive to the strength of the embedded spheres. Kiser *et al.* (1999) performed static compression tests on Al matrix syntactic foams embedded with hollow Al_2O_3 spheres of different wall-thickness-to-radius ratios (t/R). The compressive strength was found to be sensitive to t/R. With the same A202 aluminium alloy matrix, the compressive strength of the syntactic foam increased from 70 to 230 MPa with the t/R increasing from 0.12 to 0.48. The syntactic foams with high density ceramic microspheres were found to have a higher compressive strength than that of the syntactic foams with low density microspheres. Vendra and Rabiei (2007) studied

the compressive behaviour of Al 306 matrix syntactic foams with hollow steel spheres of same thickness but different compositions. They reported that syntactic foams with stainless steel spheres had much higher compressive strength than the syntactic foams with low carbon steel spheres. Wu *et al.* (2007) indicated that the size of the ceramic spheres also affects the compressive strength of the resultant syntactic foams. However, it is arguable whether the effect was genuinely attributable to the particle size. Rohatgi *et al.* (2006) reported that the compressive yield strength of the Al matrix syntactic foams increased with increasing particle size of the ceramic spheres, while Palmer *et al.* (2007) reported that larger ceramic spheres are associated with lower initial peak compressive stress values. In both studies, the variations of compressive strength were attributed to the different void contents in different sized ceramic spheres instead of different geometries.

Different metal matrices can result in significantly different compressive strengths of the syntactic foams. Balch *et al.* (2005) studied the compressive behaviour of syntactic foams with same ceramic microspheres but different Al matrices. The compressive strength of syntactic foam with an Al 7075 matrix was found to be double that of syntactic foam with a commercially pure Al matrix produced by the same process. The syntactic foams fabricated with the same metal matrix but different heat-treatment procedures were also found to have very different compressive strengths. Both Kiser *et al.* (1999) and Balch *et al.* (2005) reported that the peak-aged (T6) syntactic foam, with an A210 or Al 7075 alloy matrix respectively, had a much higher compressive strength than the annealed syntactic

foam. In general, stronger metal matrix results in higher compressive strength of the syntactic foam.

Varying the volume ratio between the metal matrix and the ceramic particles can alter the compressive strength of the syntactic foam. However, as mentioned in the previous section, the volume fraction of the metal matrix in the metal matrix syntactic foams is difficult to be increased when they are fabricated by the pressure infiltration method. Hartmann *et al.* (1999) packed the ceramic spheres in hexagonal close-pack arrays, which decreased the volume fraction of the magnesium matrix by 11% compared with randomly packed ceramic spheres. It should be noted that this procedure can only be carried out when the ceramic spheres are relatively large (more than 2.8mm in the study). The compressive strength of the syntactic foams shows an increasing trend with the decrease of volume fraction for ceramic spheres. Rohatgi *et al.* (2006) increased the matrix fraction of Al from 65% to 80% by mixing different Al particles with fly ash. The compressive strength of the syntactic foam increases with the increase of Al volume fraction. Daoud (2008) manufactured ZnAl22 matrix syntactic foam by stir casting and varied the volume percentage of the metal matrix from 50% to 94%. When the volume percentage was increased from 50% to 80%, the compressive strength of the syntactic foam had a marked increase. Further increase from 80% to 94% had the opposite effect.

Besides the effects of the matrix and cellular spheres, heating temperature and infiltration pressure can also influence the compressive strength of the syntactic foams. The Al syntactic foams fabricated with higher infiltration pressures were found to have higher compressive yield strengths, due to reduced void contents (Rohatgi *et al.* 2006). The Al 1350 matrix syntactic foams fabricated by the pressure infiltration method at 666°C had a higher compressive strength than those fabricated at a higher temperature of 750°C (Palmer *et al.* 2007). This was because the reduced temperature decreased the sphere dissolution, which would make the matrix more ductile through decreased silicon content and increase the strength of the spheres by lessening the thinning of their walls.

2.4.4.2 Predictions of compressive strength

The compressive strength of metal matrix syntactic foams is mainly dependent upon the strength of the matrix, the strength of the ceramic particles and the volume ratio of the two components, as discussed above. With known information on these three parameters, it is possible to quantitatively predict the compressive strength of the syntactic foams.

For metal matrix syntactic foams containing hollow ceramic spheres, the formula given by Hartmann *et al.* (1999) for the prediction of the compressive strength is:

$$\sigma = 0.86\sigma_c\left[1-\left(\frac{R-t}{R}\right)^2\right]+0.14\sigma_m \quad (2.4)$$

and the formula given by Wu *et al.* (2007) is:

$$\left\{\sigma_m(1-f)^{\frac{3}{2}}+\sigma_c f\left[1-\left(1-\frac{t}{R}\right)^3\right]^{\frac{3}{2}}\right\} \quad (2.5)$$

where σ, σ_c and σ_m are the compressive strengths of the metal matrix syntactic foam, the solid part of the ceramic spheres and the metal matrix, respectively, R is the radius of the ceramic spheres, t is the shell thickness of the hollow spheres, C is a constant assumed to have a value of 0.3, and f is the volume fraction of the ceramic spheres in the syntactic foam.

Eq. (2.4) was based on syntactic foams embedded with randomly packed ceramic spheres, the volume fraction of which was estimated to be 63%. It was assumed in the development of the equation: (a) that the compressive failure of syntactic foam was in the form of shear fracture, (b) the area fraction of metal matrix in the shear plane was 14% and (c) the ceramic spheres and the matrix were equally strained. Eq. (2.4) may only be applicable to a limited range of materials due to the pre-defined packing model for ceramic spheres and compressive failure mode of the syntactic foams. The estimated value of area fraction of metal matrix in the shear plane has also not been proved.

Eq. (2.5) was developed the by assuming that both the matrix and the ceramic spheres were open celled cellular materials. The author used the relationship between the relative strength and the relative density for open celled materials given by Miyoshi *et al.* (1999):

$$\frac{\sigma_{pl}}{\sigma_{ys}} = C\left(\frac{\rho}{\rho_s}\right)^{\frac{3}{2}} \tag{2.6}$$

where σ_{pl} and σ_{ys} are the compressive strengths and ρ and ρ_s are the densities of the open celled cellular material and the full dense solid, respectively. Eq. (2.6) was applied to the metal matrix and the ceramic spheres to obtain Eq. (2.5).

In order to examine the validity of Eqs (2.4) and (2.5), the predicted and experimental values of syntactic foams fabricated by Kiser, He and Zok (1999) are used to calculate the compressive strength of syntactic foams fabricated by Kiser, He and Zok (1999) is compared. The compressive strength of the Al 201-Al_2O_3 syntactic foam is predicted to be 606.37 MPa with Eq. (2.4) and 116.94 MPa with Eq. (2.5), while the experimental compressive strength was 140 MPa. Eq. (2.4) overestimated the compressive strength by several times while Eq. (2.5) underestimated the experimental results by 20%.

These two formulae were obtained when the ceramic particles were not damaged. They should be used with care, as the pattern of load partition between the metal

matrix and the ceramic particles in metallic syntactic foams can vary if the ceramic particles experience damage during compression. In contrast to solid ceramic particles, hollow or porous ceramic particles have lower strength. When the compressive stress borne by them exceeds their compressive strength, they can either collapse or undergo plastic deformation. When the volume fraction of ceramic spheres is low, the compressive strength of the syntactic foam is often determined by the strength of the ceramic spheres. With a higher volume fraction of ceramic spheres, both the ceramic spheres and the metal matrix contribute to the compressive strength of the syntactic foam.

2.4.4.3 Compressive failure modes

Metal matrix syntactic foams have some structural characteristics similar to those of metal foams, metal matrix composites and polymer matrix syntactic foams. In compression, they can behave like any one of these materials and show mainly three different failure modes as shown in Figure 2.6. The compressive failure can be either ductile in the form of collapse and crushing of ceramic spheres (Kiser *et al.* 1999, Balch *et al.* 2005, Daoud 2007, Wu *et al.* 2007), or brittle in the form of shear failure (Kiser *et al.* 1999, Balch *et al.* 2005) or in the form of fracture with cracks at around 30° to the loading direction (Zhang & Zhao 2007, Palmer *et al.* 2007).

The ductility of the metal matrix has a moderate effect on the failure mode. Balch *et al.* (2005) showed that the syntactic foam with a commercially pure Al matrix

failed by ductile plastic deformation, while the syntactic foam with an Al 7075 matrix failed by shear fracture. Palmer *et al.* (2007) also found that the syntactic foam with an Al 6061 matrix has much more stable plastic deformation than the syntactic foam with an Al 5083 matrix.

Ceramic particles with different inner structures or porosities can give rise to different failure modes. Kiser *et al.* (1999) reported that the Al matrix syntactic foams containing hollow ceramic spheres with low wall-thickness-to-radius ratio failed by shear fracture and the deformation band was inclined 45° to the loading direction; the Al matrix syntactic foams containing hollow ceramic spheres with high wall-thickness-to-radius ratio failed by collapse and crushing of the ceramic spheres. The opposite was reported by Wu *et al.* (2007). They found that the failure of syntactic foams fabricated with low wall-thickness-to-radius ratio was dominated by the ductile collapse and crushing of ceramic spheres and Al network. In contrast, the syntactic foams with higher wall-thickness-to-radius ratio failed in a brittle manner, where wedge shaped cracks were observed from the longitudinal cross-section of the cylinder sample. Therefore, wall-thickness-to-radius ratio is not an independent variable determining the failure mode of the syntactic foam.

2.4.4.4 Energy absorption

The capability of metal matrix syntactic foams in energy absorption can be characterised by two parameters: plateau strength and onset strain of densification. The former is dependent upon the strengths of the metal matrix and the ceramic

particles, as well as upon the volume ratio between the two. The densification strain is mainly dependent upon the level of porosity in the syntactic foam.

Metal matrix syntactic foams have higher strengths than metal foams and polymer matrix syntactic foams. Therefore, they often have better capability of energy absorption. Balch *et al.* (2005) achieved specific energy absorption values of 39 and 49 J/g for syntactic foams with a CP Al matrix and an Al 7075 – T6 matrix, respectively. Vendra and Rabiei (2007) reported that the syntactic foam fabricated with Al 365 and hollow steel spheres had a higher specific energy absorption than either Al foam or hollow steel sphere foam alone due to higher plateau strength and ductile plastic deformation. Metal matrix syntactic foams are particularly suited to applications where permanent deformation at low stresses is undesirable.

2.4.4.5 Dynamic compressive properties

The dynamic compressive properties of metallic syntactic foams have been studied either by low speed or by high speed impact. The properties were often different from those obtained in static compression. Balch *et al.* (2005) and Dou *et al.* (2007) studied the dynamic compressive response of Al matrix syntactic foam using split-Hopkinson pressure bars at high strain rates up to $5.3\times10^{3}s^{-1}$. The dynamic stress-strain curves had a similar shape to those obtained in static compression, but with a much higher compressive strength. Dou *et al.* (2007) also reported that the deformation of syntactic foam under high speed impact is more ductile than it was in the static compression. Zhang & Zhao (2007) studied the

low speed impact response of Al matrix syntactic foam at a speed of 4 m/s. The stress-strain curves at low strains were found to consist of many oscillations where the test hammer experienced strong vertical vibrations, which were different from the static compression. The impact peak strength was also found to be much higher than the compressive strength in static compression.

2.5 Closed cell metal foams

2.5.1 Introduction

Although metal matrix syntactic foam and metal foam are different kinds of materials in that the former is a composite and the latter is a one-phase material, both can be classified as cellular solid. This section mainly reviews the compressive properties of closed cell metal foam, which has some common characteristics in compression to metal matrix syntactic foam.

2.5.2 Fabrication

The closed cell metal foam can be made by several techniques. Two techniques are usually used to fabricate closed cell Al foam. In the Alcan process (Andrews *et al.* 1999), gas is injected into a mixture of molten aluminium and ceramic particles (either SiC or Al_2O_3). The volume fraction of ceramic particles is between 5 and 15% and the size of the particles is 1-20μm. The injected air causes bubbles to rise to the surface of the melt, forming a liquid foam which is stabilized by the presence of the ceramic particles. The liquid foam is then mechanically

conveyed off the surface of the melt and allowed to cool. The as-fabricated aluminum foams have a relative density ranging from 0.03 to 0.15. Closed cell aluminium foam can also be made by adding titanium hydride powder to either molten or powdered aluminium (Davies & Zhen 1983). The titanium hydride decomposes at 400°C, well below the melting temperature of aluminium (T_m=660 °C), releasing hydrogen gas to form bubbles in the foam. The aluminium foam fabricated by this technique has a relative density range of 0.08-0.25. The typical structure of closed cell Al foam is shown in Figure 2.7.

2.5.3 Mechanical properties

The compressive properties of closed-cell metallic foams are largely determined by their density. However, the pore size, pore structure and distribution are also important parameters determining the properties. As a general rule, there is a fairly close relationship between density and mechanical properties such as compressive strength.

The compressive stress-strain curves of closed-cell metal foams show three regimes of the elastic-plastic foams, as illustrated in Figure 2.8 (Hall, Guden & Yu 2000). The plateau region is caused by pore collapse, buckling and cell wall failure. The deformation mechanism of closed-cell foams during compression is by the bending of cell edges accompanied by stretching of the cell faces (Edwin & Daniel 2007). Gibson and Ashby (1999) suggested a general equation for the plateau stress of regular hexagonal closed-cell foam:

$$\frac{\sigma_{pl}^{*}}{\sigma_{ys}} = 0.3\left(\varphi\frac{\rho^{*}}{\rho_s}\right)^{\frac{3}{2}} + (1-\varphi)\left(\frac{\rho^{*}}{\rho_s}\right) \tag{2.6}$$

where σ_{pl}^{*} is the plateau stress of the foam, σ_{ys} is the yield stress of the cell wall material, φ is the fraction of solid contained in the cell edges, ρ^{*} is the density of foam, and ρ_s is the density of the cell wall material. Similarly, the Young's modulus for regular hexagonal closed-cell foam is given by

$$\frac{E^{*}}{E_s} = \varphi^2\left(\frac{\rho^{*}}{\rho_s}\right)^2 + (1-\varphi)\left(\frac{\rho^{*}}{\rho_s}\right) \tag{2.7}$$

where E^{*} is the Young's modulus of the foam and E_s is the Young's modulus of cell wall material.

For tetrakaidecahedral closed cell metal foam, Simone & Gibson (1998a) specified Eqs. (2.6) and (2.7) using finite element simulations and obtained:

$$\frac{\sigma_{pl}^{*}}{\sigma_{ys}} = 0.33\left(\frac{\rho^{*}}{\rho_s}\right)^2 + 0.44\left(\frac{\rho^{*}}{\rho_s}\right) \tag{2.8}$$

$$\frac{E^{*}}{E_s} = 0.32\left(\frac{\rho^{*}}{\rho_s}\right)^2 + 0.32\left(\frac{\rho^{*}}{\rho_s}\right) \tag{2.9}$$

Sugimura *et al.* (1997) studied the static compressive and tensile behaviour of three Al closed cell foams fabricated with different foaming strategies. The difference results in three types of imperfections, which were wiggles, nodal inclusions and curves. They suggested that these morphological factors can affect mechanical properties, as well as the deformation and fracture mechanism. They studied the stress-strain response and reported that non-planarity in the cell wall is the principal defect affecting stiffness and cell wall defects have a comparable role on plasticity.

Andrews *et al.* (1999) studied the compressive and tensile properties of Al closed cell foams with the relative density in the range of 0.08 to 0.14. The experimental data for the modulus and strength of the closed cell foams lay well below the model predictions from an ideal tetrakaidecahedral cell (Eqs. 2.8 and 2.9). Simone and Gibson (1998b) studied the effect of cell face curvature and corrugation on the stiffness and strength of closed cell Al foam using finite element methods. They attributed the disagreement between the mechanical properties of closed cell foam and the predicted idealized models (Eqs 2.8 and 2.9) to curved and corrugated cell faces present within the foams. Andrews *et al.* (1999) argued that other imperfections in the cell structure (e.g. cell shape, local density variations) also play a role in determining the stiffness and strength.

Motz and Pippan (2001) studied the tensile behaviour of Al closed cell foams of two different relative densities. They reported the deformation mechanism was different from that found in compression. No plateau stress regime accompanied by plastic instabilities was found in tension.

Paul and Ramamurty (2000) tested closed cell Al foam with different strain rates of 3.33×10^{-5} s^{-1} to $1.6\times10^{-1}s^{-1}$. They found that the strain-rate sensitivity characteristics of Al foam are similar to those of dense Al at room temperature. However, there are some features, such as the bilinear increase in the yield strength with the $\log(\dot{\varepsilon})$, that are distinct for the foam material. Because the buckling of cell walls is the dominate micromehcanism of the deformation in these foams, microinertial effects are thought to be the cause for the observed

bilinearity. The energy absorption was found to be increased by 50% with increasing the strain rate to the maximum value. Similar results were reported by Hall *et al.* (2000). They studied the effects of density and strain rate on the compression properties of closed cell Al foams with three different relative densities. They reported that the compressive flow stress of the foam is a function of the relative density but shows little or no strain rate sensitivity. They found that the energy absorption of the foam is also related to the foam density by a similar power law dependency as in Eq. 2.6. By metallographic observation, they suggested that the general deformation process is progressive cell wall collapse, including buckling and tearing.

2.6 Particulate reinforced metal matrix composites (PRMMCs)

2.6.1 Introduction

Particulate reinforced metal matrix composites (PRMMCs) refer to a class of materials in which rigid ceramic particles (mainly SiC or Al_2O_3) are embedded in a ductile metal or alloy matrix (mainly Al). PRMMCs combine metallic properties (ductility and toughness) with ceramic characteristics (high strength and modulus), leading to greater strength in shear and compression and to higher service temperature capabilities. The attractive physical and mechanical properties that can be obtained with PRMMCs, such as high specific modulus, strength, and thermal stability, have been documented extensively since 1980's (Fishman *et al.* 1986, Flom & Arsenalt 1986a & 1986b, Rack 1988, Mortensen & Cornie 1987, Nardone & Prewo 1986). This section mainly review the microstructure and

mechanical properties of PRMMCs, which have some common characteristics in compression to metal matrix syntactic foams.

2.6.2 Fabrication

PRMMCs are produced mainly by liquid phase processing, including stir casting (Hanumanth & Irons 1993, Seo & Kang 1995) and squeeze infiltration (Mortensen & Cornie 1987, Klier *et al.* 1991, Taha & El-Mahallawy 1998) and also by powder metallurgy (P/M) (Divecha, Fishman & Karmarkar 1981, Flom & Arsenault 1986b, Nair, Tien & Bates 1985). All these techniques are based on the addition of ceramic reinforcements to the matrix materials which are in the molten or powder form.

In terms of microstructural development, the (P/M) approach is superior in view of the rapid solidification experienced by the powders (Ibrahim, Mohamed & Lavernia 1991). It allows the development of novel matrix materials outside the compositional limits dictated by equilibrium thermodynamics in conventional solidification processes (Jones 1982). The disadvantage of the P/M method is that the matrix-particle bonding may be not as good as in the melt processing (Ibrahim, Mohamed & Lavernia 1991). In the stir casting method, a strong bond between the matrix and the reinforcement can be achieved by utilizing high processing temperatures and alloying the matrix with an element which can interact with the reinforcement to produce a new phase and effect "wetting" between the matrix and the particles (Ibrahim, Mohamed & Lavernia 1991, Hanumanth & Irons 1993).

The difficulties of the stir casting process include: agglomeration of the ceramic particles, segregation of secondary phases in the metallic matrix, extensive interfacial reactions, and particulate fracture during mechanical agitation. The advantages of the squeeze casting process includes better matrix-particle bonding, easier control of matrix structure, simplicity, low cost of processing and near net shape (Hanumanth & Irons 1993, Seo & Kang 1995, Taha & El-Mahallawy, 1998). Some of the drawbacks of the squeeze casting process include reinforcement damage, preform compression and coarse reinforcement particles.

2.6.3 Microstructure

The size of the reinforcement has a marked effect on the homogeneity of PRMMCs fabricated by powder metallurgy. Hall *et al.* (1994) found that the Al/SiC_p composite with 5μm SiC_p had a more uniform distribution of reinforcement than that with 10μm SiC_p. This result was consistent with the study of Varma *et al.* (2001), where three different sizes (1.4, 15.8 and 62.8μm) of SiC_p were used to produce PRMMCs by P/M. Some clustering tendency was observed in the composite with the fine SiC_p (1.4μm), as shown in Figure 2.9. Gnjidic, Bozic & Mitkov (2001) also observed the agglomerations of small SiC particles (0.7μm) in the microstructure of Al/SiC PRMMCs, and that some particles cracked in the PRMMCs with large SiC particles (33μm). Slipenyuk *et al.* (2006) found that both the particle size and volume fraction of reinforcement particles affected the microstructure of PRMMCs. They fabricated Al/SiC_p PRMMCs by powder metallurgy, with matrix-to-reinforcement particle size ratio ranging from

2.9 to 12.9 and volume fraction of the reinforcement ranging from 0 to 20%. It was reported that the number of clusters of SiC particles increased with increasing particle size ratio and volume fraction of SiC particles.

Hanumanth and Irons (1993) examined the microstructure of an Al/SiC_P composite manufactured by the stir casting process. Particle agglomerates and large pores were observed in the microstructure of the composite. It was also reported that the number of agglomerates and pores can be reduced by adding small amount of magnesium which can improve the contact of SiC with molten Al. Seo and Kang (1995) examined the microstructure of Al-15%SiC_P composite fabricated by the stir casting process. It was reported that the dispersion of particles was related to the crucible size, the impeller size, the temperature of the molten metal, the stirring time and the stirring speed in the melt-stirring process. The size of particles can also affect the homogeneities of PRMMCs fabricated by stir casting. Kok (2005) fabricated Al/Al_2O_3 composites with three different sizes of Al_2O_3 particles (66, 32 and 16μm). It was revealed that the dispersion of the coarser particles was more uniform while the finer particles led to agglomeration and segregation of the particles, and porosity.

Divecha, Fishman and Karmarkar (1981) studied the microstructure of Al/SiC composite fabricated by the infiltration casting method, where SiC is in the form of whiskers and particles with lengths up to 50μm and the diameters varying from 0.2-1.0μm. The composites were found to have a good macrohomogeneity. However, dark regions with high SiC content were found on a microscopic scale. The investigation under higher magnification revealed that good infiltration of the

aluminum occurred even within high SiC content regions. The microstructure of PRMMCs fabricated by the infiltration casting method was also studied by Taha and El-Mahallawy (1998). They fabricated Al/Al_2O_3 composites with three different sizes of Al_2O_3 particles (80, 95 and 115 μm). It was reported that all the composites displayed a uniform distribution in both transverse sections, independent of the particle size of Al_2O_3. However, they found that the distribution of Al_2O_3 particles was not uniform in the longitudinal section. Whilst at the top of the specimen the particles were relatively far from each other, they were closer to each other towards the bottom. A gradual increase in the inter-particle spacing was observed from the bottom to the top of the specimen.

2.6.4 Mechanical properties

Arsenault (1984) studied the strengthening effect of SiC platelets in an Al/SiC composite through a series of tensile tests. It was revealed that the level of strengthening, which was attributable to the SiC platelets, was much greater than that predicted by continuum mechanics theories. It was reported that the mechanism by which the strengthening occurred was due to the difference between the coefficient of thermal expansion of SiC and that of aluminum, which resulted in a high dislocation density in the matrix.

Arsenault and Flom (1986) investigated the magnitude of strength for the interracial bond between SiC and the Al 6061 alloy matrix. They measured the local interfacial stresses at the particle-matrix interfaces. The lower bound value

of the bond strength was determined to be at least 1690 MPa. The ductile fracture of the Al-SiC composite with a low volume percentage of SiC occured by void nucleation at SiC particulates and also at the matrix imperfections (pre-existing voids, inclusions, etc.).

Flom and Arsenault (1989) studied the effect of particle size of SiC reinforcement on the fracture process of Al/SiC composites. The fracture was confined to a very narrow band and took place within the matrix containing small SiC particles. They found that in the composites reinforced with SiC particles of 20μm and above fracture of SiC began to dominate. It was also suggested that the matrix was influenced by the high density of dislocations generated at SiC/Al interfaces due to the difference in coefficient of thermal expansion (CTE) between SiC and the Al matrix. Crack initiation did not depend on SiC particle size. Crack growth increased as the size of the SiC particle increased.

Manoharan and Lewandowski (1992) studied the effects of microstructure and reinforcement sizes, on the fracture initiation and growth in a SiC particulate reinforced 7091 aluminum alloy. They found that nucleation of reinforcement cracking was both matrix and particle size dependent. While crack initiation showed minor dependence on the size of reinforcement, the crack growth was higher for the composite with larger particles (13μm) compared with that reinforced with smaller particles (5μm).

Hall, Wayne & Sachdev (1994) evaluated the probability of particle fracture in Al/SiC composites with SiC particle sizes ranging from 2 to 20μm and volume

fraction from 10% to 35%. It was found that the strength and fatigue life of the composite increased as reinforcement particle size decreased and volume fraction increased. The frequency of particle fracture during crack propagation was found to be dependent on matrix strength, particle size and volume fraction and maximum crack tip stress intensity. Particle fracture was rationalized, phenomenologically, by the application of modified process zone models, originally derived for static fracture processes, and weakest link statistics which accounted for the dependence of matrix yield strength and flow behavior and particle strength on the probability of particle fracture during monotonic fracture and fatigue crack propagation. Gnjidic, Bozic and Mitkov (2001) suggested that both the presence of agglomerations of small SiC particles (0.7μm) and the cracking of large SiC particles (33μm) had detrimental effects on Al/SiC composite strengthening, while the greatest strengthing effects were achieved with the Al/SiC composite of medium (15μm) SiC particles. Mazen and Emara (2004) investigated the effects of particle cracking on the strength and ductility of Al-SiCp composite. It was found that particle cracking played a significant role in controlling the mechanical properties of the composite. It was shown that particle cracking was possible in a PRMMC material made with a low strength matrix (e.g. commercially pure aluminum), and increased with the increase of reinforcement volume fraction, applied strain rate, and amount of plastic deformation. The yield strength increased as a function of reinforcement volume fraction and to a lesser extent as a function of the strain rate. They also reported that the tensile strength increased at low SiCp volume fractions, then remained constant or decreased as more particles were added to the matrix.

Doel and Bowen (1996) studied the tensile behaviour of Al 7075 matrix PRMMCs with the SiC particles of three different sizes (3, 5 and 60μm). They found that all the composites had a lower ductility than the unreinforced material; the finer the particle size, the more ductile the composite was. The failure of the composite samples was suggested to be due to the accumulation of internal damage to particles either by particle fracture or interfacial failure. Such damage was believed to lead to the presence of voids which grow and result in reduced ductility in these composites. Large 60m particles fracture easily at low applied stresses, leading to reduced 0.2% proof stress and premature failure compared to the other composites. The small particles (5 and 13μm) damaged less easily, so these composites were stronger than the monolithic material and are more ductile than the composite reinforced with 60 μm particles.

Kiser *et al.* (1996) studied the compressive, tensile and flexural behaviour of PRMMCs fabricated with Al-Si-Mg alloy matrix and SiC reinforcement of two different volume percentages, 10% and 20%. The volume percentage of particles had significant effects on compressive and tensile strengths. Both composites had a higher strength than the monolithic alloy. Moreover, the more the volume fraction of particles, the more brittle the composite was.

Kok (2005) fabricated 2024 aluminium alloy PRMMCs reinforced with Al_2O_3 particles of three different sizes and weight fractions up to 30 wt.% using a vortex method with subsequently applied pressure. Hardness and tensile tests were performed on the composite samples. It was found that the hardness and the

tensile strength of the composites increased with decreasing size and increasing weight fraction of particles.

Zhang *et al.* (2004) studied the dynamic compressive behaviour of aluminum 6092/B_4Cp (boron carbide) composites. The tests were conducted over a wide range of strain rates (10^{-4} to 10^{4} s^{-1}). They found that the strength of these composites increased with increasing volume fraction of the particulate reinforcement. Strain hardening was observed to increase with increasing volume fraction of reinforcement at lower strains (<5%), but tended to be insensitive to volume fraction at higher strains. They reported that particle size effect was not significant for the particles >5μm.

2.7 Summary

Polymeric syntactic foams have a similar morphology to the metallic syntactic foams. Although both materials have the capability for energy absorption, two reasons lead to metallic syntactic foams being a better choice for energy absorption. First, polymeric syntactic foams have lower plateau strength due to lower strength of the polymer matrix. Second, the polymeric syntactic foams usually fail in a brittle manner at a low strains due to voids in the matrix.

In the previous studies on metallic syntactic foams, the volume fraction of the metal matrix was determined by the inter-particle space of the ceramic spheres and was fixed to about at 37%. The effect of volume ratio of the metal matrix and the ceramic sphere on the mechanical properties and energy absorption capability

of the syntactic foams has not been studied in detail. Moreover, although different failure modes were observed in several studies of metallic syntactic foams, the reason for different modes has not been well explained.

Although closed cell metal foams have different morphologies and mechanical properties from those of metallic syntactic foams due to the embedding of ceramic spheres in the latter, the understanding of compressive failure mechanism of closed cell metal foams can help the study of metallic syntactic foams. The analysis used in closed cell metal foams, has a potential application in metallic syntactic foams.

PRMMCs have different structures and mechanical properties from those of metallic syntactic foams because of a lower volume fractions and the solid form of the of reinforcement particles. However, the fabrication methods used in PRMMCs are also applicable to metallic syntactic foams. Stir casting, squeeze infiltration and powder metallurgy have indeed been applied in fabrication of metallic syntactic foams. The literature about the optimum fabrication parameters for microstructure and mechanical properties of PRMMCs is used in the study of microstructure and mechanical properties of metallic syntactic foams, manufactured by a similar process.

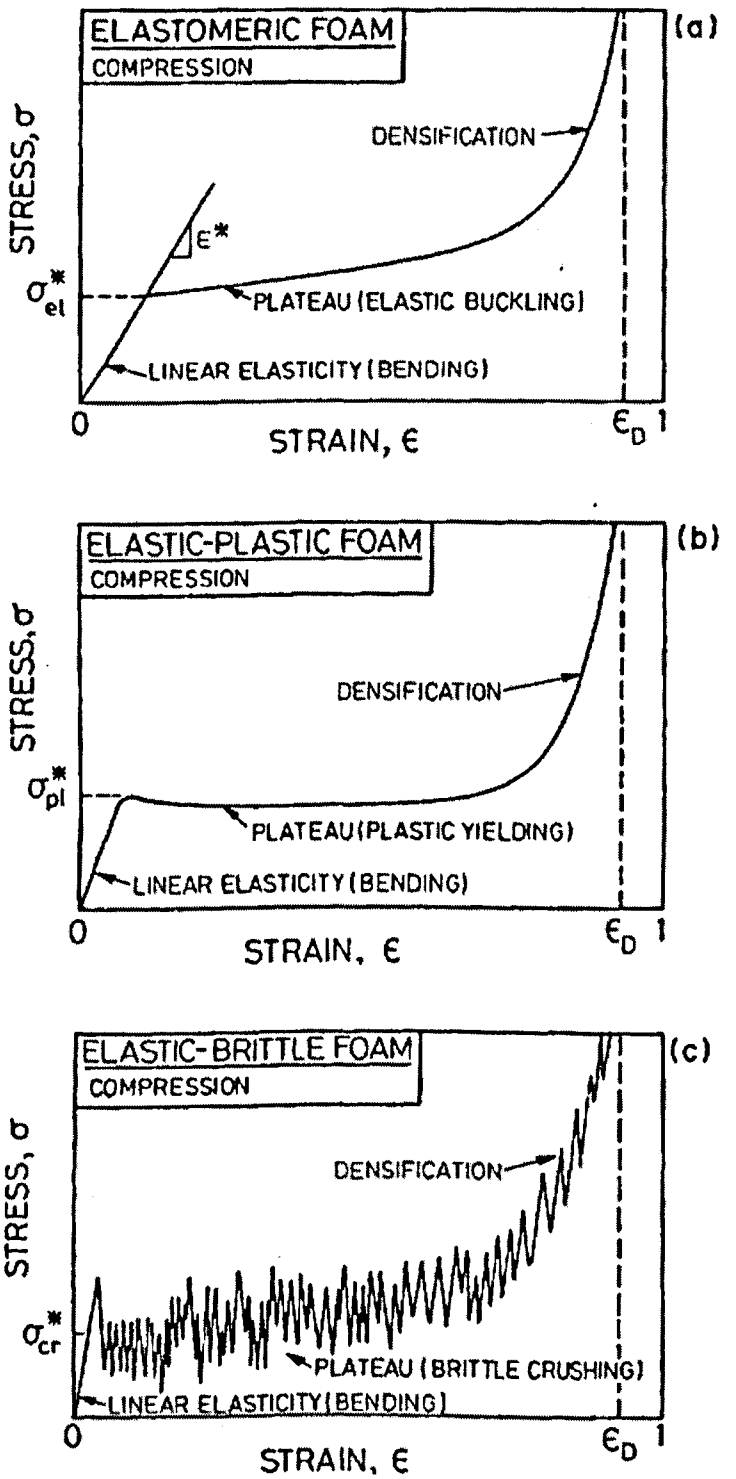

Figure 2.1 *Schematic compressive stress-strain curves for foams, showing the three regimes of linear elasticity, collapse and densification: (a) an elastomeric foam; (b) an elastic-plastic foam; (c) an elastic-brittle foam (Gibson & Ashby 1999)*

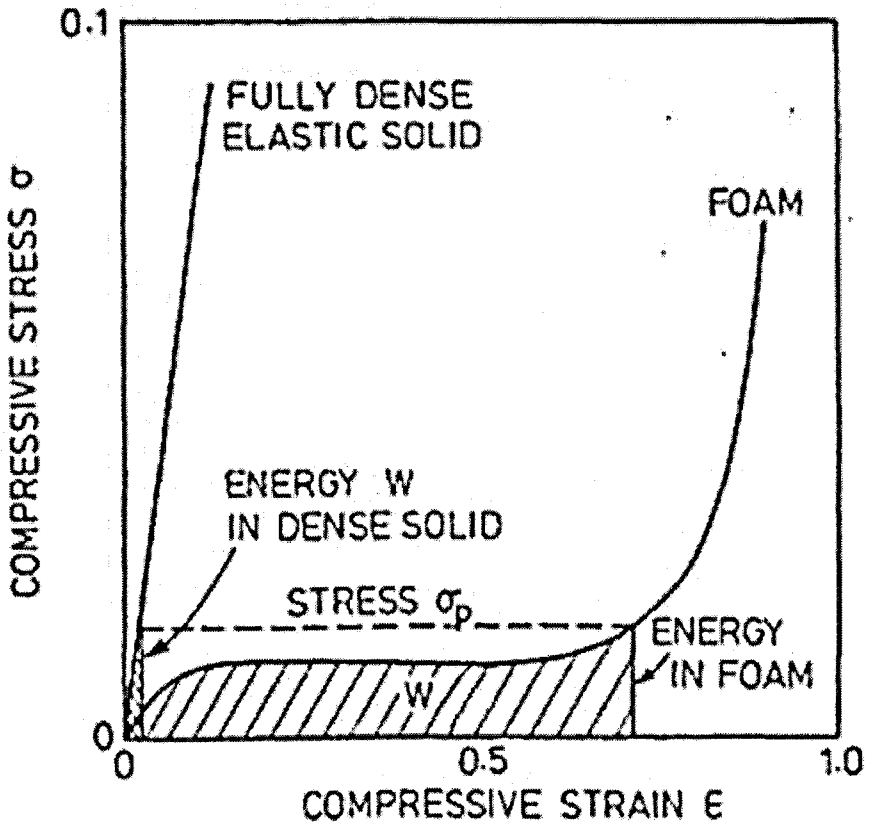

Figure 2.2 *Stress-strain curves for an elastic solid and a foam made from the same solid, showing the energy absorbed at a peak stress* σ_p (Gibson & Ashby 1999)

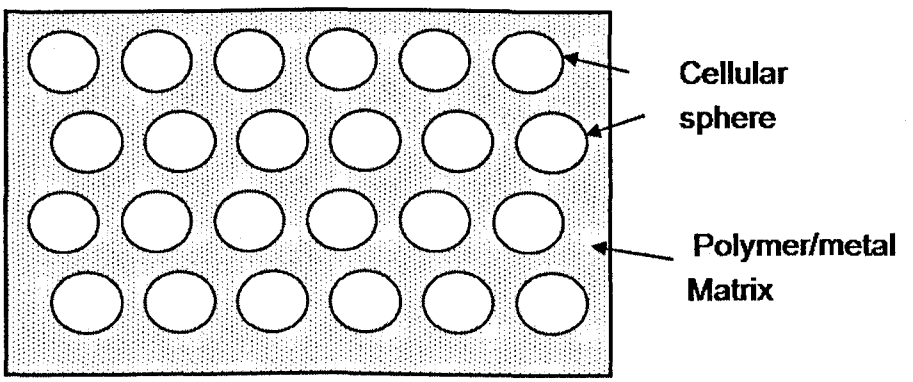

Figure 2.3 *Schematic structure of syntactic foam*

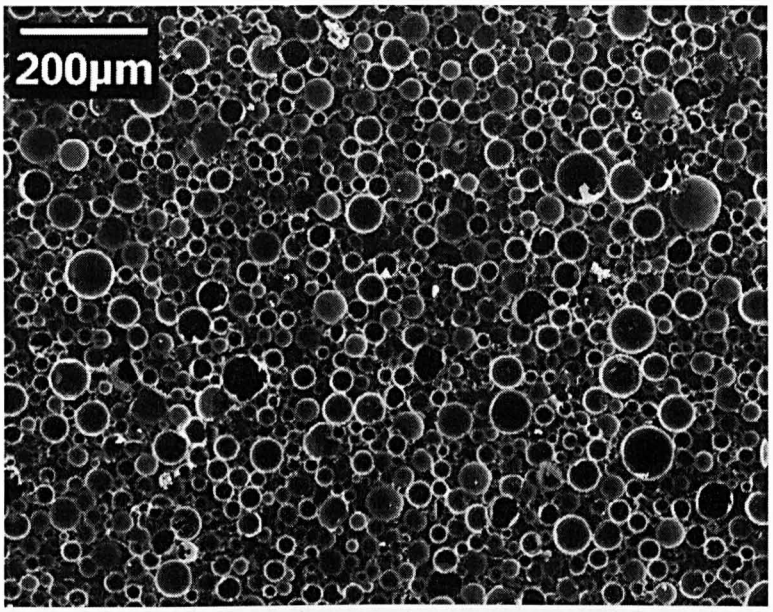

Figure 2.4 *Scanning electron micrograph of a syntactic foam (Gupta et al. 2008)*

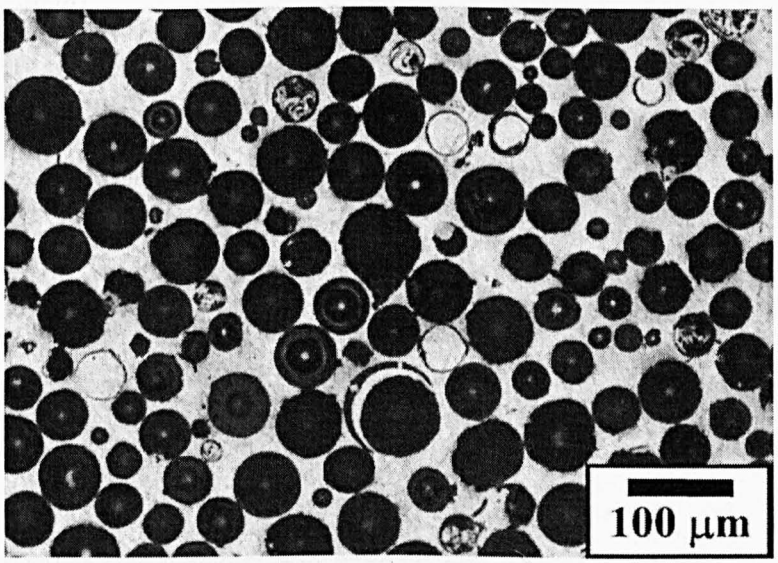

(a)

Figure 2.5 *Microstructure of metallic syntactic foams fabricated by: (a) melt pressure infiltration method (Balch 2005) and (b) stir casting method (Daoud 2007) (to be continued)*

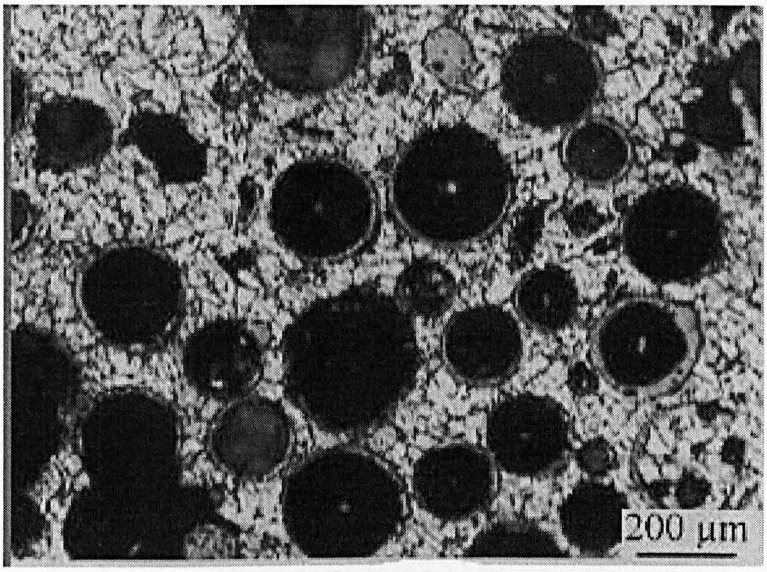

(b)

Figure 2.5 *Microstructure of metallic syntactic foams fabricated by: (a) melt pressure infiltration method (Balch 2005) and (b) stir casting method (Daoud 2007) (continued)*

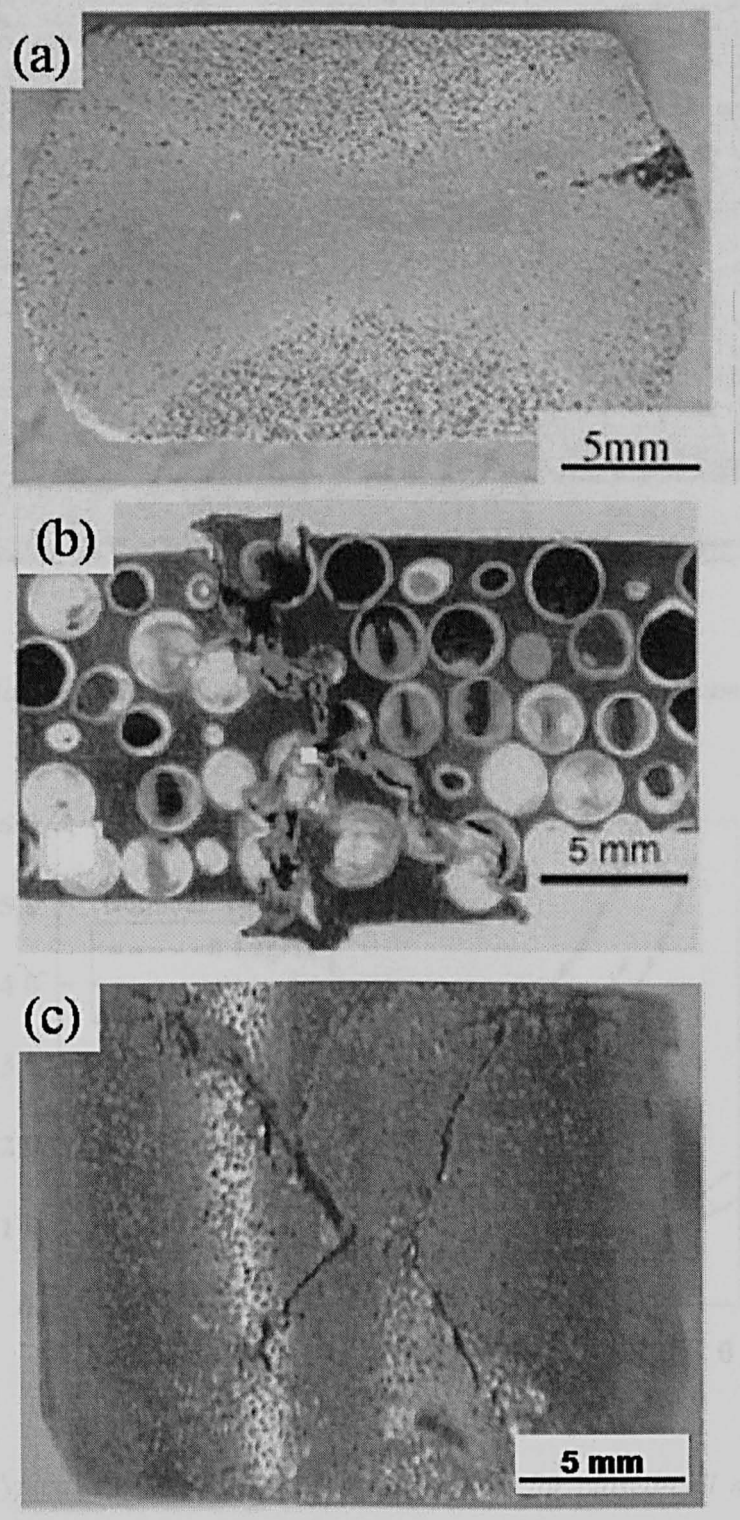

Figure 2.6 *Three different failure modes of metal matrix syntactic foams: (a) collapse and crushing (Wu et al. 2007), (b) shear failure (Kiser et al. 1999) and (c) brittle fracture (Zhang and Zhao 2007)*

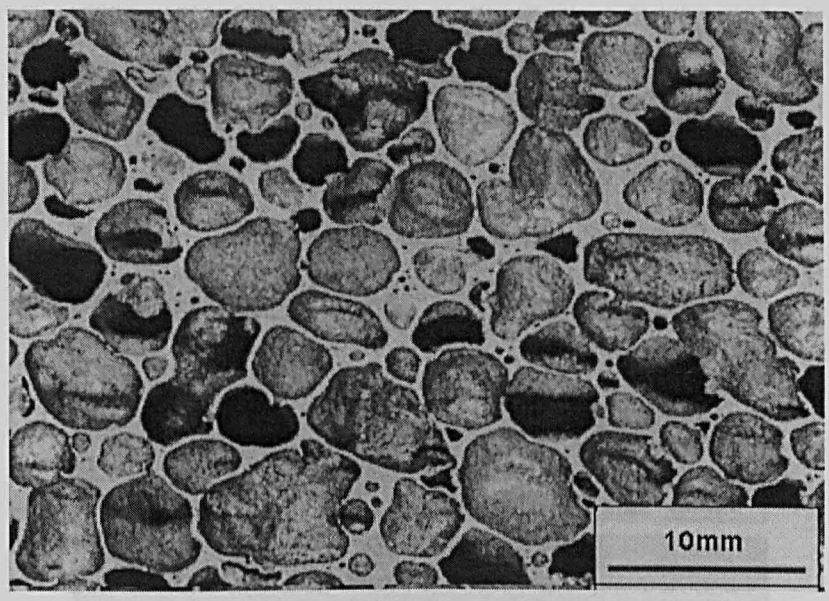

Figure 2.7 *Macroscopic view of a closed cell Al foam. (Paul & Ramamurty 1999)*

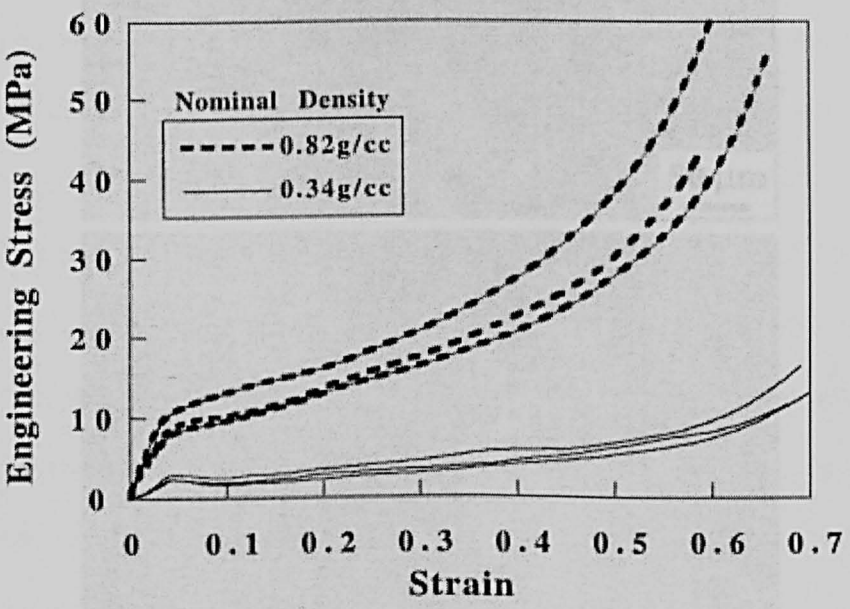

Figure 2.8 *Typical compressive stress-strain curves for closed-cell metal foam. (Hall, Guden & Yu 2000)*

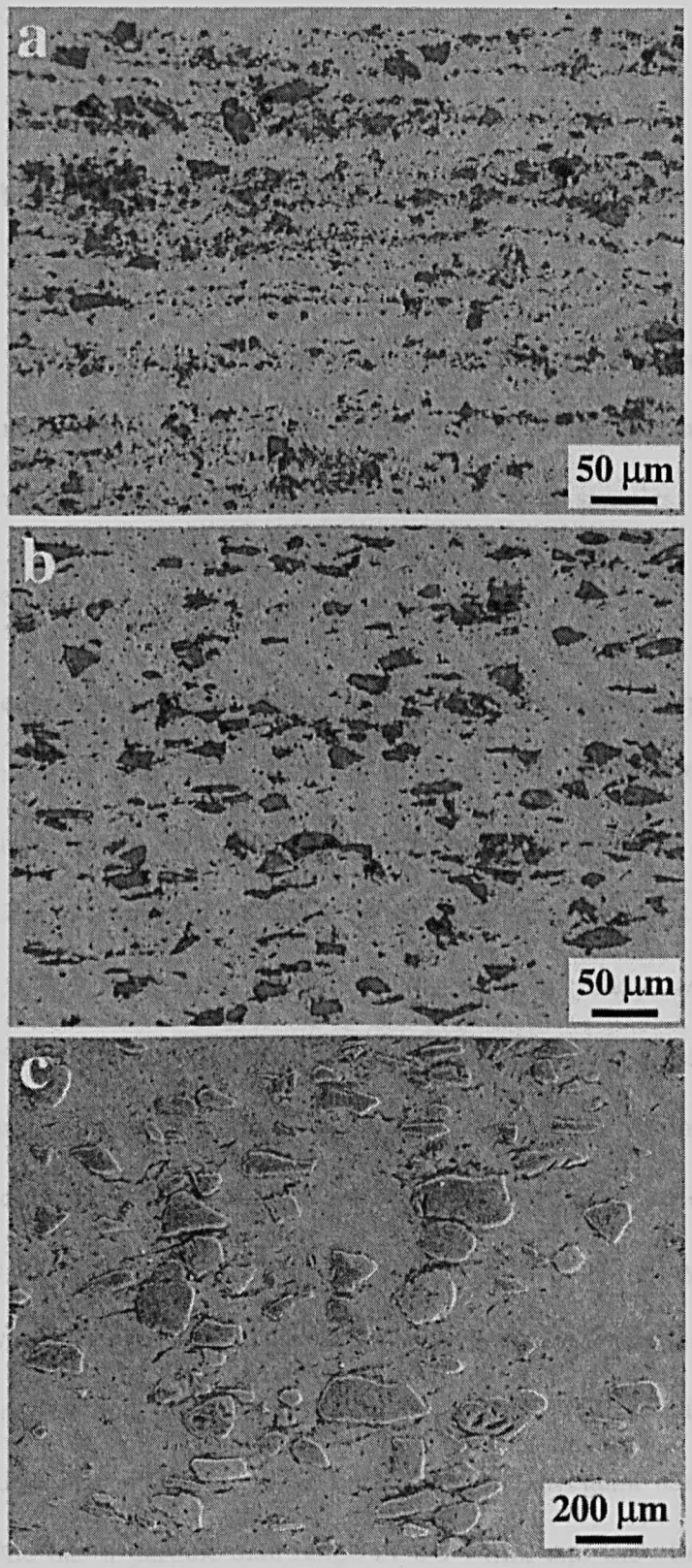

Figure 2.9 *Optical micrographs showing SiCp distribution in composites with (a) 1.4 μm, (b) 15.8 μm and (c) 62.8 μm SiCp (Varma et al. 2001)*

CHAPTER 3 EXPERIMENTAL PROCEDURE

This chapter presents a detailed description of the fabrication processes, the density measurement procedure, the mechanical testing procedures and the micro- and macro-structural observations for the Al syntactic foam samples.

3.1 Raw materials

The raw materials used for fabricating the Al syntactic foam samples were Al 6082 alloy and a ceramic microsphere (CM) powder. Al 6082, in the form of a block, was used in the manufacture of syntactic foam samples by the melt infiltration casting method. Al 6082 has a chemical composition of 1.3% Si, 0.5% Fe, 0.4% Mn, 0.8% Mg and balance for Al by weight. Al Alloys with silicon as the major alloying addition are the most important casting alloys mainly because of the high fluidity imparted by the presence of relatively large volumes of the Al-Si eutectic (Polmear 1989). Al 6082 is one of the strongest 6000 series alloys, and was therefore selected as the matrix in this study. The Al 6082 alloy, in the form of powder, was also used in the manufacture of syntactic foam samples by the liquid sintering method or by the method of melt infiltration into an Al-CM powder mixture. Two different Al 6082 powders with irregular shaped particles were used. One has a particle size range of 0.5-1mm, and the other has a size range of 30-100 μm with the average size of 53μm. The CM powder used in this study was supplied by Envirospheres Pty Ltd (Linfield, Australia). The CM

powder has a composition of ~60% SiO_2, ~40% Al_2O_3 and 0.4-0.5 % Fe_2O_3 by weight, and has an effective density of 0.6g/cm^3, which is the mass of the spheres of a CM powder divided by the volume the spheres occupy less the air void between them. The as-received CM powder was divided into four size groups with the diameter ranges of 20-75 μm, 75-125 μm, 125-250 μm and 250-500μm, which were designated as CM Powder I, II, III and IV, respectively.

3.2 Fabrication methods

The Al syntactic foams were either produced by melt infiltration casting or by liquid sintering. In the melt infiltration casting process, the syntactic foam was fabricated by infiltrating molten Al into monomodal (single particle size range), or bimodal (two particle size ranges) CMs. This method was also used to fabricate syntactic foams toughened with Al particles. In the liquid sintering process, the syntactic foam was produced by mixing, compacting and sintering a mixture of Al and CM powders.

3.2.1 Melt infiltration casting

3.2.1.1 Melt infiltration with CM preforms

The melt infiltration casting process is shown schematically in Figure 3.1. A steel tube, the bottom of which was sealed by a circular steel disc, was first partly filled with the CM powder. The diameter of the tube was either 21mm or 44mm, and the

Table 3.1 Compositions of syntactic foams fabricated by melt infiltration casting.

Sample ID No	Al Alloy	Type and Volume of CM
M1	6082	I
M2	6082	II
M3	6082	III
M4	6082	VI
B1	6082	30% II, 70% IV
B2	6082	50% II, 50% IV
B3	6082	70% II, 30% IV
B4	6082	20% I, 80% IV
B5	6082	40% I, 60% IV
B6	6082	60% I, 40% IV

length was 55mm. The height of the CM contained in the tube was 25mm. An Al block, with a predetermined weight was then placed on the top of the CM powder. The volume ratio of Al to CM was maintained at 1:2, at which the Al is slightly more than the amount needed to ensure full infiltration of the CM powder. Another circular steel disc, which was slightly smaller than the internal diameter of the tube, was placed above the Al block. The assembly was placed in an electric furnace, heated up and maintained at 730°C for 30 minutes to ensure that the Al block was fully molten. The assembly was then removed from the furnace and the molten Al alloy was instantly pressed to infiltrate into the CM powder by a piston at a pressure of 3 MPa. After complete solidification, the syntactic foam sample was removed from the tube. The CM powder was either monomodal or bimodal. The compositions of the as-fabricated syntactic foams are shown in

Table 3.1, where syntactic foams of M series were fabricated with different monomodal CMs and syntactic foams B series were fabricated with bimodal CMs, respectively. Three more syntactic foams with the same composition as M4 were fabricated with higher infiltration pressures of 4, 7 and 9 MPa, and are designated as M4-H1, M4-H2 and M4-H3, respectively.

3.2.1.2 Melt infiltration with Al/CM powder mixture

The melt infiltration casting method was also used to produce the syntactic foams toughened with additional Al 6082 particles. Four sets of samples were fabricated by infiltrating molten Al 6082 into a mixture of Al 6082 (with a particle size range of 0.5-1 mm) and the CM powder. The target total volume fractions of Al 6082 in the four sets of samples were 43%, 50%, 60% and 70%. To achieve the target Al volume fraction, predetermined amounts of Al powder and CM powder were firstly mixed with small amount of ethanol as binder before packed in a steel tube with the diameter of 44mm. An Al 6082 block, with a predetermined volume about half of the volume of the Al/CM powder mixture, was placed on the top of the mixture. The assembly was placed in an electric furnace preheated to 650°C and then heated to 710°C and maintained for 10 min. The assembly was removed from the furnace and the molten Al alloy was instantly pressed to infiltrate into the CM powder by a piston at a pressure of 3 MPa. After complete solidification, the syntactic foam sample was removed from the tube. The four sets of syntactic foams embedded with Al particles, with total Al volume fractions of 43%, 50%, 60% and 70%, were designated as T1, T2, T3 and T4, respectively.

3.2.2 Liquid sintering

The liquid sintering method used to fabricate the syntactic foams in this study is shown schematically in Figure 3.2. The Al 6082 powder with an average particle size of 53 μm and a monomodal CM powder, CM II, III or IV, were first mixed. A small amount of ethanol, roughly 1 vol.% of the Al-CM mixture, was added during the mixing to serve as a binder. In most cases, the volume fraction of Al in the Al-CM mixture, excluding voids, was maintained at 0.4. A range of Al volume fractions from 0.4 to 0.7 were used for the Al-CM mixtures with CM IV. After mixing, the Al-CM mixture was poured into a mild steel tube, the bottom side of which was pre-sealed with a layer of iron powder in order to prevent the molten Al from flowing out. A thin steel disc with the size equal to the inner diameter of the tube was used to cover the top of the Al-CM mixture. The mixture was compacted at 50 MPa by a hydraulic press. The whole assembly was heated in an electric furnace under the protection of argon to 700°C at a heating rate of 10 °C/min and maintained at this temperature for 10 minutes. The assembly was removed from the furnace and the Al-CM mixture was immediately pressed by a piston in a hydraulic press with the amount of displacement controlled to be sufficient to remove the voids included in the mixture. After complete solidification, the syntactic foam sample was removed from the tube. The compositions of the syntactic foams fabricated by the liquid sintering method are named as S series and are presented in Table 3.2.

Table 3.2 Compositions of syntactic foams fabricated by liquid sintering

Sample ID No	Volume Percentage of Al 6082 Powder (%)	CM Type
S1	40	II
S2	40	III
S3	40	IV
S4	50	IV
S5	60	IV
S6	70	IV

3.3 Pre-test heat treatment

The fabricated samples were machined to the desired dimensions for different experimental tests. Most samples were subjected to microstructural observations and mechanical tests directly without any heat treatment. Samples M1-M4 were also subjected to the standard T6 heat treatment (ASM 1991) before the mechanical tests. Specifically, the syntactic foam samples with Al 6082 matrix were homogenized in air at 540°C for 100 min and then quenched in water, followed by aging at 180°C for 12h.

3.4 Microstructural observations

The syntactic foam samples were ground and polished by grinder before optical or electron microscopy. Nikon optical microscopes with different magnifications

and a Hitachi S-2460N scanning electron microscope (SEM) were used to investigate the distribution of the CMs in the Al matrix and the bonding condition between them. The chemical compositions of the CMs and the syntactic foams were analyzed by Energy Dispersive X-Ray Spectroscopy (EDS) in the Hitachi scanning electron microscope. The Hitachi scanning electron microscope was also used to study the fracture surfaces of samples after indentation, compression, shear and tension.

3.5 Measurement of density

The density of the as-fabricated syntactic foams was measured by the Archimedes method using water as the working medium. The density of the four CM powders, I, II, III and IV, was also measured by the Archimedes method. Because some defective CM particles can be penetrated with water, the following procedure was adopted to achieve accurate values. A certain amount of pure wax was melted in a glass container and then cooled to full solidification. The volume of the wax together with the glass container was measured by the Archimedes method using water as the working medium. The wax was re-melted at 80°C without any evaporation. An amount of the CM powder was weighed, poured into the liquid wax, gently stirred with a steel wire to eliminate any air bubbles and then allowed to cool to room temperature and solidify. After complete solidification, the total volume of the wax, CM powder and glass container was measured again by the Archimedes method. The volume of the CM powder was the difference between

the two measurements. The density of the CM powder was determined using the measured values of its weight and volume.

3.6 Measurement of Young's modulus

The Young's modulus of Foams M1-M4 was measured by the impulse excitation method. The method is based on the principle that the mechanical resonant frequencies of a specimen that are determined by the elastic modulus of a material under a oscillatory applied force can therefore be determined by measuring mechanical resonant frequencies of a suitable (rectangular or cylindrical geometry) test specimen. Dynamic Young's modulus is determined using the resonant frequency in either the flexural or longitudinal mode of vibration.

In this study, rectangular specimens (40mm×15mm×15mm) and resonant frequency in flexural mode of vibration were used to determine the dynamic Young's modulus, which by (ASTM E 1876 – 01):

$$E = 0.9465\left(\frac{mf_f^2}{w}\right)\left(\frac{l^3}{t^3}\right)T \qquad (3.1)$$

where m is the mass of the sample, w the width, I the length, t the thickness, f_f the flexural frequency and T a correction coefficient.

A resonant frequency and damping analyser (RFDA) tester provided by IMCE

N.V. damping analyser (RFDA) tester provided by IMCE N.V. (Genk, Belgium) was used in this study. The test specimen was excited RFDA tester measures the flexural frequency of test specimens by exciting them mechanically by a singular elastic strike. The mechanical vibration of the specimen was detected by a transducer and transformed them into electric signals, as shown in Figure 3.3. The signals were analyzed by the signal analyzer, which provides a numerical reading of the flexural frequency of the specimen. The apparatus was available for a limited period of time. Therefore only the Young's modulus of foams M1-M4 was measured by this method in this study.

3.7 Mechanical tests

Most of the mechanical tests described below were performed on an Instron 4045 machine supplied by Instron Corporation, Canton, USA. The low speed impact tests, however were performed on an impact test facility. In all tests, at least three samples were tested for each fabrication condition to verify the repeatability.

3.7.1 Indentation test

Axisymmetric indentation tests were performed on cylinder samples of M2, M3 and M4 using a cylindrical punch with a semi-sphere head. The samples had a diameter of 20 mm and a length of 10 mm. The punch had a diameter of 5 mm,

thus the indentation was at a distance of more than 2 indenter diameters from the sample edge such that the edge effect was negligible. All the three types of syntactic foams were tested in two different conditions: either being indented directly without a spreader or with a spreader, as shown in Figure 3.4. The spreader was used to simulate the role of the facesheet in a sandwich structure, in order to evaluate the potential applications of syntactic foam in a sandwich structure against concentrated loading. The spreader was a circular mild steel disc with a diameter of 20 mm and a thickness of 0.5, 1, 1.5 or 2 mm. The tests were performed at a cross-head speed of 1mm/min and stopped when the displacement exceeded 8mm.

3.7.2 Compression test on CM powders

Quasi-static compression tests were carried out on the four CM Powders. In each test, a steel tube with an inner diameter of 19mm and a height of 50mm was placed on the lower platen of the test machine. The CM powder was poured into the tube to a free-packing height of 40mm and a steel punch with a diameter of 19mm was placed above the powder inside the tube. The punch was pressed by the upper platen of the test machine with a cross-head speed of 1mm/min. The load-displacement curve was recorded.

3.7.3 Quasi-static compression tests on syntactic foams

3.7.3.1 Unconfined

Uniaxial quasi-static compression tests were carried out on all the syntactic foams. The shapes of the samples were either cylinders with a circular cross-section or rectangular parallelepipeds with a square cross-section. The details of the geometry and heat treatment condition of the samples are listed in Table 3.3. Each sample was tested with a cross-head speed of 1mm/min and the stress-strain curve was recorded. The stress was calculated by dividing the applied load to the original cross-sectional area of the sample and the strain was calculated by dividing the displacement to the original length of the sample.

Table 3.3 *Geometry and heat treatment condition of the syntactic foam samples for quasi-static compression tests*

Samples	Shape	Diameter/ Width (mm)	Length (mm)	Heat Treatment
M1-M4	cylinder	21	21	no
M4-H1, -H2, -H3	cylinder	21	21	yes
M1-M4, B1-B6, T1-	cylinder	10	10	yes
S1-S6	parallelepiped	8	8	yes

3.7.3.2 Confined

Constrained compression tests were performed on syntactic foams M1-M4. The samples were cylindrical with both diameter and length of 19mm. In each test, the sample was confined within a cylindrical steel tube with the inner diameter equal to the sample diameter and thickness of 4mm. Each test was conducted with a cross-head speed of 1mm/min and the stress-strain curve was recorded.

3.7.4 Low speed impact test

Low speed impact tests were conducted on syntactic foams Ml-M4 using an instrumented drop-weight impact tower as shown in Figure 3.5. The samples were cylindrical with both the diameter and length about 10mm. In each test, the sample was placed on the base and the impactor was released from a certain height. For each foam, three different heights, 0.4, 0.66 and 1.08 m, were used to give constant impact velocities of approximately 2.8, 3.6 and 4.6 m/sec respectively. The impactor was cylindrical with a diameter of 20mm and had a 2.14kg impact carriage. The vertical guides of the impact tower were lubricated to minimize any friction generated during the descent of the carriage. The instant impact load-time data was recorded by a Kistler 9021A piezoelectric load cell with a 35kN capacity.

3.7.5 Shear test

The shear tests were conducted on syntactic foams M1-M4 using a test fixture composed of two halves of an occlusive cylinder as shown in Figure 3.6. Each syntactic foam specimen had a diameter of 19mm and a length of 24mm. The specimen was placed in a through hole of the setup and a screw bolt was used to adjust the position of specimen to ensure the shear fracture take place at the middle of the sample. The two halves of the fixture were subjected to tension to generate a shear condition on the specimen. The tests were performed at a cross head speed of 0.1mm/min.

3.7.6 Tensile test

Tensile tests were performed on syntactic foams M1-M4. The tests were conducted on parallelepiped samples with an approximate size of 38×12×5mm. In each test, each side of the sample was stuck onto two rectangular steel shims using cyanoacrylate super-glue to ensure a satisfactory testing length, as showing in Figure 3.7. The steel shims were clamped between the vices of the machine. One steel block was filled between each pair of steel shims to avoid stress concentration during the clamping. The tests were performed at a cross-head speed of 0.1mm/min and the stress-strain data were collected to generate the tensile stress-strain curves.

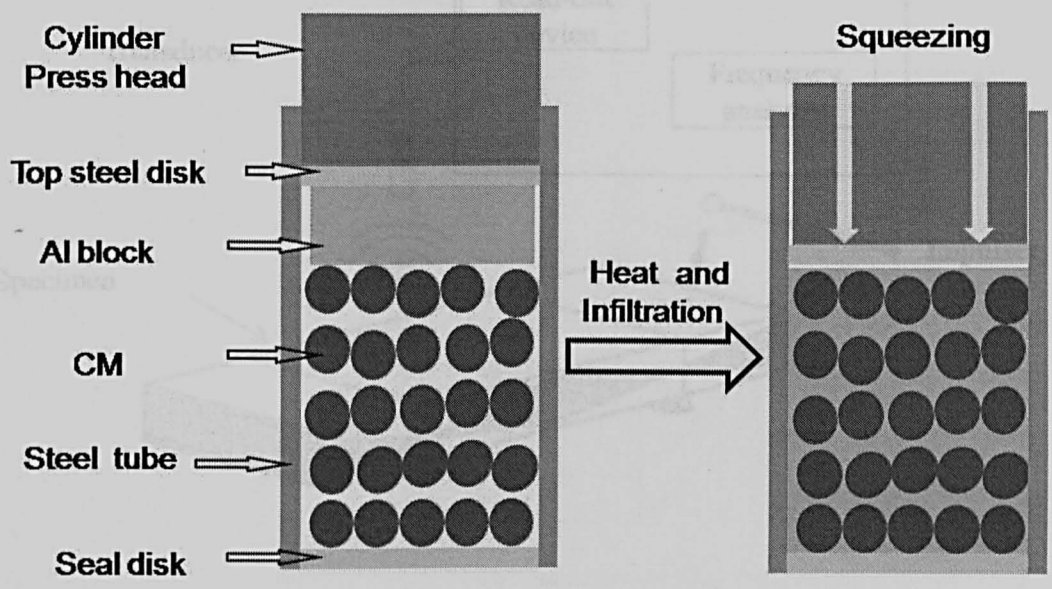

Figure 3.1 Schematic of melt infiltration casting

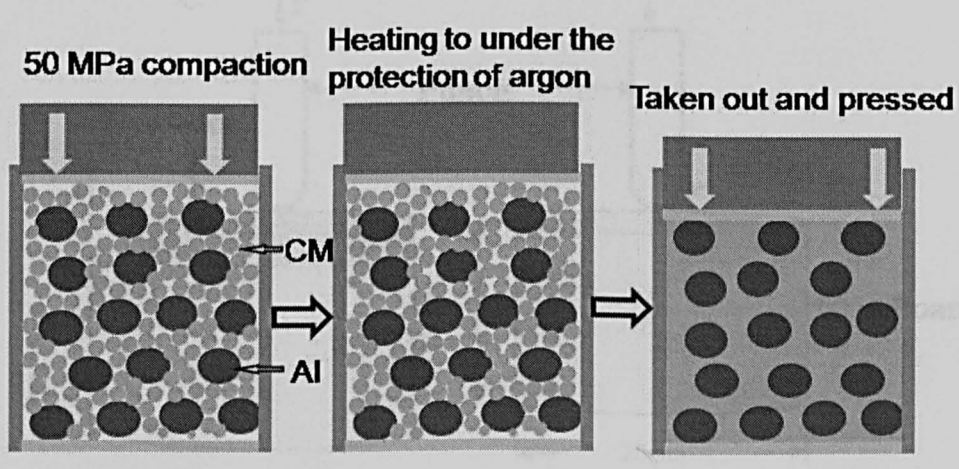

Figure 3.2 Schematic of liquid sintering process

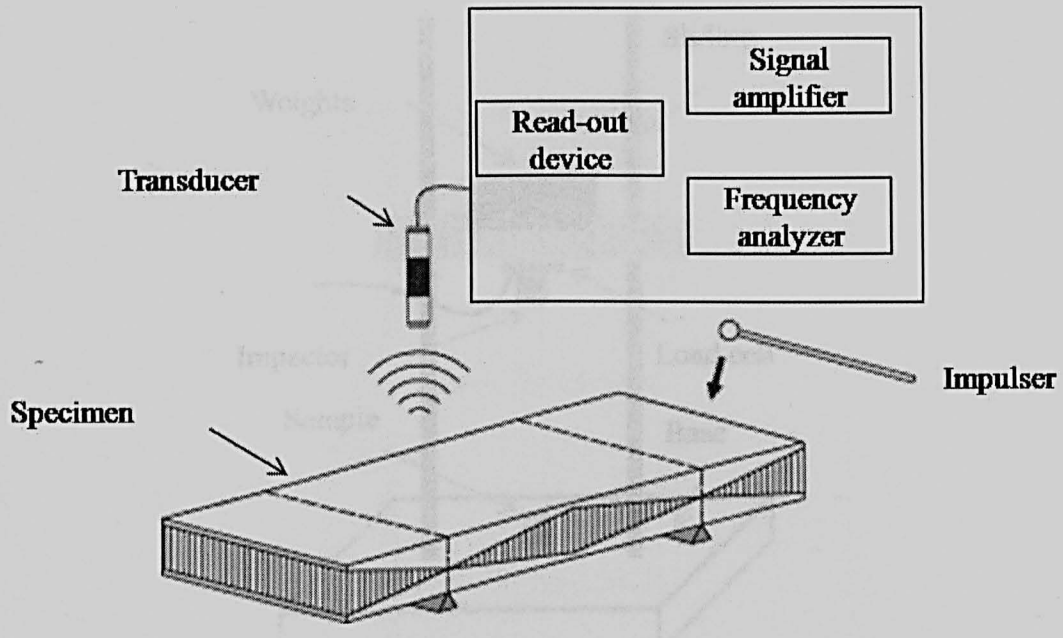

Figure 3.3 *Schematic diagram of a rectangular sample for the measurement of the flexural vibration frequency using the RFDA equipment*

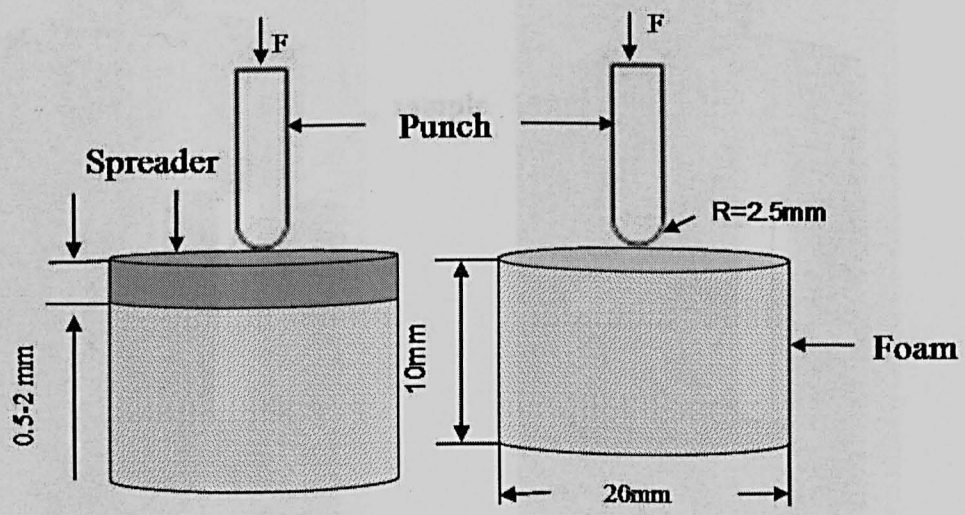

Figure 3.4 *Schematic of the indentation test arrangement*

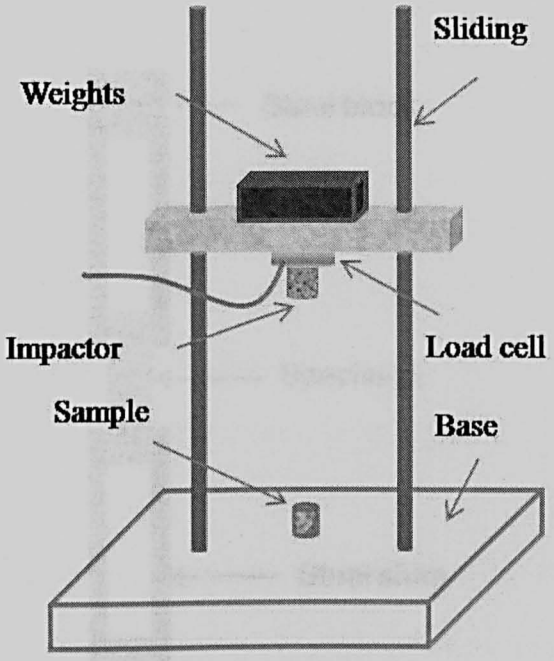

Figure 3.5 *Schematic diagram of impact test using falling weight impact tower*

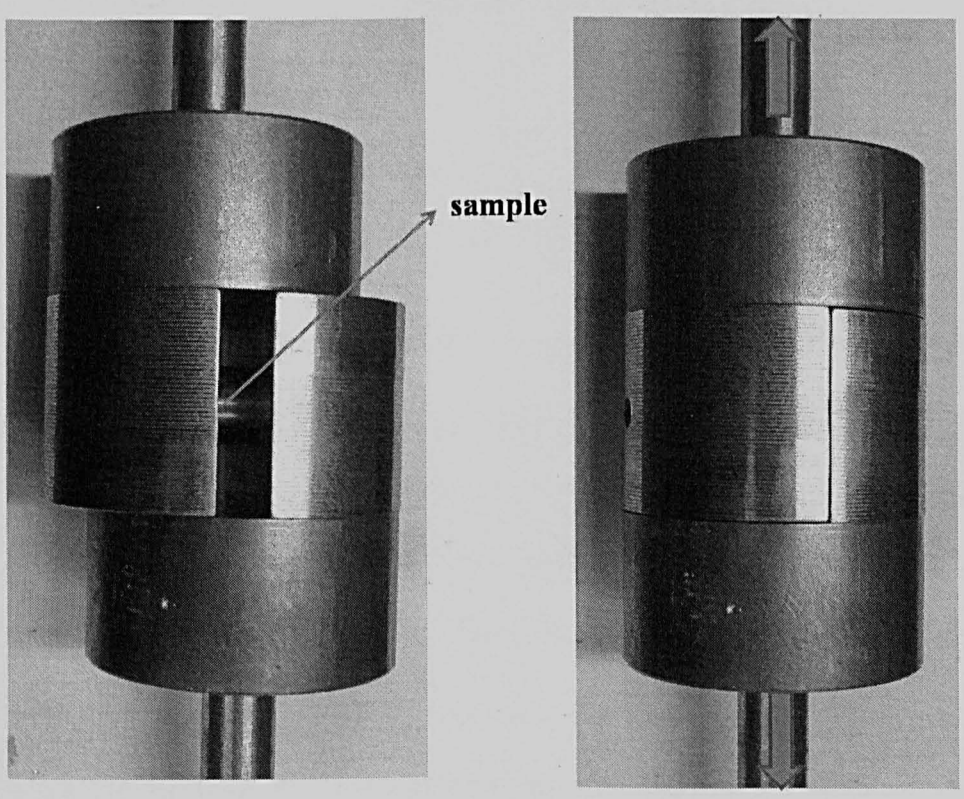

Figure 3.6 *Fixture for shear test*

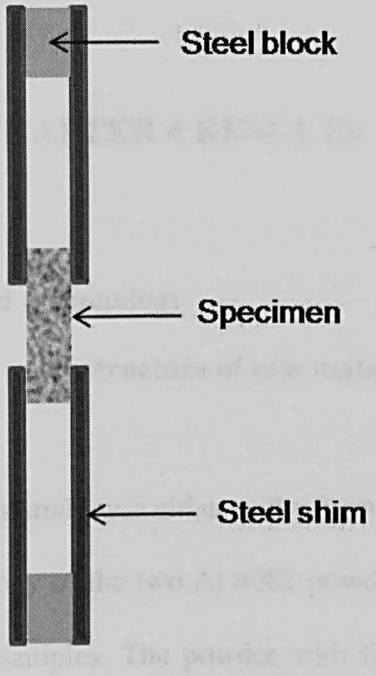

Figure 3.7 *Schematic of tensile test arrangement*

CHAPTER 4 RESULTS

4.1 Microstructure and morphology

4.1.1 Morphology and microstructure of raw materials

The Al alloy used in this study was either in the form of a lump or powder. Figure 4.1 shows the morphology of the two Al 6082 powders used in the fabrication of the Al syntactic foam samples. The powder with fine particles was used in the liquid sintering process and the powder with coarse particles was used in the melt infiltration method. Both powders have irregular shaped particles.

4.1.2 Microstructure of the CMs

The spheres of the CM powder have two different kinds of inner structure, either porous or hollow, as shown in Figure 4.2. The porous and hollow CMs have a similar effective density of $0.6g/cm^3$ and a similar porosity of about 80%. The appearances of the two kinds of CMs are slightly different. The porous CMs are roundish with a rough surface. They have a spongy like inner structure, normally containing a few big pores and numerous small pores. Most of these pores are spherical or quasi-spherical and the rest have irregular shapes. The

hollow CMs are nearly perfect spheres with a solid shell and a smooth surface and the average thickness-to-radius ratio is 0.1.

The EDS graphs showing the chemical compositions of these two types of CMs are presented in Figure 4.3. The weight percentages of the major constituent elements, O, Al and Si, at the indicated point were 42.61%, 31.39% and 24.82% in the hollow CM and 43.86%, 28.36% and 27.78% in the porous CM, which were close to each other. Considering the non-homogeneous chemical distribution of the CMs, it is confirmed that both types have a similar chemical composition.

Figure 4.4 shows the morphology of the four CM powders. The majority of the particles in CM Powder I and II have a regular spherical shape and a smooth shining surface, indicating that they are hollow CMs. The majority of the particles in CM Powder IV have a quasi-spherical shape and a coarse surface, indicating that they are porous CMs. CM Powder III contains both types of particles and is a mixture of hollow and porous CMs. The proportions of hollow and porous particles in Powders I, II, III and IV were determined quantitatively by examining 1000 CMs each in the optical micrographs of the polished cross-sections of Foam M1, M2, M3 and M4 samples. The four CM powders have very different proportions of hollow and porous particles. The percentages of hollow particles in Powders I, II, III and IV are 98.2%, 90.5%, 32.2% and 2.0%, respectively.

4.1.3 Microstructure of syntactic foams

4.1.3.1 Microstructure of monomodal syntactic foams

Figure 4.5 shows the microstructure of the four different types of syntactic foams, M1-M4. The CMs are distributed randomly in the Al 6082 matrix in all cases, resulting in a homogeneous macroscopic structure. While most CMs in the syntactic foam samples were intact during fabrication, a small number of CMs were infiltrated with molten Al, as indicated by arrows in a polished cross-section of foam M2, as shown in Figure 4.5 as examples. The percentage of the infiltrated CMs was determined quantitatively by examining 3000 CMs on the polished cross-sections for each type of syntactic foam samples. The infiltrated CMs account for 0.8%, 0.9%, 5.1% and 7.6% of the total embedded CMs for Foams M1, M2, M3 and M4, respectively. It seems porous CMs are more defective because of their thin surface membranes and therefore more apt to be invaded by molten Al under pressure during the melt infiltration process. As a consequence, Foams M3 and M4 have more infiltrated CMs than Foams M1 and M2.

4.1.3.2 Microstructure of syntactic foams fabricated with higher infiltration pressures

Figure 4.6 shows the microstructure of three foams M4-H1, M4-H2 and M4-H3, in which a large number of embedded CMs were infiltrated with Al under infiltration pressures of 4, 7 and 9 MPa respectively. It was found during the experiments that when the infiltration pressure was higher than 3 MPa, more CMs would be invaded by the molten Al during the infiltration process. When the samples were fabricated with a low infiltration pressure, only a small number of

CMs were broken and infiltrated with Al, as shown in Figure 4.5, and they did not have a significant effect on the density and porosity of the as-fabricated foams. However, when a high infiltration pressure was applied, more CMs were fractured and invaded by molten Al, which led to a higher density and lower porosity of the foam. Foam M4 is more sensitive to the high infiltration pressure due to the thin membrane of CM IV. In most invaded CMs in Foam M4, Al only filled part of a CM, as shown in Figure 4.6. In comparison, the invaded CMs in Foam M2 were fully filled by Al, as shown in Figure 4.5. The different filling effect is due to the different inner structures of the CMs embedded in Foams M2 and M4. The majority of the CMs in Foam M2 are hollow. When their walls are fractured, the CMs will be fully filled by the Al. Most CMs in Foam M4 are porous and contain numerous cells of different sizes separated by thin membranes. When the surface of a CM is broken, liquid Al may flow into some of the cells but not the whole CM. The Al inside the invaded CMs is not well connected with the Al matrix between the CM particles. They are separated by the walls or membranes of the CMs, as shown in Figures 4.5 and 4.6.

4.1.3.3 Microstructure of bimodal syntactic foams

Figures 4.7 and 4.8 show the microstructures of foams B1-B3 and B4-B6, which contain bimodal CMs of Powders II & IV and Powders I & IV, respectively. The CMs in all the samples are randomly distributed in the Al 6082 matrix. However, the microstructure is different from that of the syntactic foams containing monomodal CMs. The syntactic foams containing either fine or coarse CMs have

a similar microstructure except different scales, as shown in Figure 4.5. The former has small interparticle spaces and thus thin Al matrix network (M1 and M2); the latter has large interparticle spaces and thus thick Al matrix network (M3 and M4). The syntactic foams with bimodal CMs, however, can have different microstructures. In the syntactic foams containing relatively low fractions of fine CMs (B1 in Figure 4.7 and B4 in Figure 4.8), the coarse CMs are nearly close-packed and the fine CMs distribute in the area between the coarse CMs. The fine CMs replace the pure Al matrix, which would have existed as in Foam M4 (Figure 4.5), and have little effect on the distribution of the coarse CMs. When the volume percentage of the fine CMs increases to above 30% (B2, B3, B6), however, the fine CMs not only distribute in the gaps of the coarse CMs, but also disperse in large areas in their own, as shown in Figures 4.7 and 4.8.

Although the distributions of coarse CMs in Foams B1-B3 and Foams B4-B6, the distributions of the fine CMs in these two types of foams are somewhat different due to the different sizes of the fine CMs. In Foams B1, B2 and B3, even when the volume fraction of fine CMs increases to 70%, there are still some thick Al regions between the CM particles. In Foams of B4, B5 and B6, which have finer CMs, the fine CMs disperse more widely between the coarse CMs.

4.1.3.4 Microstructure of syntactic foams toughened with Al particles

Figure 4.9 shows the microstructure of the syntactic foams fabricated by the melt infiltration method with additional Al particles pre-mixed with the CMs. The Al particles are randomly distributed in a uniform Al/CM matrix from a macroscopic point of view. The random distribution indicates that the Al particles remained in their original locations without movement during the infiltration process. This may be because the Al particles were either in the solid or semi-solid state due to poor thermal conductivity of the surrounding CMs or, although in the liquid state, were contained within a solid oxide skin. A representative interface between the additional Al particles and the regions where the interstices of CMs were infiltrated with Al is shown in Figure 4.10. The additional Al particle is observed to be well connected with the infiltrating Al matrix.

4.1.4 Microstructure of syntactic foams fabricated by liquid sintering

Figure 4.11 shows the representative micrographs of the syntactic foams fabricated by the liquid sintering method. The microspheres show that the CMs are reasonably well distributed. In Foams S1 and S2, some Al particles have been partly melted and bonded with the adjacent Al particles to enclose the CMs particles. However, there are still a larger number of CMs without being surrounded by Al particles. In Foam S3, the majority of the Al particles have been melted and bonded well with the CM particles. Only a small number of CMs are agglomerated, without being surrounded by Al particles. In Foams S4 to S6,

nearly all the Al particles have been melted and very well bonded with each other; no clear boundaries of individual particle were observed. The embedded CMs are in close contact with the Al matrix, showing no discernible gaps. Some dark spots are observed in the Al matrix in syntactic foam S3 shown in Figure 4.11. They are proved to be voids as shown by the SEM micrograph in Figure 4.12.

4.2 Density and porosity

4.2.1 Density and porosity of CMs

Figure 4.13 shows the measured average effective densities of the four types of CMs. The effect density for each type of CMs is obtained by averaging the measured values of three samples. The variations among each set of three samples, due to slight variations in particle size distribution and compositional inhomogeneity, are less than 5%. Small errors may be caused by some voids trapped in the wax in the measurement process and are less than 6%. Although they have different particle size ranges, their effective densities are very similar and have an average value of approximately 0.6 g/cm^3, which will be used as the density of all types of CMs in the subsequent calculations throughout the thesis. The solid parts of all the four types of CMs have the same chemical composition and thus the same density, which is estimated to be 3.05 g/cm^3. Based on the above values of the effective and solid densities of the CMs, the porosity of all types of CMs is calculated to be approximately 80%.

4.2.2 Density and porosity of monomodal syntactic foams

Figure 4.14 shows the average densities of four types of syntactic foams (M1, M2, M3 and M4) fabricated by melt infiltration, containing monomodal CMs I, II, III and IV, respectively. The density for each type of foam is obtained by averaging the measured values of three 10 samples. The variations among each set of 10 samples, due to different number of CMs infiltrated with Al in different samples, are less than 6%. The syntactic foams containing CMs III and IV have slightly higher densities than those containing CMs I and II. This difference is due to the different numbers of infiltrated CMs in these foams. As discussed in Section 4.1.3.1, CMs III and IV have more porous particles, which have thin surface membranes and are therefore more apt to break during delivery, packing and melt infiltration. Therefore, the syntactic foams containing CMs III and IV have more infiltrated CMs and have higher densities than those containing CMs I and II.

The densities of these syntactic foam samples fall in a narrow range of 1.4—1.5 g/cm^3. Given a volume percentage of CMs in the foams being 63%, the theoretical density of the foams is 1.38 g/cm^3. The experimental density values are slightly higher than theoretical value, because of the small number of CMs infiltrated with Al matrix.

The porosity of the foams is provided by the embedded porous or hollow CMs. While the density of the solid shell of the CMs is 3.05 g/cm^3, an effective density of 0.6 g/cm^3 results in a porosity of 80% in the CMs. Given the densities of the Al

matrix and the foams, the porosities of Foams M1-M8 were calculated by Eq. (2.3). These foams contain monomodal CMs and have a narrow porosity range between 45% and 48%. The differences in the porosity between these foams are again due to the different numbers of infiltrated CMs.

4.2.3 Density and porosity of syntactic foams fabricated with higher infiltration pressures

The average densities of Foams M4-H1, M4-H2 and M4-H3 are shown in Figure 4.15. The density of for each type of foam is obtained by averaging the measured values of three samples. The variations among each set of three samples, due to different numbers of fractured CMs in the samples, are less than 7%. The density of the foams is found to increase with increasing infiltration pressure. At an infiltration pressure higher than 3 MPa, more CMs were infiltrated with Al, as shown in Figure 4.6. As a consequence, the foams will have a higher density. With the density values of Foams M4-H1, M4-H2 and M4-H3 being 1.62, 1.81 and 1.96 g/cm^3, the volume percentages of Al in them are calculated to be 48.6%, 57.0% and 63.8%, respectively. Given a theoretical volume percentage of Al in a syntactic foam with free packed monomodal CMs being 37% (Hartmann, 1999), the volume percentages of Al-infiltrated CMs in Foams M4-H1, M4-H2 and M4-H3 are 11.6%, 20% and 27.8%, respectively. When no molten Al is infiltrated into the CMs, as in the case of Foam M4, the porosity of the foam is 50%. The porosities of Foams M4-H1, M4-H2 and M4-H3 are therefore estimated to be 39.4%, 30% and 23.8%, respectively.

4.2.4 Density and porosity of bimodal syntactic foams

The average densities of the syntactic foams containing bimodal CMs of II & IV or I & IV are presented in Table 4.1. The density for each type of foam is obtained by averaging the measured values of three samples. The variations among each set of three samples, due to different numbers of CMs infiltrated with Al in different samples, are less than 8%. The porosities of these six foams are calculated from the measured densities using Eqn. (2.3) and are also presented in Table 4.1. While syntactic foams with monomodal CMs have a similar density and porosity due to a similar volume percentage of CMs in the foams, the syntactic foams with bimodal CMs have lower densities and higher porosities due to increased volume percentage of CMs in the foams. The key parameter affecting the density and porosity is the volume ratio of the fine and coarse CMs. When the volume percentage of CM II is increased from 30% (B1) to 50% (B2) and then to 70% (B3) the density of the foam increases and the porosity decreases. Similarly, when the volume percentage of CM I is increased from 20% (B4) to 40% (B5), the density and porosity have a similar variation trend as that in Foams B1, B2 and B3. However, when the volume percentage of CM I is increased further from 40% (B5) to 60% (B6) the density of the foam increases and the porosity decreases instead. The results indicate that there is an optimum volume ratio of fine and coarse CMs in bimodal syntactic foams which gives the lowest density and highest porosity.

Table 4.1 Density and Porosity of Foams B1-B6

Foam ID	B1	B2	B3	B4	B5	B6
Density (g/cm^3)	1.29±0.05	1.31±0.05	1.36±0.05	1.30±0.05	1.23±0.05	1.28±0.05
Porosity (%)	53.7±2.1	52.8±2.1	51.4±2.1	53.3±2.1	55.5±2.2	54.1±2.2

4.2.5 Density and porosity of syntactic foams toughened with Al particles

Figure 4.16 shows the theoretical and measured densities of the syntactic foams embedded with Al particles, T1, T2, T3 and T4. The density of each type of foam is obtained by averaging the measured values of three samples. The variation, the variations among each set of three samples are less than 8%. The experiment values are slightly lower than the theoretical values, but they are very close to each other in all the foams. The largest difference between the theoretical and experimental values is in foam B3, which has 60% Al in volume in the foam. Even in this case, Its mean measured density (1.81 g/cm^3) is only 3% less than the theoretical value.

4.2.6 Density and porosity of syntactic foams fabricated by liquid sintering

Figure 4.17 and 4.18 compares the theoretical and the measured densities of the syntactic foams fabricated by the liquid sintering method. The density for each type of foam is obtained by averaging the measured values of three samples. The variations are within 9%. The theoretical values were estimated according to the

volume percentages of Al and CMs in the foams when the mixture was prepared, assuming no damages of CMs and no voids between Al and CMs. The measured densities of the syntactic foams containing 40% Al and different sized CMs was found to be higher than the theoretical values, as shown in Figure 4.17. It was also found that the experimental value increased with increasing CM size.

When the syntactic foams were fabricated with the same CMs, foam density increased with the increase of Al volume fraction in the foam. For the foam with 40% Al, the theoretical value is lower than the measured value. For other foams, the theoretical values are greater than the measured ones.

4.3 Young's modulus of monomodal syntactic foams

The values of Young's modulus for Foams M1-M4 are shown in Figure 4.19. The Young's modulus for each type of foam is obtained by averaging measured values of three samples. The variations are less than 7%. The errors may result from the different densities of the samples. The Young's modulus value is found to be sensitive to foam density but not to the foam type. With an increase in the density of 11%, the Young's modulus of the syntactic foam is increased by 17%. However, the values are within a relatively narrow range of 23-28 GPa.

4.4 Indentation response

4.4.1 Indentation response without a spreader

Figure 4.20 shows the vertical cross-section of a Foam M4 sample after the indentation test. It illustrates the different deformation zones, which are present in all the samples tested. A hole was created in the top part of the sample where the indenter penetrated through. Directly below the hole, a crush zone was formed due to compaction. Inside the indentation hole, traces of tearing were observed at the perimeter.

Figure 4.21 shows the typical indentation load-displacement curves of the three types of syntactic foams, Foams M2, M3 and M4. For each curve, the load initially increases nearly linearly with displacement. At a certain displacement, the load starts either to drop abruptly or to increase with a lower gradient. With increasing displacement further, the load increases steadily as the foam directly under the indenter densifies. For Foam M4, the curve is nearly linear up to a displacement of roughly 2 mm but has small oscillations. The load increases steadily with displacement up to a displacement of about 8 mm, at which a drop in load appears. For Foams M3 and M2, the load increases nearly linearly with displacement until a sudden drop at a displacement of about 2.5 and 3.5 mm, respectively. The load then increases again with displacement. The curves of Foams M3 and M2 are much smoother than that of Foam M4 with no discernible oscillations. The load at which the curve deviates from linearity corresponds to the start of a significant collapse of the foam and is designated as indentation collapse load, which is equivalent to the indentation yield load in some cases. The average

indentation collapse loads of Foams M4, M3 and M2 are 2.2, 3.2 and 4.9 kN, respectively, obtained by averaging the values from three samples for each type of foam. The values varied less than 8%.

Figure 4.22 shows the macro- and micrographs of the three types of syntactic foams after indentation tests. In foam M4, no macroscopic damage is visible except within the indentation area, and the damage at the perimeter of the indentation hole is not significant. This explains the steady load-displacement curve of Foam M4 in Figure. 21. The small oscillations in the curve are a result of the repeating cycles of yield, collapse and densification of the ceramic microspheres (Olurin *et al.* 2000). In Foams M2 and M3, cracks spanning from the indentation hole to the outer edge of the samples are observed. Considerable deformation is also observed in the region at the perimeter of the indentation hole, indicating significant tearing damage. The initiation of the cracks is believed to result in the abrupt drop in the load-displacement curves for Foams M2 and M3 in Figure 4.21.

4.4.2 Indentation response with a spreader

Figure 4.23 shows the load-displacement curves of Foams M2, M3 and M4 under indentation with a mild steel disc of 0.5, 1, 1.5 or 2 mm thick. The load-displacement curves obtained without a spreader is also included for comparison purposes. For Foam M4, the load-displacement curve is very sensitive to the

thickness of the disc. For Foams M2 and M3, however, increasing disc thickness from 0.5 mm to 1 mm or from 1.5 mm to 2 mm has no significant effect on the load-displacement curve. The sharp drops in the indentation load-displacement curves are associated with the perforation of the discs, whereas the small drops are associated with cracking of the samples.

Figure 4.24 shows the top surfaces of the samples of Foam M4 after indentation with discs of different thicknesses, before the discs were penetrated. In the indentation test with a disc on the top of the syntactic foam sample, the disc acts as a load spreader. The indentation load is distributed to a larger area than the cross section of the punch before the disc is perforated. When the thickness of the disc increases, as shown in Figure 4.23, the disc transfers the indentation load to a larger area on the foam. At any fixed displacement, the indentation load increases with increasing disc thickness, as shown in Figure 4.23(a). Due to the good ductility of Foam M4, no shear cracks are observed in the samples for the four test conditions.

Figure 4.25 shows the top surfaces of the samples of Foams M2 and M3 after indentation with discs of different thicknesses, before the discs were penetrated. The effect of load spreading of a 0.5 mm disc is similar to that of a 1 mm disc, and the effect of a 1.5 mm disc is similar to that of a 2 mm disc. This phenomenon is also evidenced in the load-displacement curves in Figure 4.23 (b) and (c). This is likely to be due to the higher compressive strengths of Foams M2 and M3 than

that of Foam M4, which makes the load spreading less sensitive to disc thickness. When the disc thickness is increased from 0.5-1 mm to 1.5-2 mm, however, there is a significant difference in the response of the foam to indentation. With a thick disc, the indentation load is spread to a greater area, resulting in fewer and shorter cracks in the region outside the indentation hole, as shown in Figure 4.25. The indentation load at any fixed displacement is also increased as shown in Figures 4.23 (b) and (c).

4.4.3 Indentation facture

Figure 4.26 shows the SEM micrographs of the fracture surfaces of Foams M2 and M3 after the indentation tests. All fractures took place either in the Al matrix or across the CMs and no fractures were observed to occur at the interface between the Al and the CMs. This fracture mode indicates that the bonding between the Al matrix and the CMs is very good.

4.5 Compressive response

4.5.1 Compressive response of Al matrix alloy

Figure 4.27 shows the quasi-static compressive stress-strain curves of the Al 6082 alloy, both in standard heat treated and cast conditions. The two curves start with a linear elastic region and followed by a strain hardening region where the stress is gradually increasing with the increase of the strain. Some characteristic compressive properties of the Al alloy are displayed in Table 4.2. The

compressive yield strength is determined by the offset method and the apparent modulus is calculated from the slope of the elastic region, as described in ASTM E9-89 (Lima & Otterman 1989). The heat treated Al alloy has a much higher strength and elastic modulus than the cast alloys.

***Table 4.2** Characteristic compressive properties of the Al 6082 alloy*

Condition	Compressive strength (MPa)	Apparent modulus (GPa)
6082 casting	106±3.7	7.1±0.3
6082 T6	316±11	14.4±0.5

Figure 4.28 shows the deformation of the two Al samples at a large strain of 0.5. The two samples were barreled, as shown in Figure 4.28. However, the heat treated sample was observed to have a smooth surface, whereas the cast sample was showed orange peel wrinkles and shear cracks with an orientation of approximately ±45° on the surface.

4.5.2 Compressive response of CMs

Figure 4.29 shows the compressive load-displacement curves of the four CM powders. All curves have three characteristic regions, namely, packing, crushing and densification. In the low compressive load region (packing), the particles undergo reordering and elastic deformation without significant damage and

collapse. The load-displacement curve in this region has a relatively steep slope. In the medium load region (crushing), the particles are gradually crushed and the displacement increases more rapidly with increasing load. At the end of this region, the majority of the particles will have been crushed. In the high load region (densification), the broken pieces of particles undergo densification. The load-displacement curve becomes steep again.

The transition from the packing region to the crushing region can be defined as the point at which the load-displacement curve deviates from the linear relation. The average crushing loads of Powders I, II, III and IV are thus determined to be 0.85, 0.58, 0.65 and 0.61 kN, respectively, based on the values of three tests. The variations are less than 7%. The transition from the crushing region to the densification region, however, is not clearly defined. The two regions can be regarded as being separated by the intersection of the tangents of the curves in the crushing and densification regions, as illustrated on the load-displacement curve in Figure 4.29. The average densification loads of Powders I, II, III and IV are thus determined to be 5.2, 4.36, 5.0 and 4.5 kN, based on the values of three tests. The variations are less than 7%. The corresponding displacements are 24.1, 23.8, 23.6 and 25.5 mm, respectively. It is worth noting that for all powders the densification region starts at a similar displacement, largely because they have a similar porosity.

4.5.3 Compressive response of non-heat treated syntactic foams

Figure 4.30 shows representative quasi-static compressive stress-strain curves of non-heat treated foams, M1-M4. The three typical regions found in the compression of cellular solids, namely linear elastic, plateau and densification, are observed in all the stress-strain curves. All the curves start with a linear elastic region, followed by plastic deformation. The maximum stress of the linear region, i.e. the compressive strength of the foam, appears at a strain in the range of 0.03-0.07. The stress-strain curve then enters the plateau region after a small stress drop. The plateau region is either flat (e.g., M4), or with small fluctuations (e.g., M1), or with strain hardening (e.g., M2). All curves enter the densification region at a strain in the range of 0.48-0.55, where the stress increases to high values with a small increase of strain.

The average characteristic compressive properties of the four foams are presented in Table 4.3. The average values of the properties for each type of foam are based on measurements of three samples. The variations are less than 9%. The compressive strength is defined as the maximum stress at fracture or collapse of the foam according to ASTM standard E 9-89 (Lima and Otterman 1989). The four foams have different compressive strengths. The compressive strength of foams M1-M4 is gradually decreasing with the embedded CMs varying from I to II, III and IV. The values of apparent modulus of the syntactic foams (Table 4.3) are lower than the value of the cast Al 6082 alloy (Table 4.2).

Table 4.3 Characteristic compressive properties of non-heat treated foams

Foam ID No	Compressive strength (MPa)	Apparent modulus (GPa)	Plateau strength (MPa)	Onset strain of densification	Specific energy absorption (J/g)
M1	115.4±5.2	3.3±0.14	106.9±4.8	0.41±0.02	26.5±1.2
M2	96.6±4.3	3.9±0.18	111.9±5.1	0.42±0.02	26.6±1.2
M3	49.5±2.2	2.2±0.10	82.1±3.7	0.43±0.02	20.4±0.9
M4	31.6±1.4	1.9±0.08	43.9±2.0	0.43±0.02	9.7±0.4

The specific energy absorption values of the four foams are also shown in Table 4.3. The specific energy absorption is defined as the energy absorbed by a unit mass of the syntactic foam from the start of the compression up to the onset of the densification. It is mainly determined by three factors: density, plateau strength and onset strain of densification. The onset strain of densification is in turn mainly determined by the porosity of the syntactic foam. As Foams M1-M4 have similar values of porosity and density, their energy absorption values are mainly determined by their plateau strength values. The higher plateau strength the foam has, the larger energy the foam can absorb.

4.5.4 Compressive response of monomodal syntactic foams

Figure 4.31 shows representative quasi-static compressive stress-strain curves for heat treated Foams M1, M2, M3 and M4. All four curves have an initial elastic region with a linear stress-strain relationship, followed by plastic deformation. These four foams show different characteristics in the subsequent deformation. Foams M1 and M2 have several large and sharp stress drops. The first drop appears immediately after the stress reaches compressive yield strength and another large drop appears at the strain of about 0.15 for Foam M1 and 0.25 for Foam M2. Foams M3 and M4 show a near-plateau region of deformation where the strain increases extensively under a relatively narrow range of stresses. Foam M3 has a few small stress drops in the early stage of plastic deformation. In contrast, Foam M4 has only a very small stress drop after the elastic region.

Table 4.4 shows the characteristic compressive properties of these four foams. The average values of the properties for each type of foam are based on the measurements of three samples. The variations are less than 8%. The average values of compressive yield strength for Foams M1, M2, M3 and M4 are 128.8, 123.7, 73 and 54 MPa, respectively. Foams M1 and M2 also have higher apparent modulus than Foams M3 and M4. These four foams have much higher apparent modulus and energy absorption values than the non-heat treated foams displayed in Table 4.3. The higher capability of energy absorption of Foams M1and M2 is believed mainly due to their higher plateau strength, as shown in Table 4.4. The

onset strain of densification for Foams M1 and M2 seems higher than M3 and M4. This difference can be explained by the brittle failure of Foams M1 and M2.

Table 4.4 *Characteristic compressive properties of heat treated Foams, M1-M4*

Foam ID No	Compressive strength (MPa)	Apparent modulus (GPa)	Plateau strength (MPa)	Onset strain of densification	Specific energy absorption (J/g)
M1	128.8±5.2	4.8±0.2	110.2±4.4	0.42±0.02	33.5±1.3
M2	123.7±5.0	5.3±0.2	86.4±3.5	0.42±0.02	25.0±1.0
M3	73.0±2.9	3.5±0.1	70.0±2.8	0.40±0.024	20.6±0.8
M4	54.0±2.2	2.7±0.1	71.2±2.9	0.43±0.02	18.6±0.7

Figure 4.32 shows the macrographs of the exterior of the four foams compressed to a strain of 0.2. Foams M1 and M2 have single or X-shaped cracks with angles of 32±2.5° to the loading direction. Many small cracks emerged in Foam M3, accompanied by radial expansion, in the top 2/3 of the sample. No visible shear crevasses or cracks are displayed on Foam M4, but barreling is observed with radial expansion in the middle part of the specimen.

Fig. 4.33 shows the macrographs of the longitudinal cross sections of the above samples. The failure modes can be seen more clearly from these photographs. In syntactic foams M1 and M2, there are two pairs of major cracks. One pair develops from the top corners and another pair develops from near the bottom corners. They are inclined at an angle of about 30° to the loading direction and meet at a distance about one third from the top of the sample. A narrow, horizontal layer of crushed CMs can be observed at the meeting location. The deformation in syntactic foams M3 and M4 is dominantly plastic with a broader crushed region, although small cracks are also present in syntactic foam M3.

Fig. 4.34 shows the macrographs of the four foams compressed to a strain of 0.6. Foams M1 and M2 were completely shattered into small pieces; Foam M3 was barely holding together and many cracks appeared; Foam M4 was still in one piece and no visible shear crevasses or cracks appeared.

Figure 4.32-34 show that in the static compression, Foams M1 and M2 were brittle, Foam M4 was ductile and Foam M3 showed medium ductility. The sudden stress drops of brittle foams in the stress-strain curves were caused by the formation of cracks. The deformation behaviour of the foams was similar to that found in the indentation tests of these foams.

The fracture surfaces of Foams M1, M2 and M3 were shown in Figure 4.35. Cleavage fracture stripes were found in the matrix as indicated by the arrows in the enlarged micrographs in the right-hand side. The cleavage fracture stripes found in Foam M3 are much deeper than that of Foams M1 and M2. The fracture surface found in Foam M3 is less flat than that in Foams M1 and M2, indicating that fracture of Al matrix in Foam M3 is less brittle than that in Foams M1 and M2.

4.5.5 Compressive response of syntactic foams fabricated with higher infiltration pressures

Figure 4.36 shows the compressive response of Foams M4-H1, M4-H2 and M4-H3. The stress-strain curves of these three syntactic foams have different plateau and densification behaviours from those of M4 in Figure 4.31. In comparison with the compressive response of Foam M4, the stress-strain curves of H1-H3 have a similar linear elastic region but a much shorter plateau region followed by brittle fracture, i.e., no densification region.

The characteristic compressive properties of the three foams are displayed in Table 4.5. The average values of the properties for each of foam are based on the measurements of three samples. The variations are less than 10%. The higher the infiltration pressure, the more CMs were infiltrated by molten Al during fabrication, and the higher compressive strength and apparent modulus the as-fabricated foam has, due to more Al in the foam. The apparent modulus increases

gradually with increasing foam density, with its values being 3.9, 4.5 and 4.8 GPa corresponding to the densities of 1.55, 1.8 and 1.96 g/cm^3. The compressive strength increases more rapidly with increasing foam density. Foam M4-H2 is 15% heavier than M4-H1 but has a compressive strength 30% higher. Similarly, Foam M4-H3 is 8% heavier than M4-H2 but has a compressive strength 80% higher. No densification regime appeared in the stress-strain curves. Instead, a sudden drop in stress happened at a strain of about 0.2-0.35. The values of specific energy absorption for these three foams are based on the accumulation of energy absorbed up to the strain of sudden stress drops.

Table 4.5 *Characteristic compressive properties of M4-H1, M4- H2 and M4-H3.*

Foam ID No	Compressive strength (MPa)	Apparent modulus (GPa)	Strain at sudden drop	Specific energy absorption (J/g)
M4-H1	72.7±36	3.9±0.2	0.35±0.02	13.5±0.7
M4-H2	95.9±4.8	4.5±0.2	0.21±0.01	11.8±0.6
M4-H3	173.2±8.7	4.8±0.2	0.17±0.01	12.5±0.6

Figure 4.37 shows the macrographs of the three foams after complete compression failure. These foams failed in a brittle mode, showing large cracks or broken into pieces. The behaviour of these foams is very different from that of Foam M4 produced with a low infiltration pressure, as displayed in Figures 4.33 and 4.34, where the failure was plastic deformation by layered crush. It seems that increased

Al in these three foams does not increase the ductility of the foams but make them more brittle. The strains at which Foams M4-H1, M4- H2 and M4-H3 completely fractured, corresponding to the final stress drops in Figure 4.36, are 0.35, 0.21 and 0.17, respectively.

The capability of energy absorption of these three foams, as shown in Table 4.5, is much lower than that of the Foam M4 produced with a low infiltration pressure, as displayed in Table 4.4. Due to the lack of a densification region, the specific energy absorption values of these three foams are calculated from the start of compression up to complete fracture. Although these three foams have very high compressive yield strengths, the specific energy absorption is low due to the low plateau strength and short plateau region.

4.5.6 Compressive response of bimodal syntactic foams

The representative compressive stress-strain curves of Foams B1-B3 and B4-B6 are displayed in Figures 4.38 and 4.39, respectively. The compressive stress-strain curves of all samples exhibit the classic regimes for cellular solids, namely the linear, plateau, and densification regimes. Foams B1and B4, which are embedded with low volume percentages of fine CMs, show no stress drops following the elastic region. Foams B2, B3, B5 and B6, which are embedded with large volume percentages of either CM I or II, have different degrees of stress drops after the elastic region. By combining fine CM II and coarse CM IV, Foams B1-B3 show a

nearly perfect plastic plateau regime, where a flat plateau stress is observed before entering the densification regime. Foams B4 and B5 show a similar flat, stable plateau region to that of Foams B1-B3. Foam B6 shows stress drops in the plateau region.

The macrographs of Foams B1-B3 and B4-B6 compressed to a strain of 0.2 are shown in Figure 4.40 and 4.41, respectively. When compressed to the strain of 0.2, the deformation of Foams B1 and B4 is dominated by collapse of CMs and layered crush of the foam. Orange peel or barrel effect is observed in the middle area of the foams. Cracks together with layered crush are observed in Foams B2, B3, B5 and B6.

The characteristic compressive properties of the two types of bimodal syntactic foams B1-B3 and B4-B6 of bimodal foams are listed in Table 4.6. The average values of the properties for each type of foam are based on measurement of three samples. The variations are less than 9%. In both types, the compressive strength increases with increasing the volume percentage of fine CMs. Foams B3 and B6, with 70% CM II and 60% CM I, have the highest compressive strength in their own types of bimodal foams.

The bimodal foams exhibit different capabilities of energy absorption due to different onset strains of densification and plateau strengths. Among the syntactic

foams containing CMs II and IV, B1 has a lower density and longer plateau region as the densification starts at a higher strain. However, B2 and B3 have much higher plateau strengths than B1, due to higher volume percentages of CM II, and therefore higher specific energy absorptions.

Table 4.6 *Characteristic compressive properties of syntactic foams containing bimodal CMs.*

Foam ID No	Compressive strength (MPa)	Apparent modulus (GPa)	Plateau strength (MPa)	Onset strain of densification	Specific energy absorption (J/g)
B1	57.3±2.6	3.8±0.2	44.4±2.0	0.50±0.02	20.0±0.9
B2	67.5±3	2.9±0.1	60.6±2.7	0.47±0.02	22.7±1.0
B3	78.5±3.5	3.1±0.1	62.9±2.8	0.46±0.02	23.8±1.1
B4	71.1±3.2	3.8±0.2	87.5±3.9	0.48±0.02	32.3±1.5
B5	91.3±4.1	4.3±0.2	81.7±3.7	0.52±0.02	35.9±1.6
B6	82.0±3.7	3.4±0.2	87.0±3.9	0.47±0.02	30.9±1.4

The syntactic foams containing CMs I and IV, Foams B4-B6, have energy absorptions about 50% higher than those of Foams B1-B3. Among B4-B6, B5 has the highest specific energy absorption. This is because B5 has a higher onset strain

of densification and a lower density than B4 and B6, although it has a lower plateau strength than both B4 and B6.

4.5.7 Compressive response of syntactic foams toughened with Al particles

Figure 4.42 shows the representative quasi-static compressive stress-strain curves for the syntactic foams T1, T2, T3 and T4, which are embedded with Al particles with total volume percentages of Al of 43%, 50%, 60% and 70%. The deformation of the foams is also divided into linear region, plateau region and densification region. In the first region up to the maximum stress, i.e. the compressive strength, the syntactic foam deformed first linearly (largely elastically) and then plastically. The compressive strengths of the syntactic foams T1, T2, T3 and T4 are 135.7, 162.2, 154.2 and 153.3 MPa, respectively. The strains corresponding to the compressive strengths are low (0.05 - 0.09) for all four syntactic foams. The plastic deformation of all foams was then followed by a stress drop, as shown in Figure 4.42. The magnitudes of the stress drop for the syntactic foams T1, T2, T3 and T4 are about 23, 21, 17 and 7 MPa, respectively. Following the stress drop, the deformation entered into the plateau region. In the plateau region, the stress of Foam T1 fluctuates and falls whereas the stress of syntactic foams T2, T3 and T4 is quite flat and stable. The densification of the syntactic foams starts at the strain of about 0.5, except for Foam B4, which starts at a lower strain of about 0.35, due to the lower overall porosity in the foam.

The strength of the syntactic foam is clearly affected by the volume percentage of the Al matrix. When the volume percentage of the matrix increases from 43% to 50%, the compressive strength increases markedly. When this value continues to increase from 50% to 70%, however, the compressive strength remains at a similar value.

The volume percentage of the Al matrix has a marked effect on the failure mode of the syntactic foams. The stress-strain curves of the four foams show that the foam becomes more ductile with increasing Al matrix in the foam. Figure 4.43 shows the macrographs of the four foams at the compressive strain of 0.2. In Foams T1 and T2, with 43% and 50% Al, X-shaped cracks were present in the centre part of the sample. In Foams T3, with 60% Al, barreling plastic deformation dominated, although cracks can still be observed. Although the syntactic foams have slightly different porosity values, they seem to start densification at a similar strain. This phenomenon is believed to be a result of the barreling effect of Foams T2 and T3 under high strains of compression. In Foam T4, with 70% Al, only very small cracks were observed and the densification starts at a lower strain due to the low level of porosity.

Figure 4.44 shows the vertical cross-section of syntactic foam T2, with 50% Al, compressed to a high strain of 0.35. Cracks are observed near the surface in the middle of the sample. These cracks are formed after barrelling plastic deformation, other than outright shear fractures described by Kiser *et al.* (1999) and Balch *et al.*

(2005), in which the cracks propagated throughout the whole sample. However, the plastic deformation does not take place uniformly throughout the sample; instead, it largely takes place in the middle regions. In the non-deformed regions, the Al particles remain in the original shapes. In the deformed region, the Al particles are compressed into prolonged shapes without any crack passing through, as indicated by arrows in Figure 4.44.

Table 4.7 *Characteristic compressive properties of the syntactic foams embedded with Al particles*

Foam ID No	Compressive strength (MPa)	Apparent modulus (GPa)	Plateau strength (MPa)	Onset strain of densification	Specific energy absorption (J/g)
T1	135.7±6.8	3.1±0.2	127.4±6.4	0.52±0.03	43.4±2.2
T2	162.2±8.1	6.2±0.3	149.1±7.5	0.55±0.03	50.6±2.5
T3	154.2±7.7	4.4±0.2	156.7±7.8	0.54±0.03	47.1±2.4
T4	153.3±7.7	4.3±0.2	207.7±10.4	0.37±±0.02	41.7±2.1

Table 4.7 lists the characteristic compressive properties of the four syntactic foams. The average values of properties for each type of foam are based on the measurements of three samples. The variations are less than 10%. It shows that the specific energy absorption capability of syntactic foam T1 is lower than that of

T2. This is because the former has a lower compressive strength and even lower plateau strength due to a large stress drop. The specific energy absorption capability of Foam T3 is also lower than that of Foam T2. This is because the former has only a plateau strength 5% higher but a density 10% higher than the latter. The specific energy absorption capability of Foam T4 is lower than Foam T2. This is because the former has a much higher density and shorter plateau region, although a much higher plateau strength.

4.5.8 Compressive response of syntactic foams fabricated by liquid sintering

Figure 4.45 shows the representative quasi-static compressive stress-strain curves for Foams S1-S6. In Figure 4.45(a), Foams S1, S2 and S3 contain the same 40% of Al but different CM powders, II, III and IV respectively. In Figure 4.47(b), Foams S3, S4, S5 and S6 contain the same CM powder, IV, but with different Al volume percentages of 40%, 50%, 60% and 70%, respectively. All stress-strain curves in both graphs have an initial elastic region with a linear stress-strain relationship, followed by plastic deformation where the stress reaches the plastic-collapse strength at a similar strain around 0.3. A large stress drop was then observed in the stress-strain curves for all six foams. This stress loss was caused by the appearance of cracks during the compression as displayed in Figure 4.46. After the stress drop, the stress-strain curves of Foams S5 and S6 show a near-plateau region where stress varies in a small range and densification of the foam starts at a strain of about 0.5. The deformation of Foams S1-S4 is much more unstable and the stress decreases to a small value at a strain of about 0.5.

Figure 4.47 shows the relationship between the compressive collapse strength and density of Foams S1-S6. The collapse-strength and density values were obtained by averaging six samples for each type of foam, with the results varying no more than 8%. Foams S1 and S3 have a similar density, but quite different compressive strengths. Foams S2 and S3 have a similar compressive strength but different densities. However, the compressive strength of the foams S1-S6 as a whole is found to increase linearly with foam density. In comparison with Foam S3, the collapse strength of Foam S6 is increased by 50% with its density only increased by 30%.

4.5.9 Confined compressive response of syntactic foams

The confined compressive stress-strain curves of Foams M1, M2, M3 and M4 are shown in Figure 4.48. The confined compressive strengths of Foams M1, M2, M3 and M4 are 146, 98, 46 and 42 MPa, respectively, which were obtained by averaging three samples for each type of foam. The variations are less than 9%. With the confinement of the tube, the strain in the transverse direction is very small. Deformation of the sample can only proceed in the vertical direction. Therefore, the plastic deformation is dominated by the crushing of the CMs and subsequent deformation of the Al matrix. Similar to the three distinctive regions observed in unconfined compression in Figure 4.31, the stress-strain curves of Foams M3 and M4 consist of linear region, near-plateau region and densification region. However, the confined compression response of Foams M1 and M2

differed from that under the unconfined compression condition. Foams M1 and M2 do not show the three distinctive regions. Instead, the stress increased monotonically with increasing stain. Small stress drops, which are caused by the occurrences of cracking, are observed in the low strain stage. These stress drops are impeded when the propagation of cracks is prevented by the confining tube. The samples were then forced to deform in a progressive manner, where the CMs collapse and Al matrix deforms.

Figure 4.49 displays the polised longitudinal cross-sections of Foams M1, M2, M3 and M4 after confined compression to a strain of 0.35. Under the constraint of the tube, the deformation of all foams is in the form of progressive crushing of the CMs and accompanied by the plastic defromation of the Al network

4.6 Impact response

Figure 4.50 shows the typical impact stress-time traces of Foams M1, M2, M3 and M4 at three different impact speeds. The impact stress represents the stress pulse produced by the impact of the drop-weight on the cylindrical specimen. It is calculated by dividing the real time impact load by the cross-sectional area of the specimen. In general, the stress response has a sharp peak followed by some oscillations, which is similar to the existing impact research on aluminium honeycomb or foams (Goldsmith & Sackman, 1992, Lopatnikov *et al.* 2002,

Radford *et al.* 2005, Tan *et al.* 2005). The stress-time curves can be divided into two regions, a linear elastic region and an oscillating plateau region.

Figure 4.51 shows the macrographs of the four foams after the impact tests under different speeds. The pattern of the impact deformation is similar to that observed in quasi-static compression. The deformation of M1 and M2 is still dominated by brittle fracture. M4 is ductile. M3 has both ductile and brittle deformation. However, Foams M1 and M2 did not break into pieces with large deformation at the impact speed of 4.6 m/s.

The impact peak stress, which is the maximum stress before plastic deformation, is found to increase with increasing strain rate, as shown in Figure 4.52. The strain is computed by dividing the shortened length by the original length of the test specimen and the strain rate is calculated by dividing the strain by the impact time. The average peak stress for each type of foam is obtained by averaging measurements of four samples. The results varied less than 7%. The peak stress is particularly sensitive to impact speed at a higher speed. When the impact speed is increased from $120s^{-1}$ to 145 s^{-1}, the average peak stress of the four foams is increased by 40 MPa. When the impact speed is increased from 145 s^{-1} to 200 s^{-1}, the average peak stress is increased by 80 MPa. The impact peak stress is also related to the yield strength of the foam in the static compression. Foams M1 and M2 have a higher static compressive yield strength than Foams M3 and M4. They also have a higher impact peak stress at all three impact speeds.

The impact specific energy absorption is found to increase with increasing strain rate, as shown in Figure 4.53. The specific energy absorption of each sample was calculated by dividing the impact energy by the mass of the deformed part of the syntactic foam sample. The average specific energy absorption is obtained by averaging the values of four samples, which varied less than 7%. The specific energy absorption of Foams M1 and M2 is more sensitive to strain rate at higher impact speeds than Foams M3 and M4. When the strain rate is increased from 145 to 200s^{-1}, the specific energy absorption of Foams M1 and M2 is increased by more than 30%, while that of Foams M3 and M4 is increased by less than 20%.

4.7 Tensile response

Figure 4.54 shows the typical tensile stress-strain curves of Foams M1, M2, M3 and M4. All the samples fractured perpendicular to the loading direction with a small elongation, about 1% for Foams M1 and M2 and 2% for Foams M3 and M4. Foams M1 and M2 have similar tensile strengths, with the average value of 15.2 and 15.8 MPa. Foams M3 and M4 have similar tensile strengths which are higher than those of Foams M1 and M2, with the average values of 19.0 and 18.2 MPa. The average tensile strength of each type of foam is obtained by averaging the values of three samples, which varied less than 6%. All the specimens fractured in a brittle manner at 90°C to the loading direction during the tensile test. The micrographs of the tensile fracture surfaces of Foams M1, M2, M3 and M4 are displayed in Figure 4.55. In all four syntactic foams, the fracture was found

occurring across the CMs and Al network and no fracture occurred at the interface between the Al network and the CMs.

4.8 Shear response

Figure 4.56 shows typical shear stress-strain curves of Foams M1, M2, M3 and M4. The foams had similar shear strengths and shear fracture strains. The average shear strengths of Foams M1, M2, M3 and M4, are 15.4, 14.6, 14.2 and 14.6 MPa, and the average fracture shear strains are 0.045, 0.039, 0.043 and 0.038, respectively. The shear stress and fracture strain for each type of foam are obtained by averaging the values of three samples, which varied less than 7%. The micrographs of the shear fracture surfaces of Foams M1, M2, M3 and M4 are shown in Figure 4.57. Similar to tensile fracture, the fracture occurred mainly across the CMs and the Al network instead of at the interface between the Al network and the CMs.

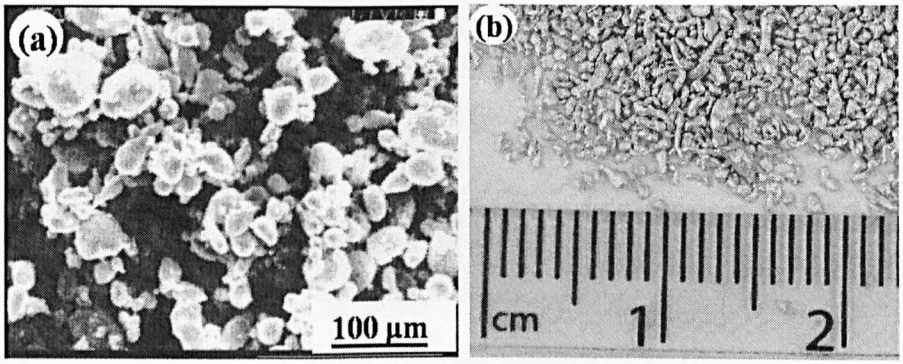

Figure 4.1 *The morphology of the two Al 6082 powders: (a) fine particles with an average size of 53 µm and (b) coarse particles with size range of 0.5-1 mm*

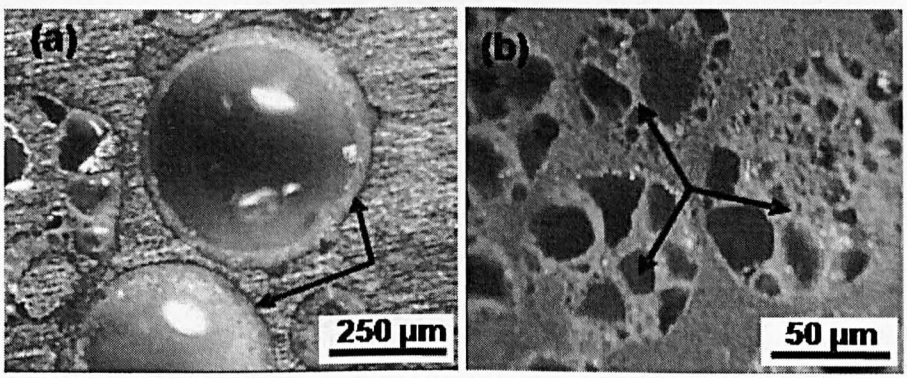

Figure 4.2 *Optical micrographs of the polished cross sections of two syntactic foam samples showing the two different inner structures of (a) hollow CMs and (b) porous CMs, as indicated by the arrows*

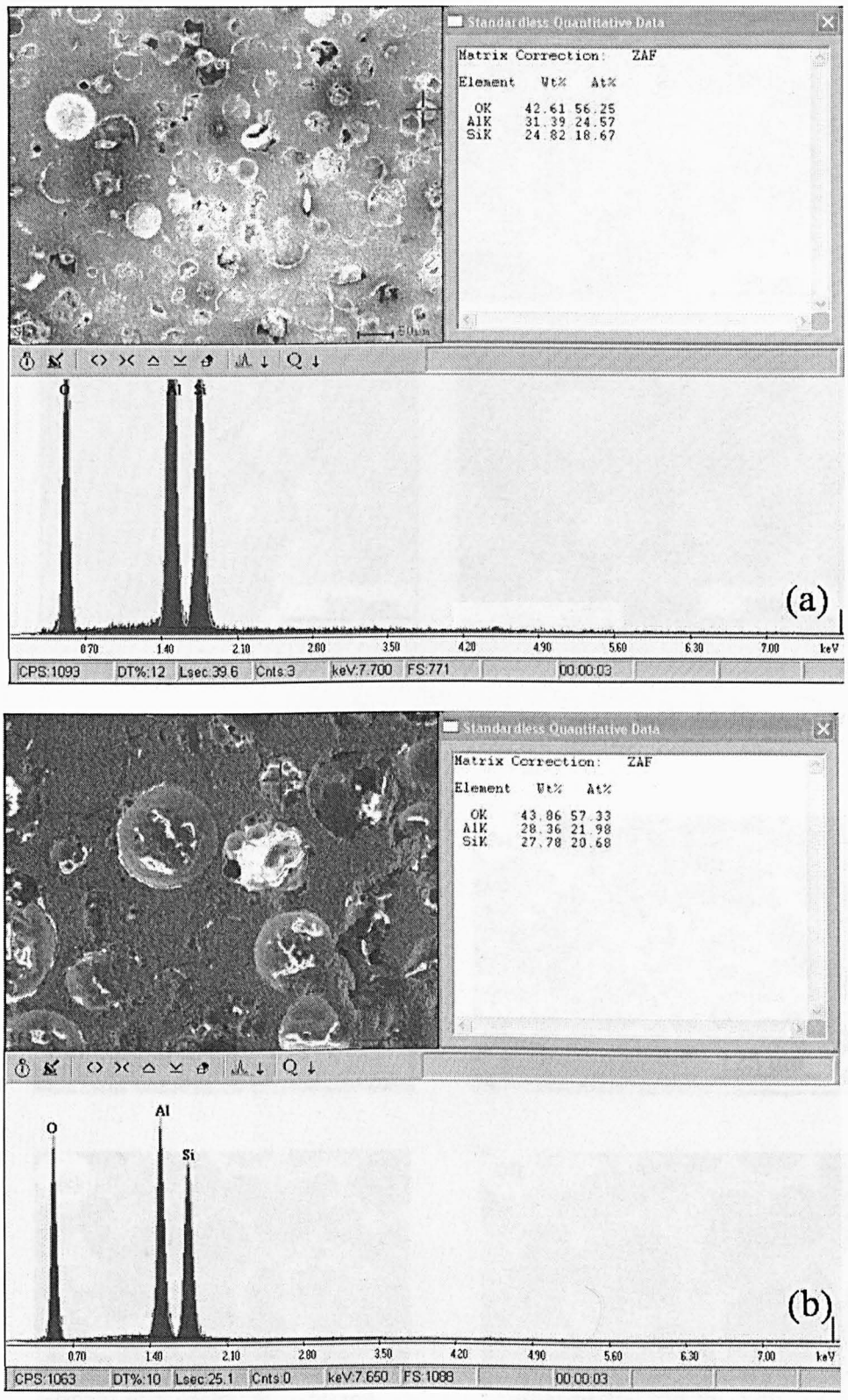

Figure 4.3 *EDS graphs for the two types of CMs: (a) hollow and (b) porous*

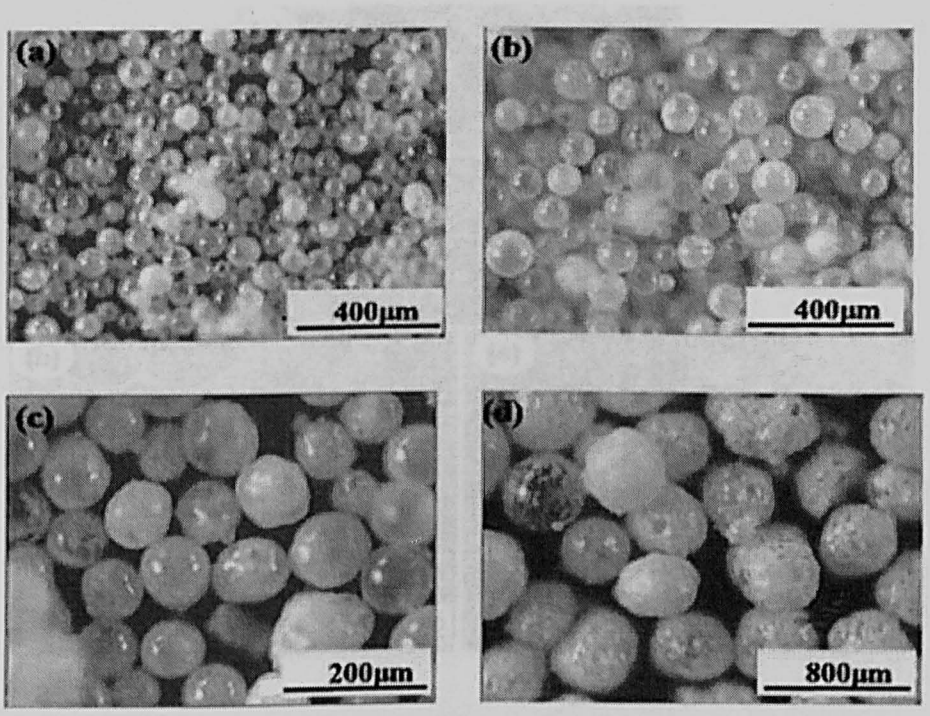

Figure 4.4 *Optical images of the four types of CMs: (a)I, (b)II, (c) III and (d) IV*

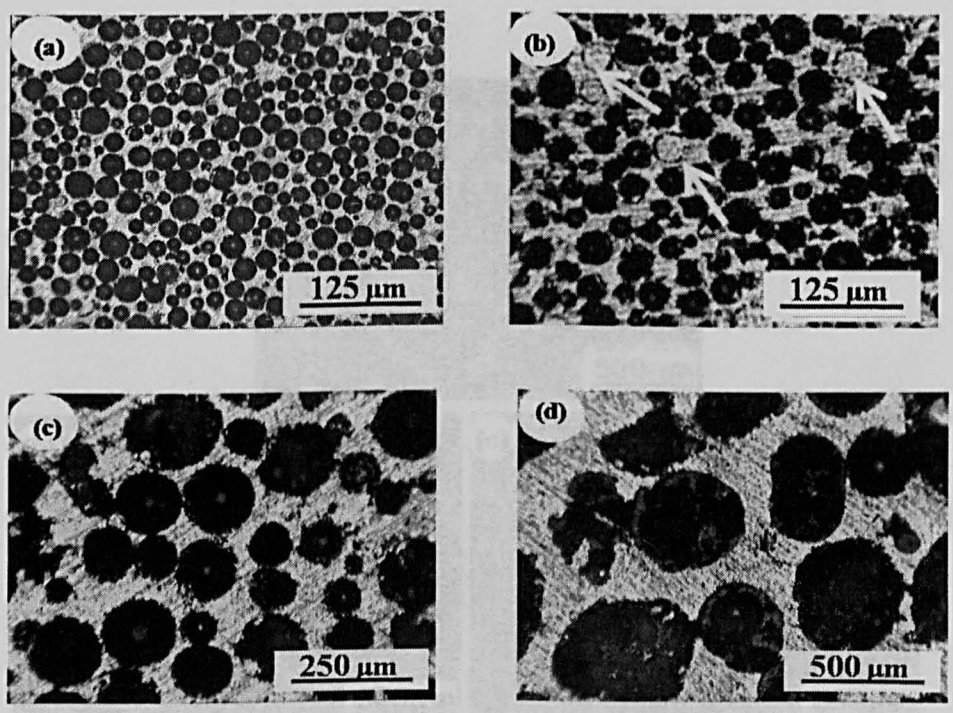

Figure 4.5 *Optical micrographs of the polished cross-sections of Foams (a) M1, (b) M2, (c) M3 and (d) M4. Arrows in (b) show examples of CMs penetrated by Al*

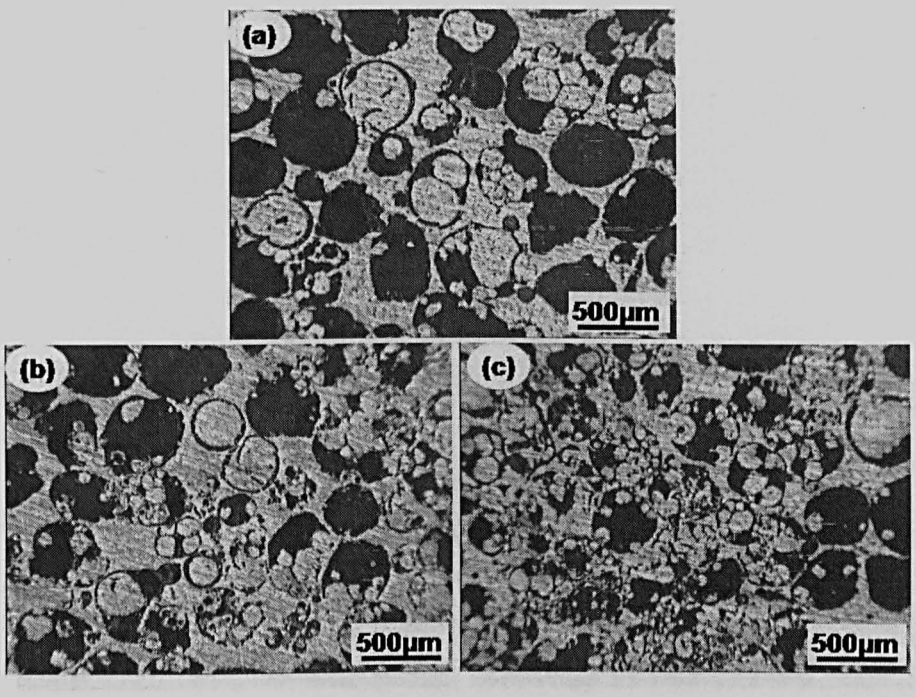

Figure 4.6 *Polished cross-sections of the Foams: (a) M4-H1, (b) M4- H2 and (c) M4- H3*

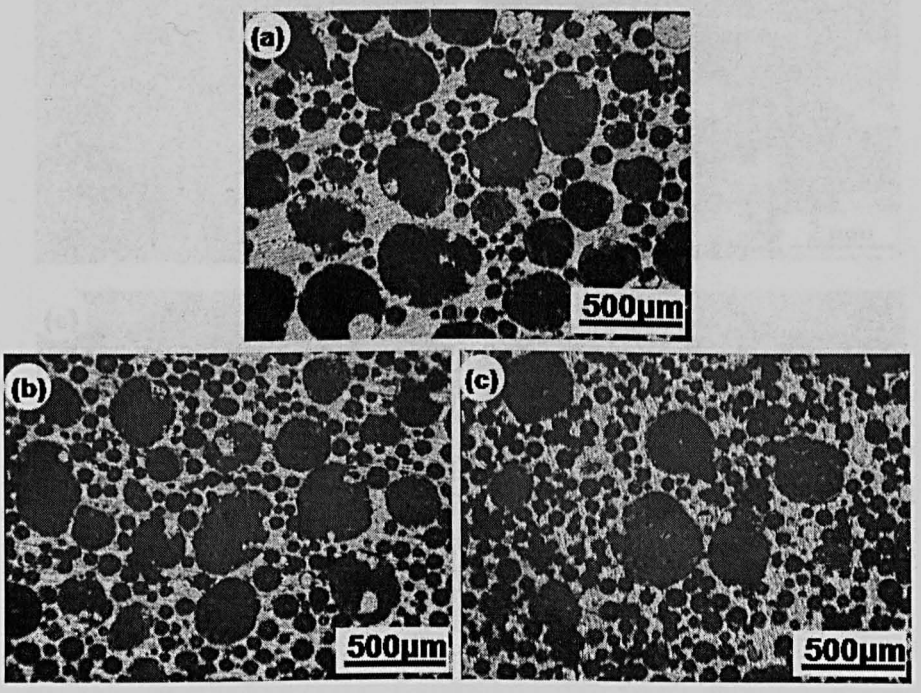

Figure 4.7 *Polished cross-sections of Foams (a) B1, (b) B2 and (c) B3*

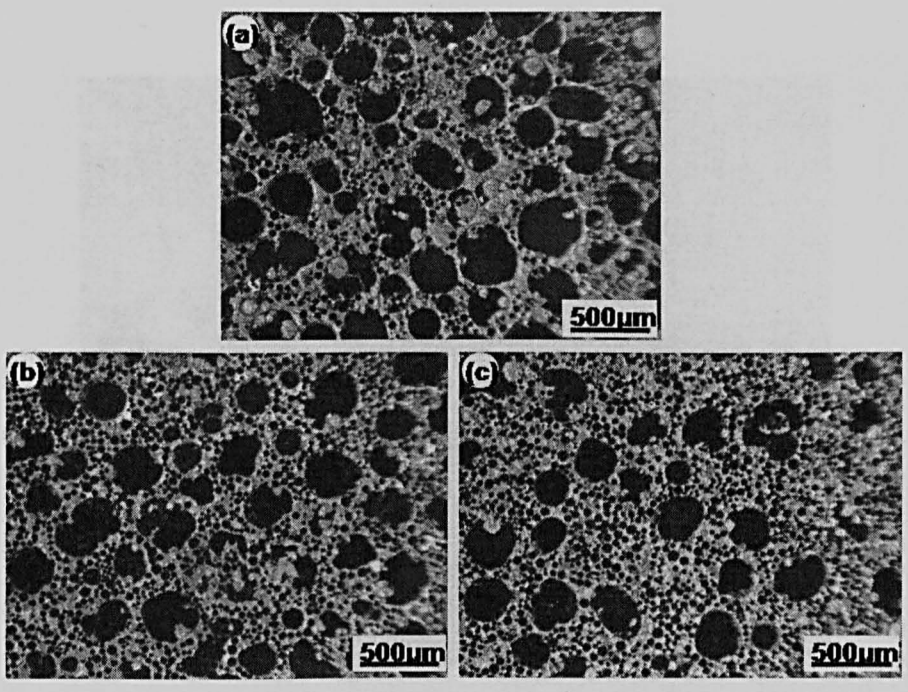

Figure 4.8 *Polished cross sections of Foams (a) B4, (b) B5 and (c) B6*

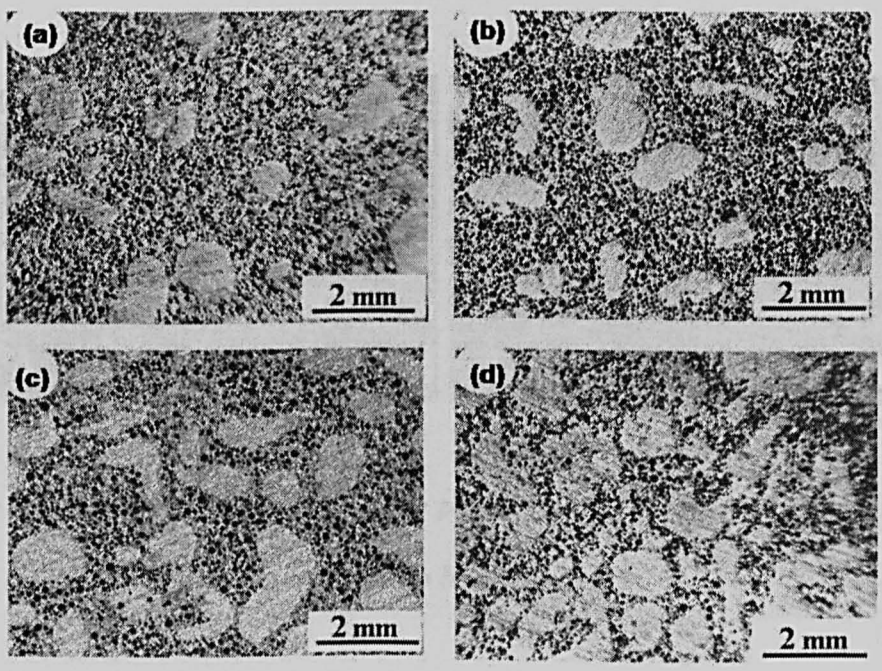

Figure 4.9 *Optical micrographs of the polished cross sections of the four Al toughened syntactic foams, (a) T1, (b) T2, (c) T3 and (d) T4*

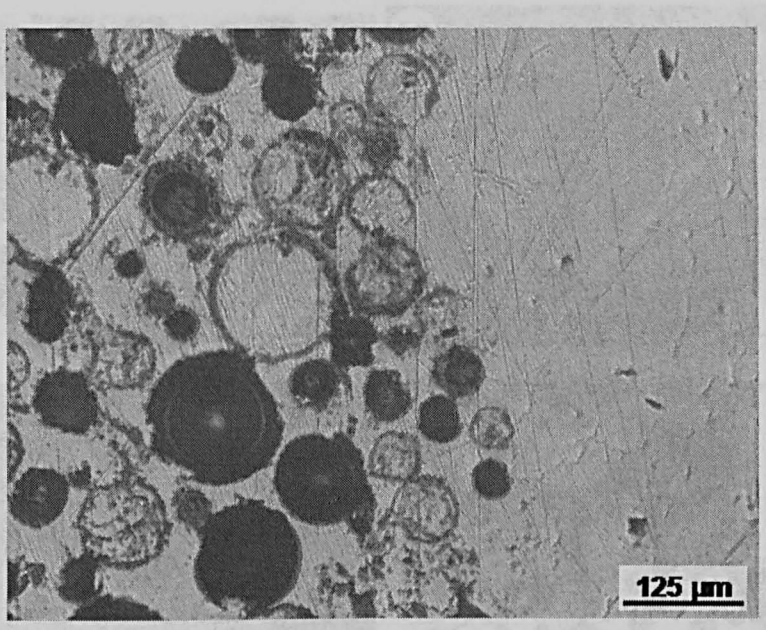

Figure 4.10 *Optical micrograph of polished cross section of Foam T2 showing the interface between an Al particle and the Al/CM matrix*

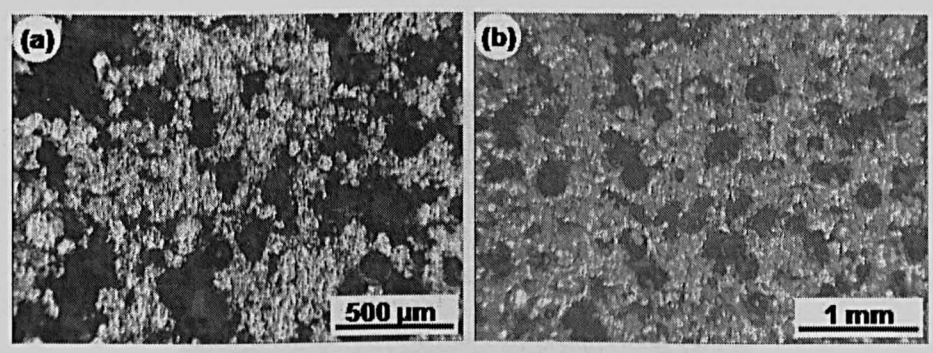

Figure 4.11 *Optical micrographs of the polished cross sections of Foams (a) S1, (b) S2, (c) S3, (d) S4, (e) S5 and (f)S6 (to be continued)*

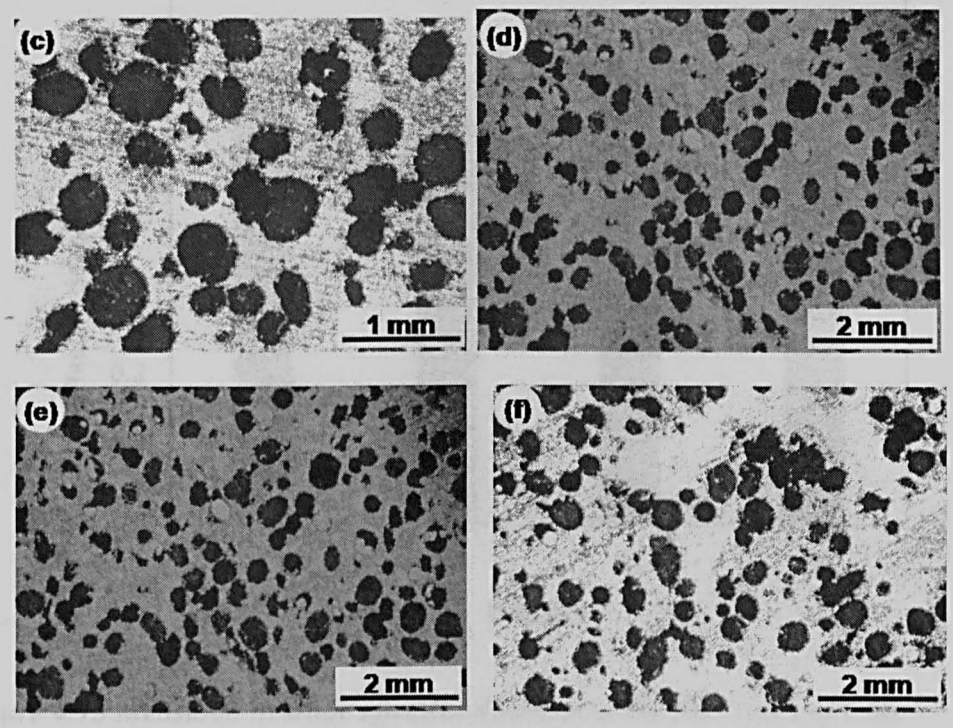

Figure 4.11 *Optical micrographs of the polished cross sections of Foams (a) S1,(b) S2, (c) S3, (d) S4, (e) S5 and (f)S6 (continued)*

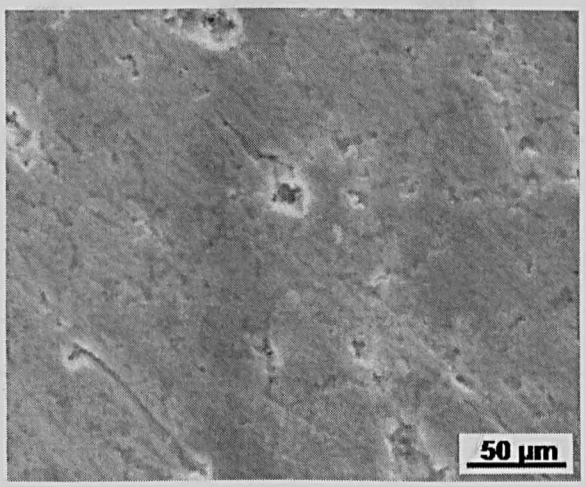

Figure 4.12 *SEM micrograph of a polished section of syntactic foam S3*

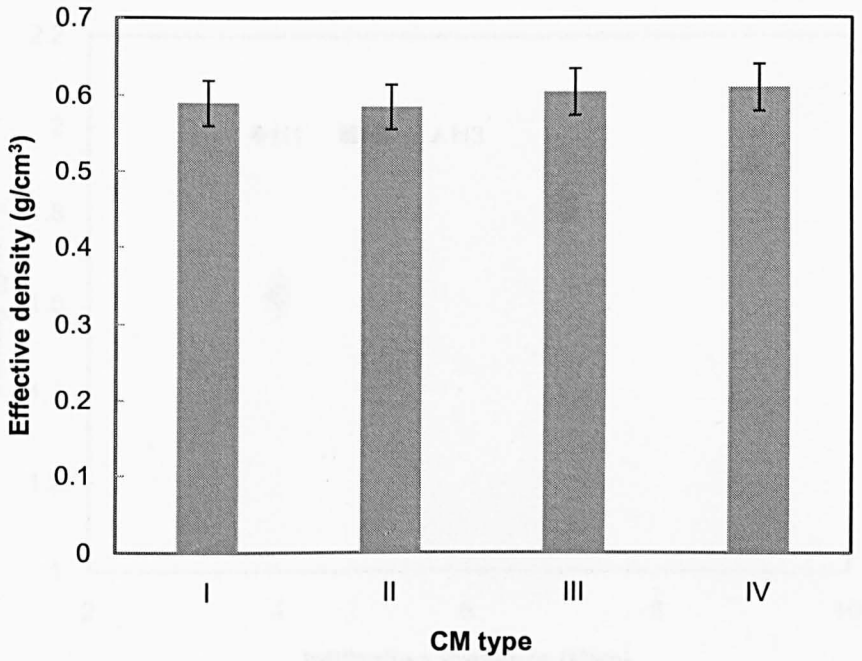

Figure 4.13 *Measured average effective densities of the four types of CMs*

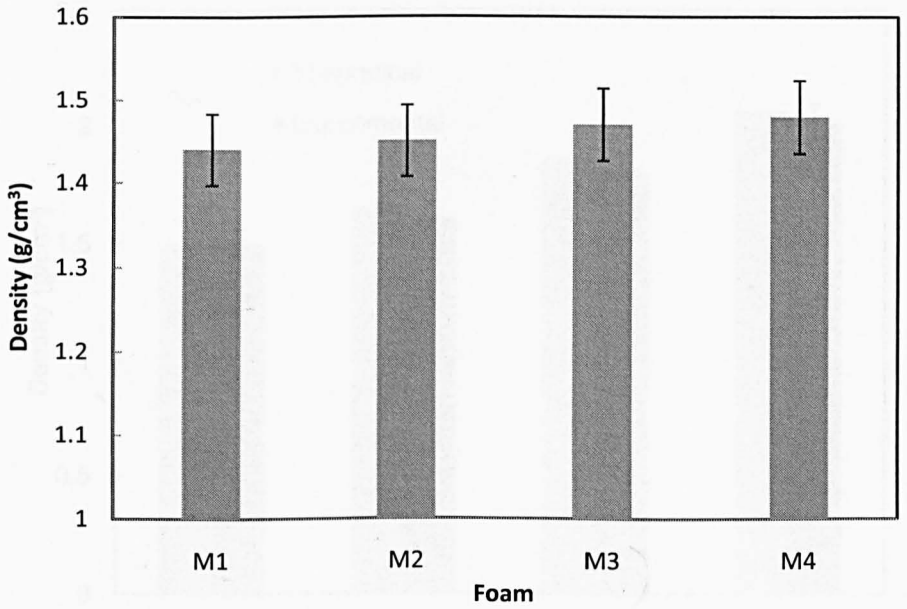

Figure 4.14 *Densities of syntactic foams containing monomodal CMs*

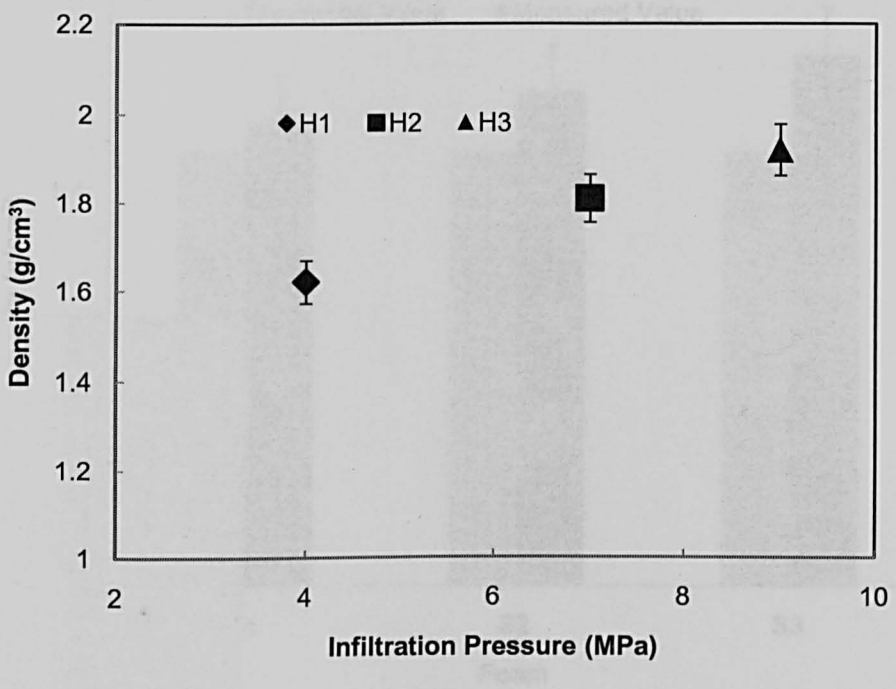

Figure 4.15 *Densities of syntactic foams M4-H1, M4-H2 and M4- H3 fabricated at different infiltration pressures*

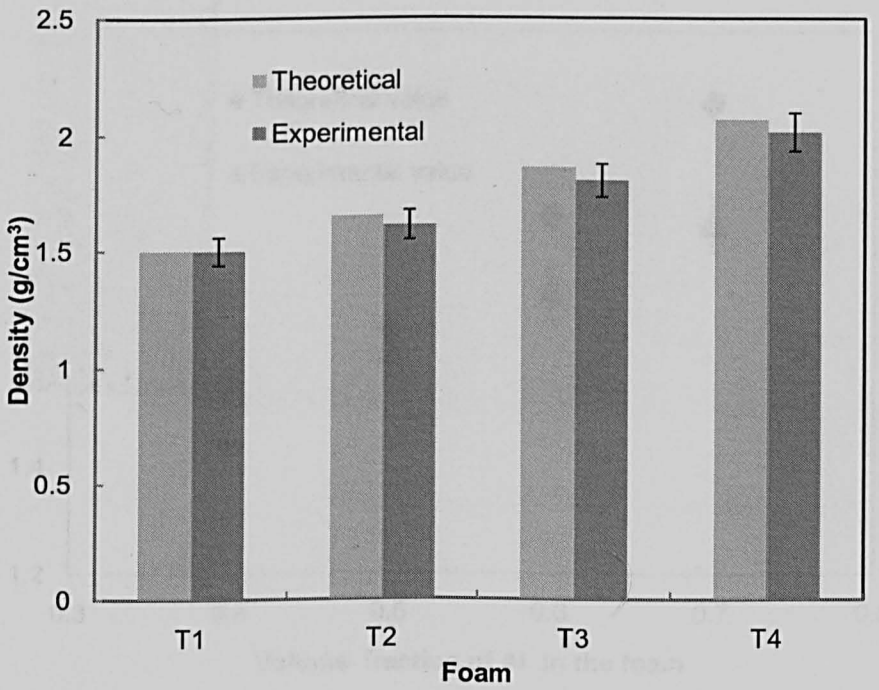

Figure 4.16 *Theoretical and measured density values of syntactic foams T1, T2, T3 and T4*

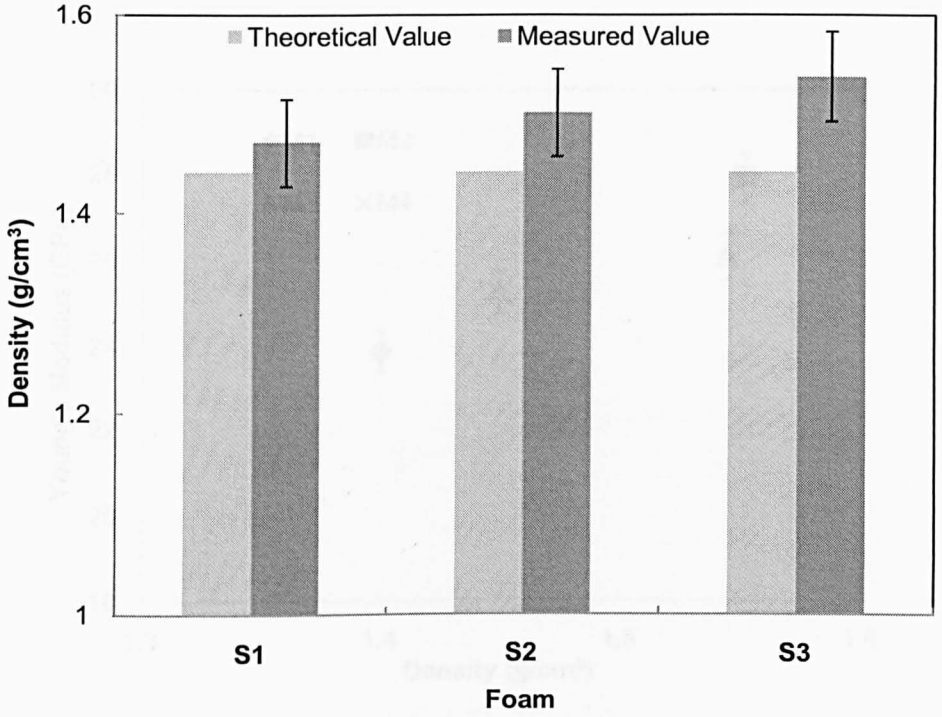

Figure 4.17 *Theoretical and measured densities of foams with different types of CMs (S1, S2 and S3)*

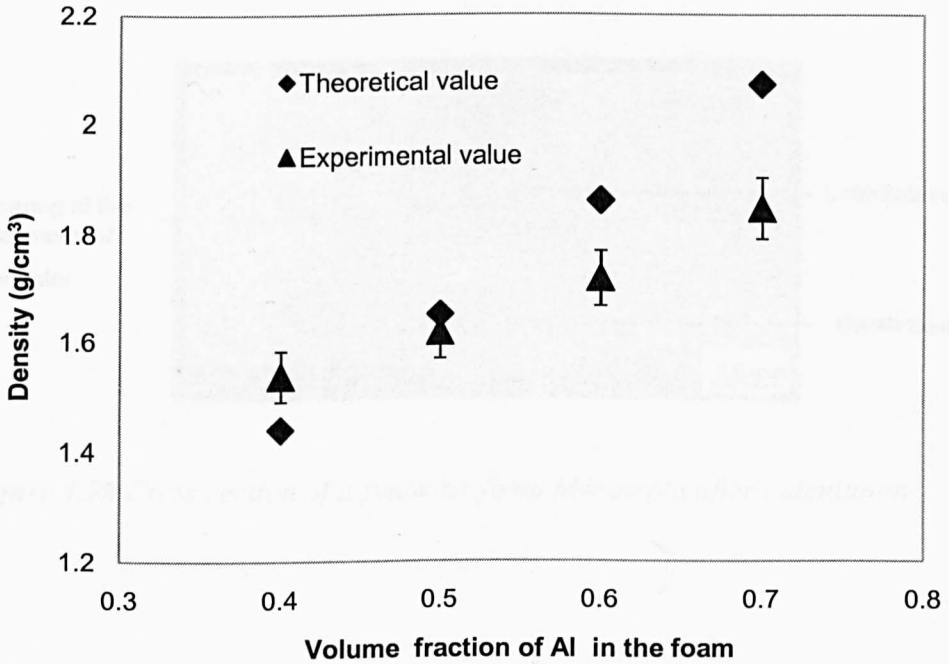

Figure 4.18 *Theoretical and measured densities of foams with different Al volume fractions (S3, S4, S5 and S6)*

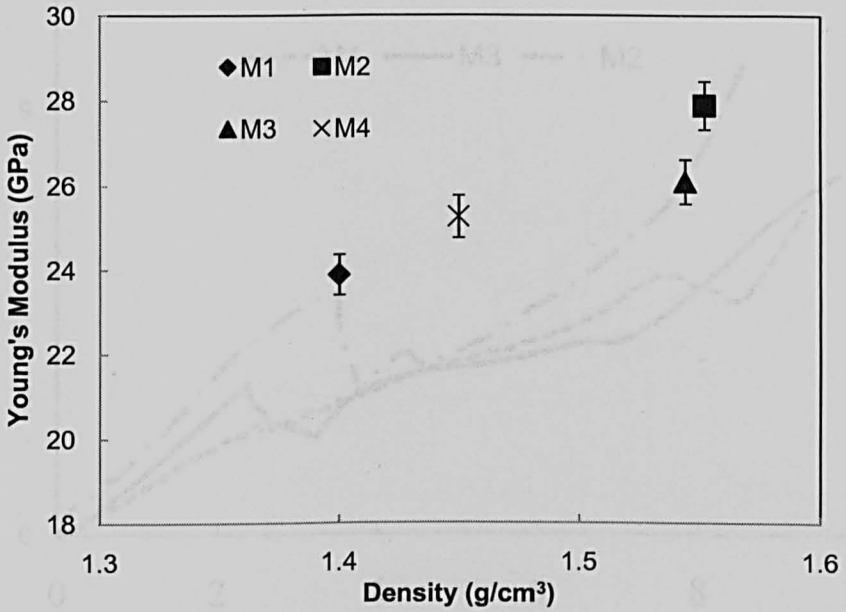

Figure 4.19 *Measured Young's modulus values of Foams M1-M4 plotted against their densities*

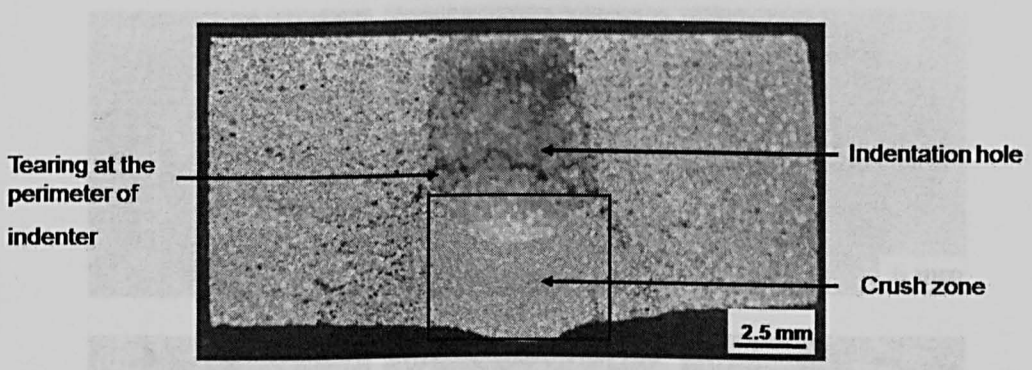

Figure 4.20 *Cross section of a syntactic foam M4sample after indentation*

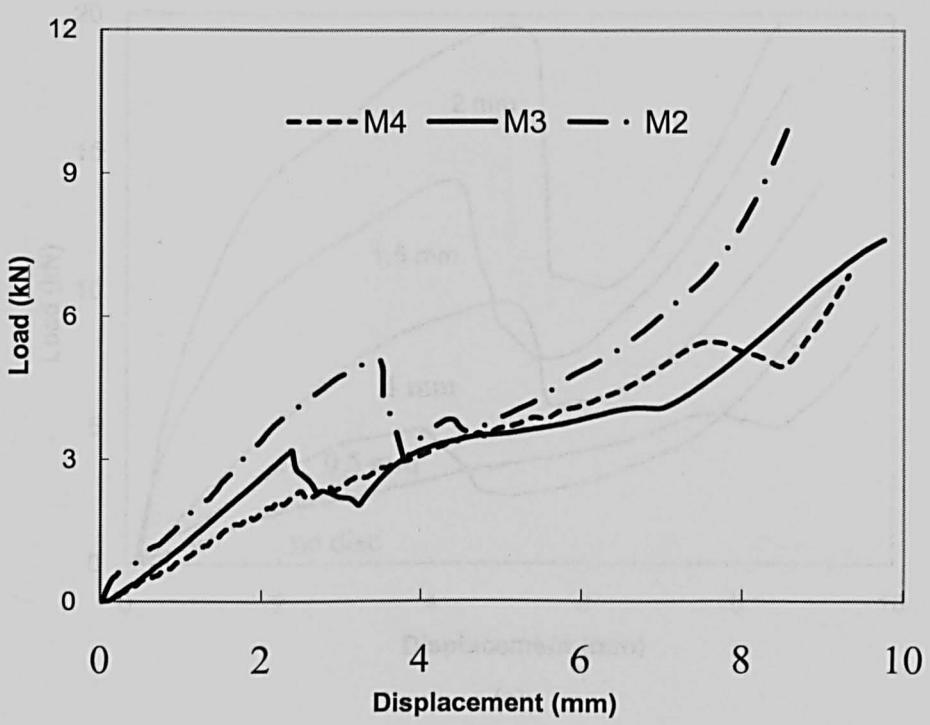

Figure 4.21 *Indentation load-displacement curves of M2, M3 and M4 without a spreader.*

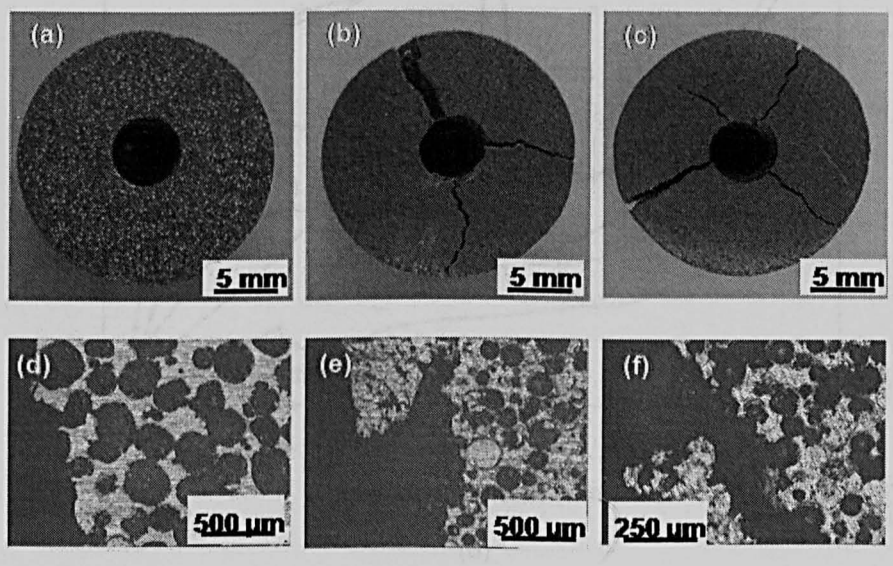

Figure 4.22 *Macrographs of the three types of syntactic foams after indentation: (a) M4, (b) M3 and (c) M2; and micrographs of the regions near the indentation holes of the three types of syntactic foams: (d) M4, (e) M3 and (f) M2*

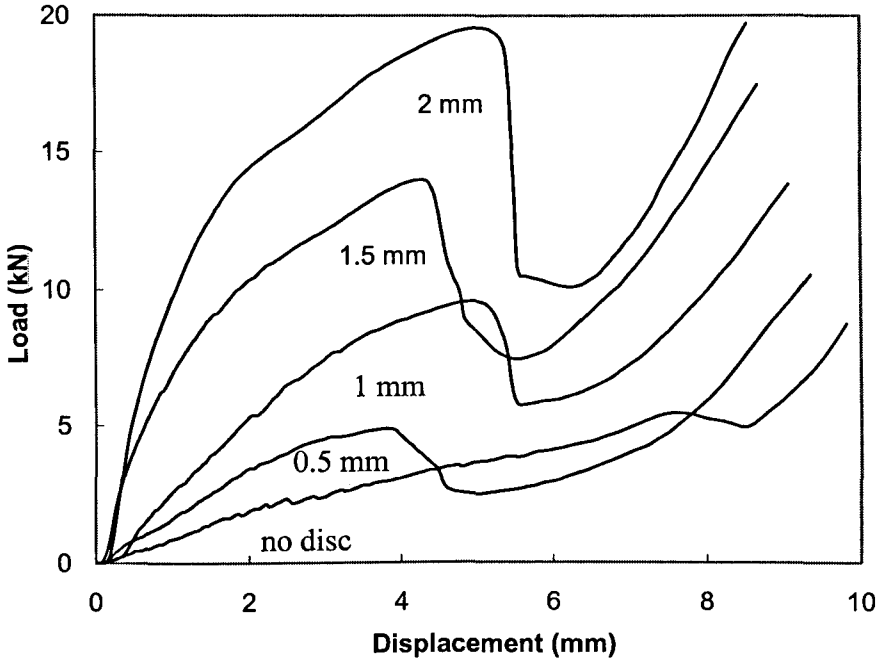

(a)

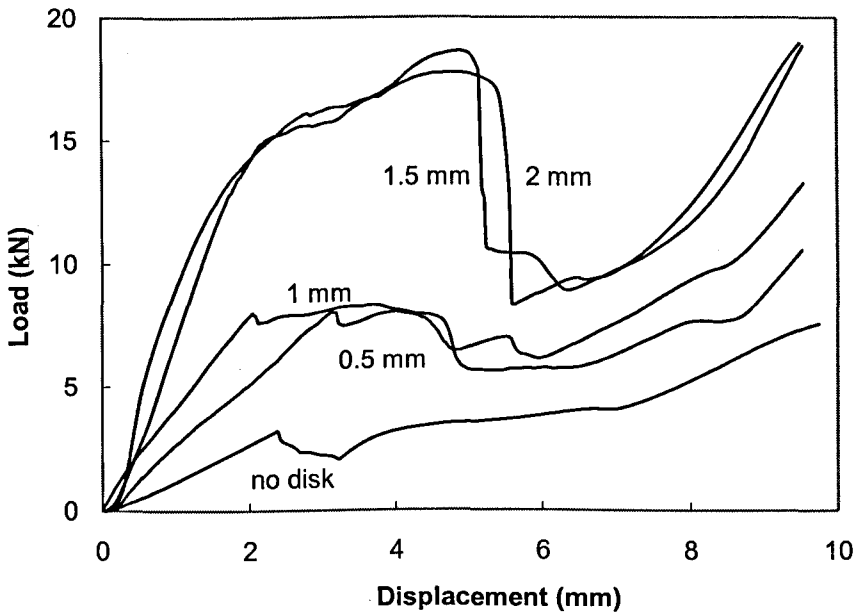

(b)

Figure 4.23 *Indentation load-displacement curves for the three types of syntactic foams with or without discs (a) Foam M4, (b) Foam M3 and (c) Foam M2 (to be continued)*

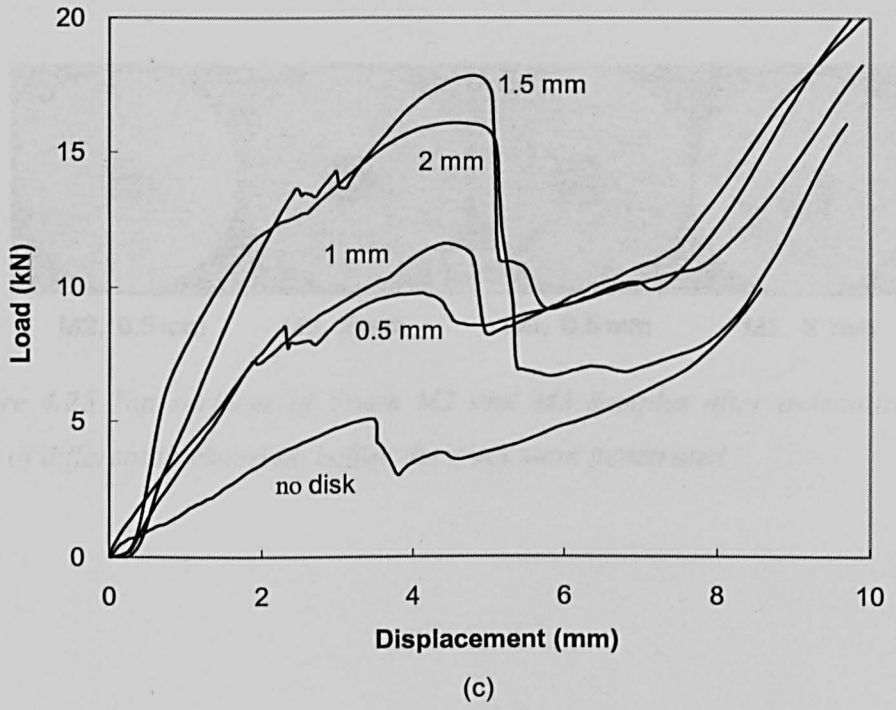

Figure 4.23 *Indentation load-displacement curves for the three types of syntactic foams with or without discs (a) Foam M4, (b) Foam M3 and (c) Foam M2 (continued)*

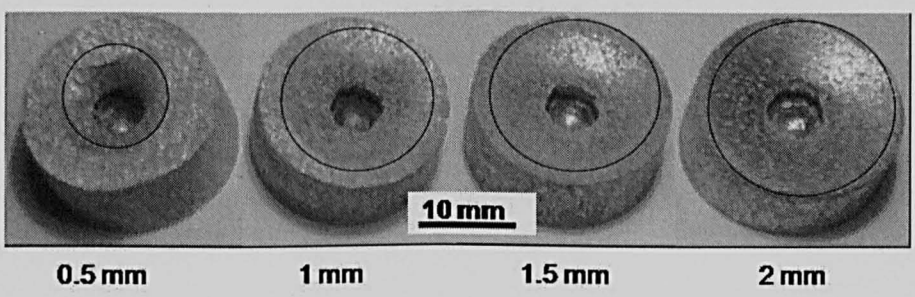

Figure 4.24 *Top surfaces of Foam M4 samples after indentation with discs of different thicknesses, before the discs were penetrated. The plastic deformation areas are indicated by circles*

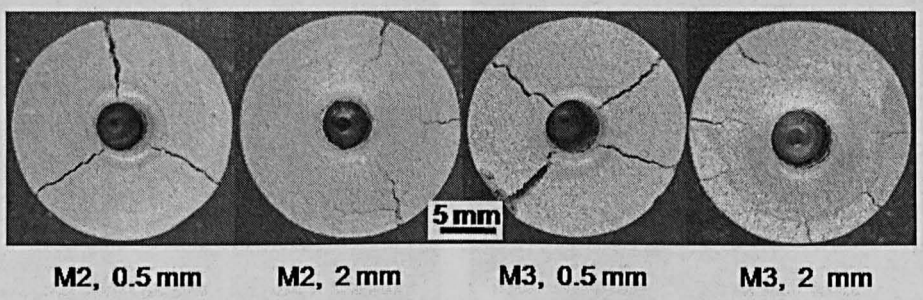

Figure 4.25 *Top surfaces of Foam M2 and M3 samples after indentation with discs of different thicknesses, before the discs were penetrated*

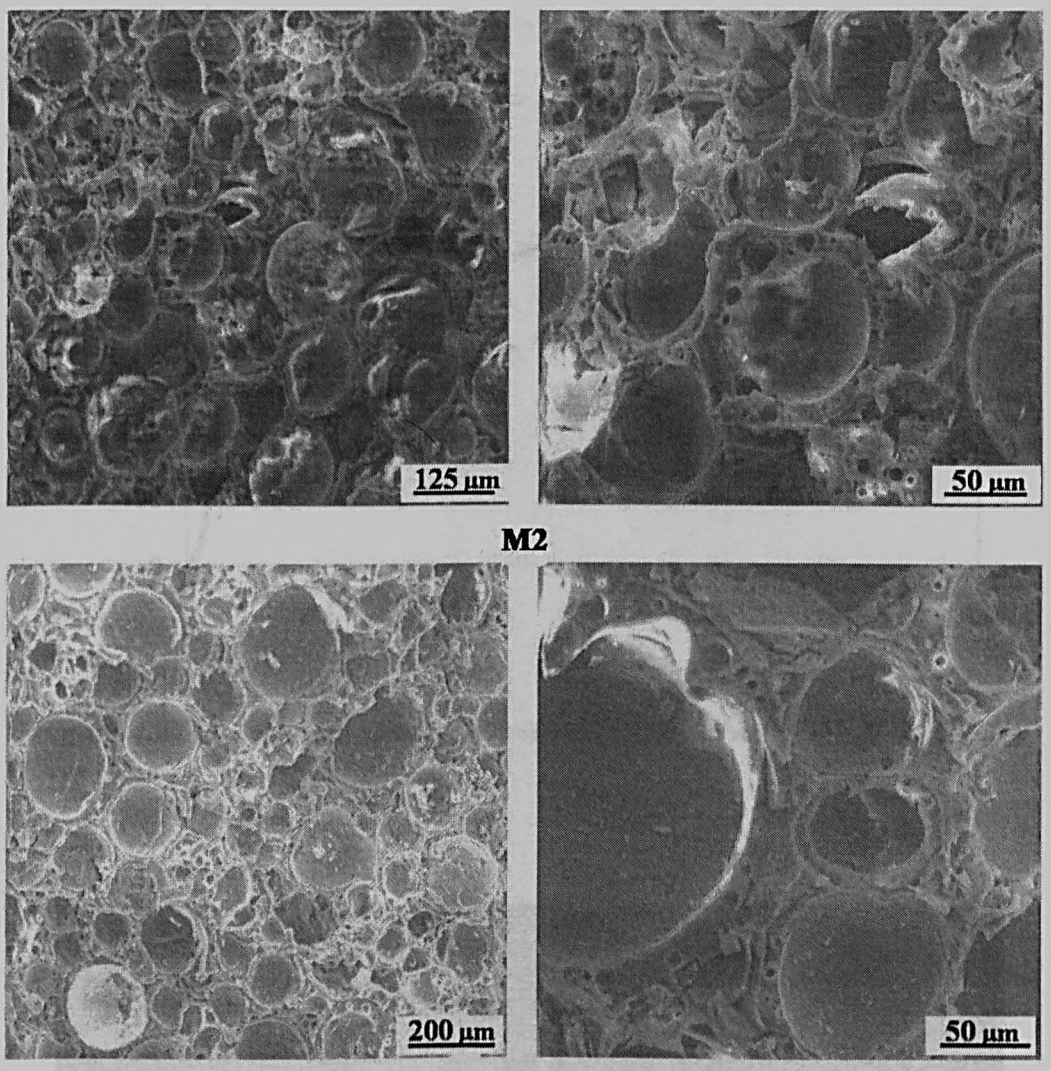

Figure 4.26 *SEM micrographs of indentation fracture surface for Foams M2 and M3 at different magnifications*

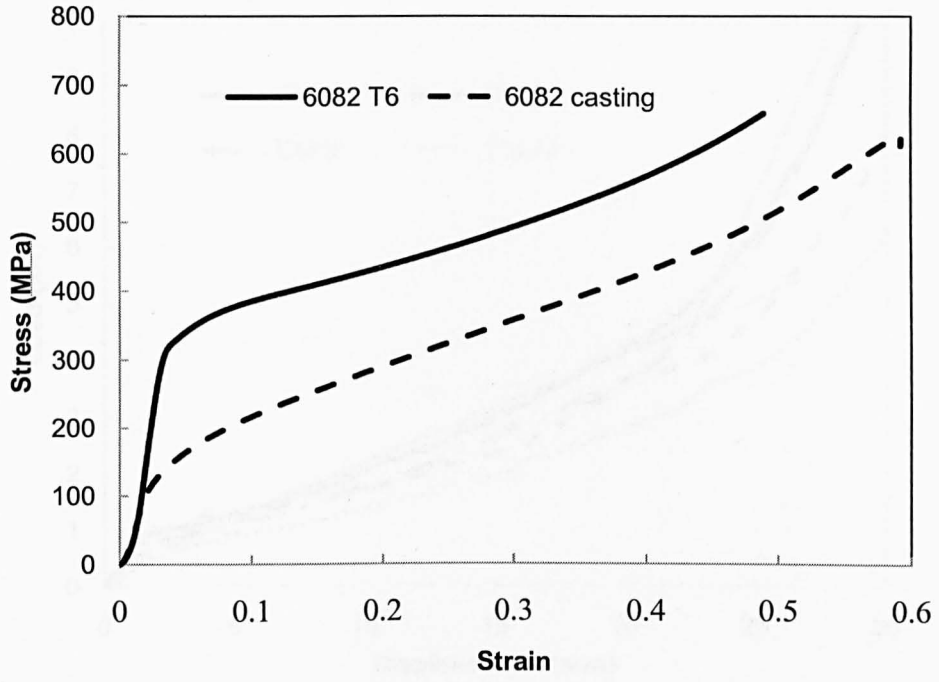

Figure 4.27 *Quasi-static compressive stress-strain curves of the Al 6082 alloy*

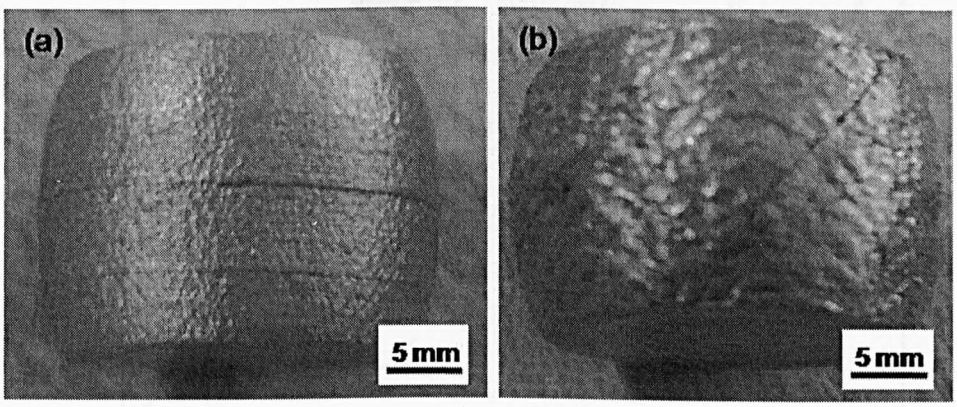

Figure 4.28 *Macrographs of Al alloy samples after compression plastic deformation at a strain of 0.5: (a) 6082 T6, (b) 6082 cast*

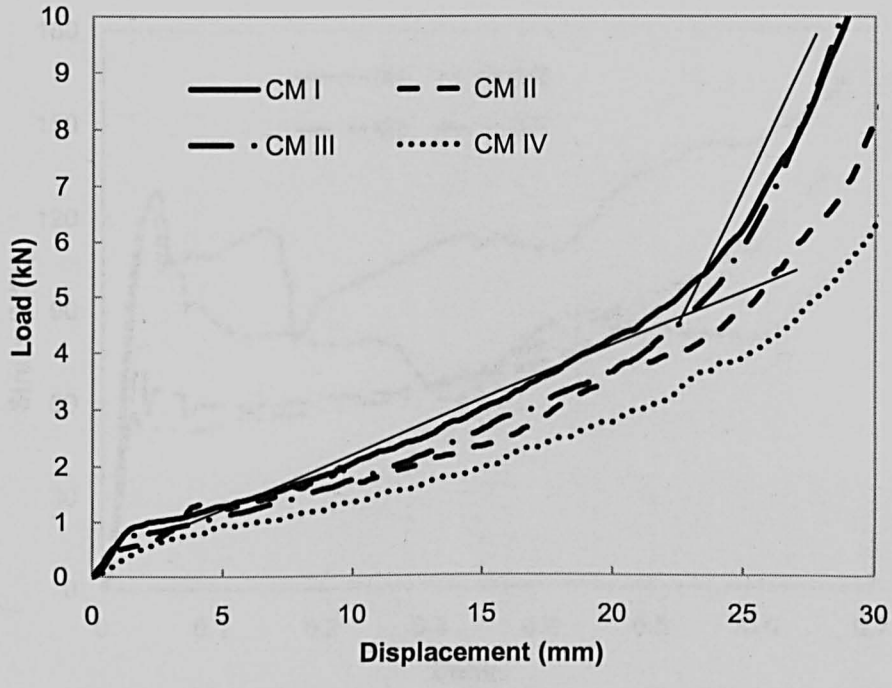

Figure 4.29 *Quasi-static compressive load-displacement curves of the four CMs*

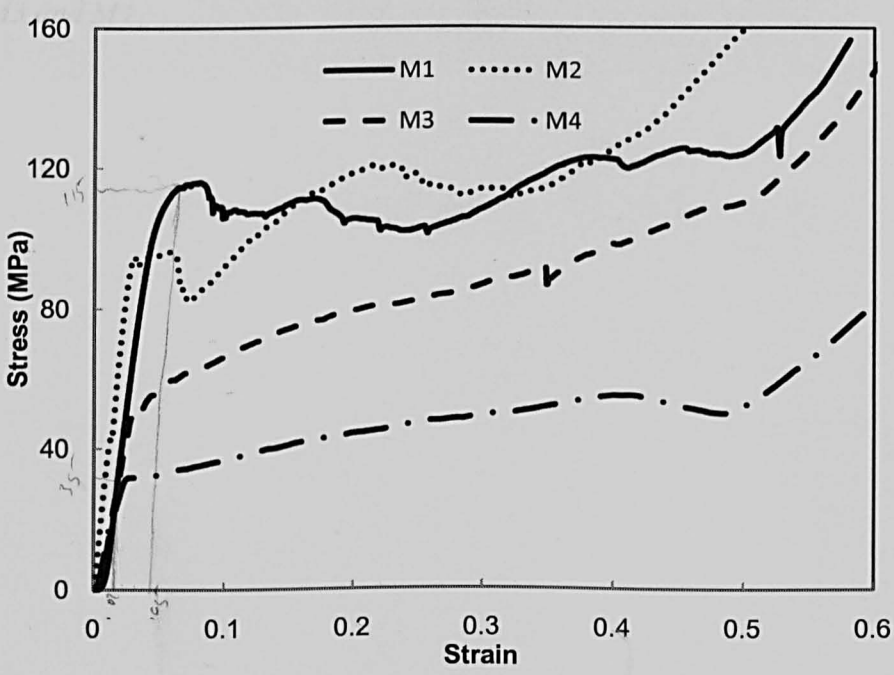

Figure 4.30 *Quasi-static compressive stress-strain curves for non-heat treated syntactic foams, M1, M2, M3 and M4*

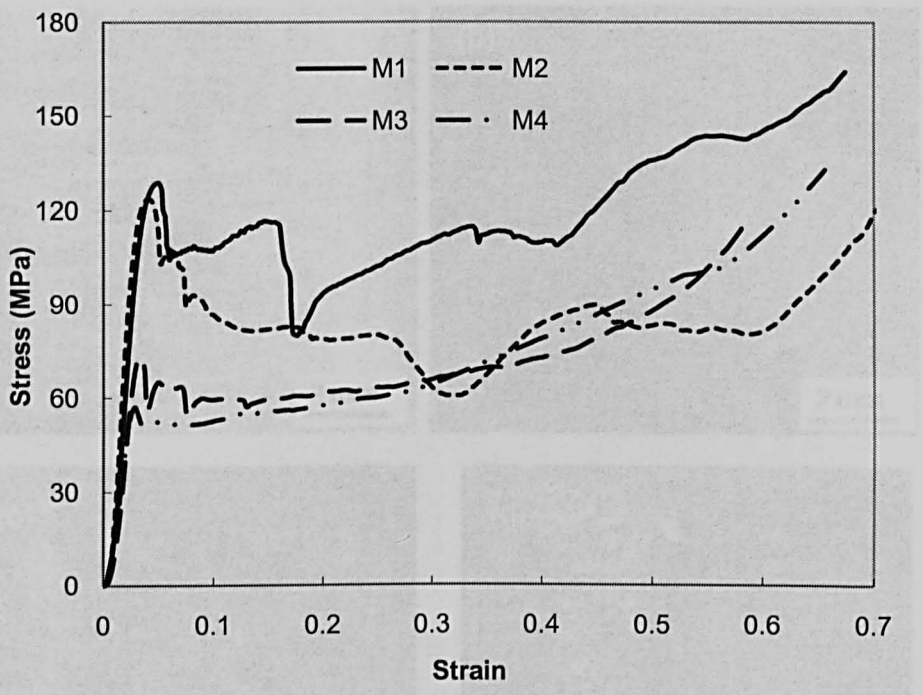

Figure 4.31 *Quasi-static compressive stress-strain curves of syntactic foams M1, M2, M3 and M4*

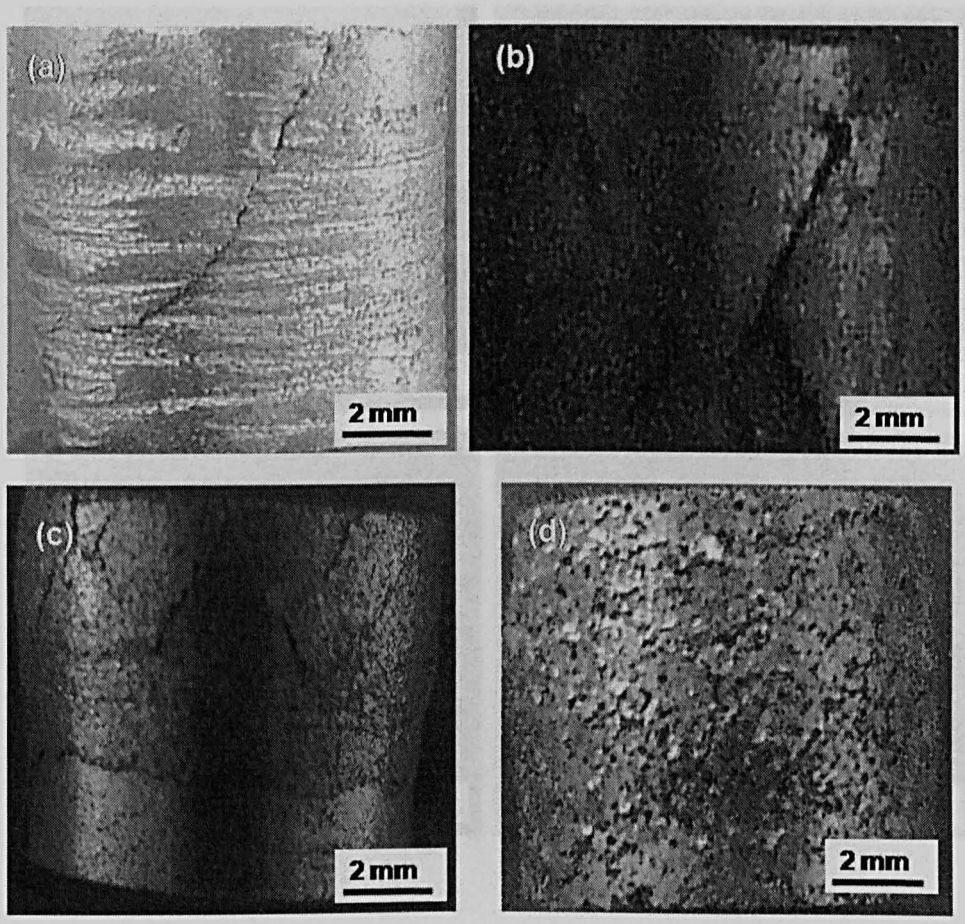

Figure 4.32 *Macrographs of syntactic foams (a) M1, (b) M2, (c) M3 and (d) M4 compressed at a strain of 0.2*

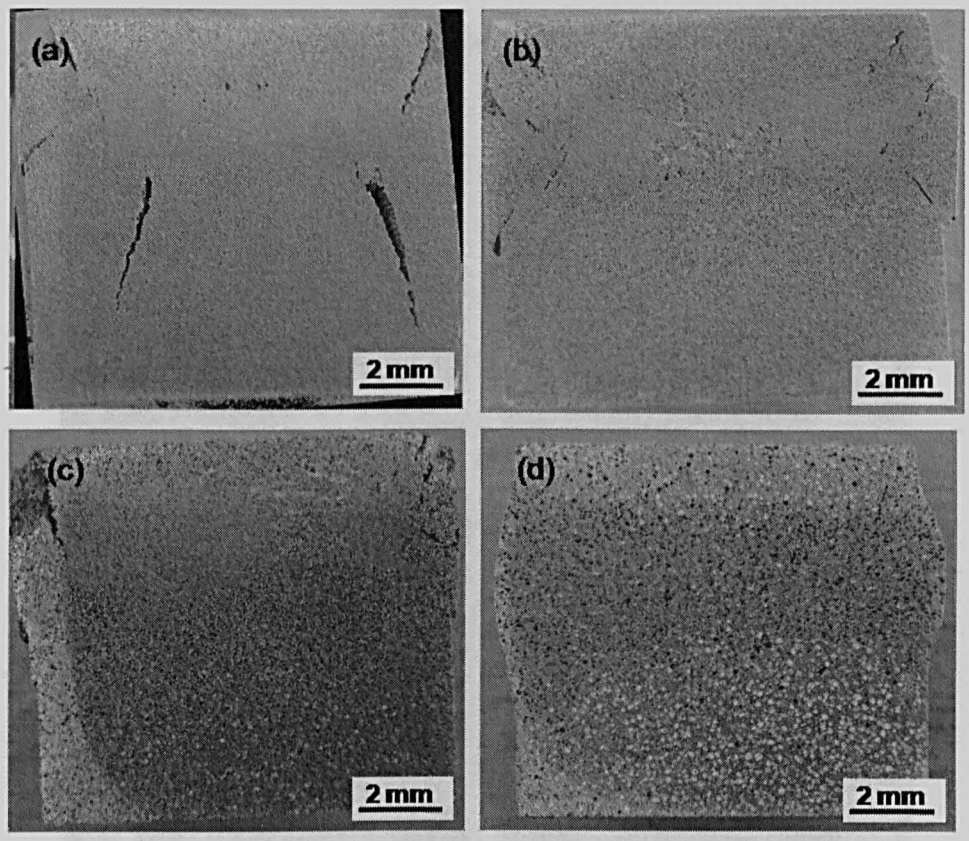

Figure 4.33 *Macrographs of longitudinal cross sections of syntactic foams (a) M1, (b) M2, (c) M3 and (d) M4*

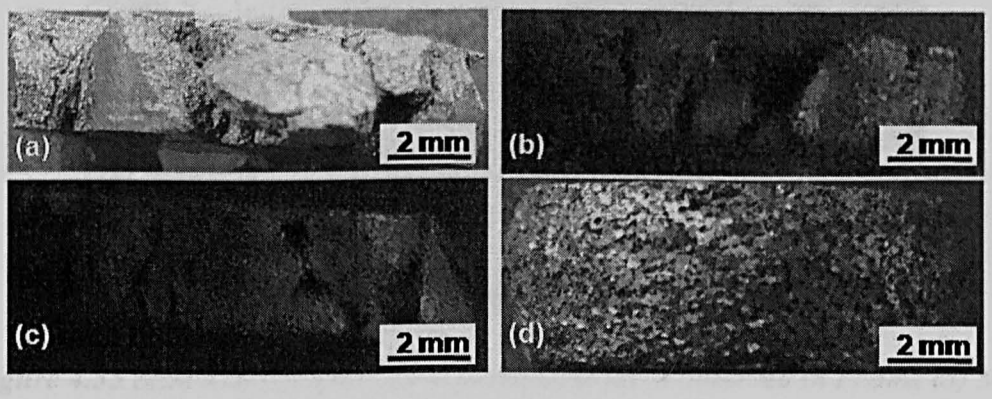

Figure 4.34 *Macrographs of syntactic foams (a) M1, (b) M2, (c) M3 and (d) M4 compressed to the strain of 0.6*

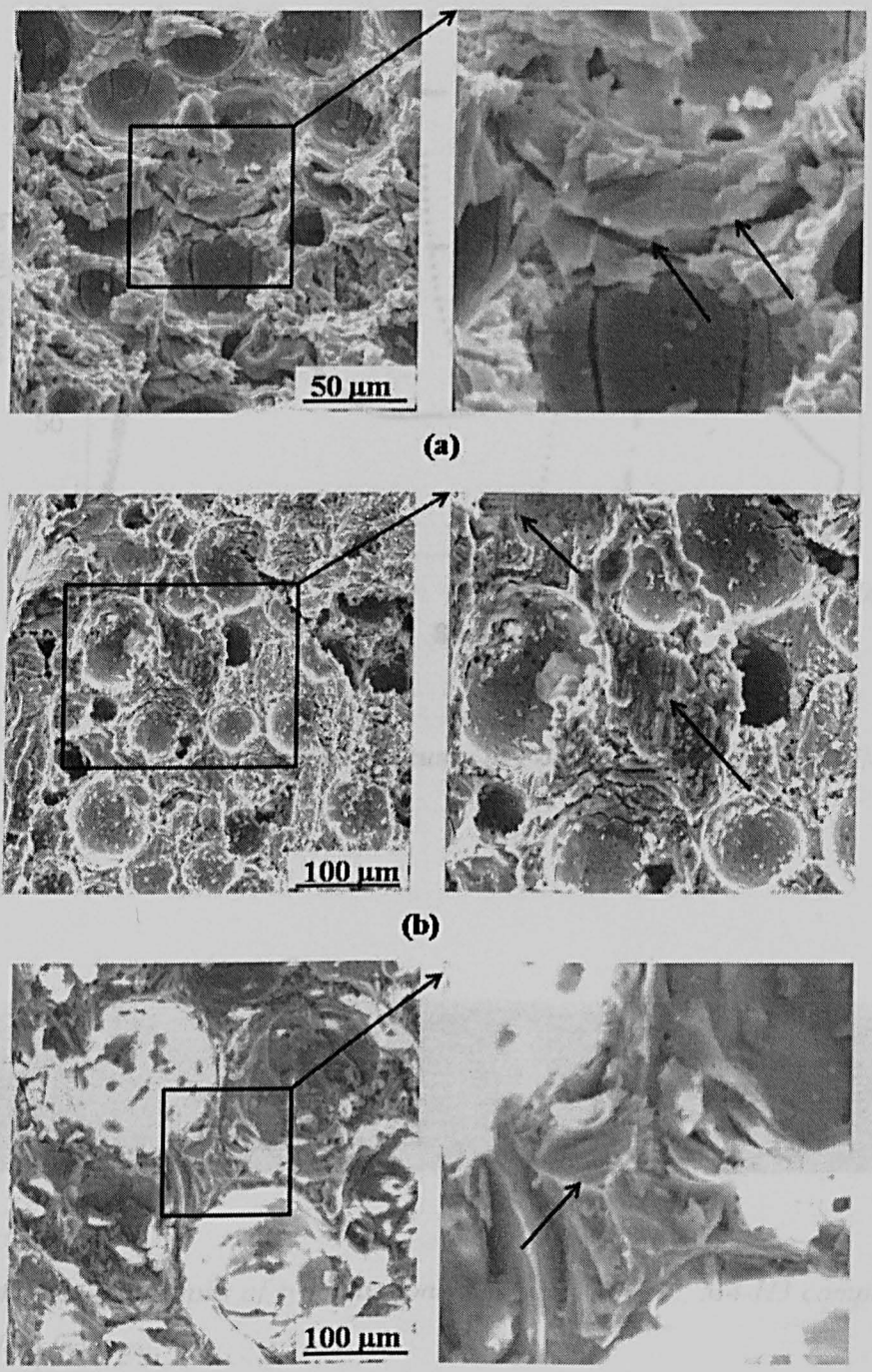

Figure 4.35 *SEM micrographs of the fracture surfaces observed in Foams (a) M1, (b) M2 and (c) M3 formed during compression. Arrows indicate the cleavage fracture stripes in the Al matrix*

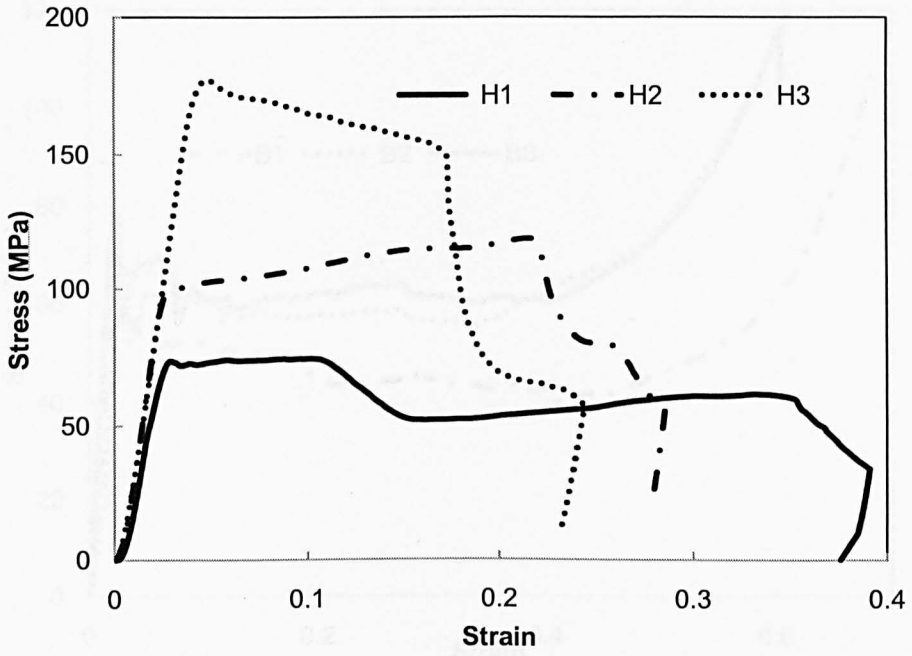

Figure 4.36 *Compressive stress-strain curve of Foams M4-H, M4- H2 andM4-H3*

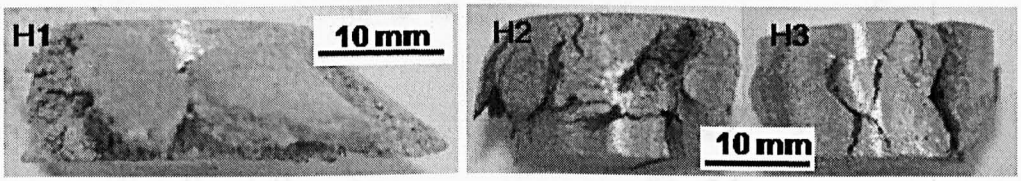

Figure 4.37 *Macrographs of syntactic foams M4-H1, M4-H2, M4-H3 compressed to complete fracture*

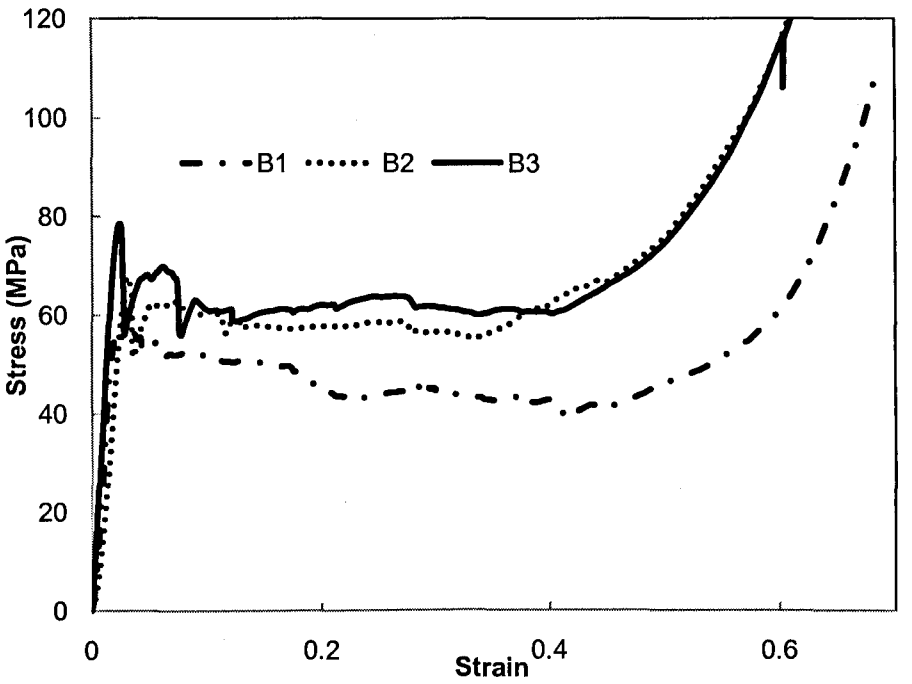

Figure 4.38 *Quasi-static compressive stress-strain curves of syntactic foams B1, B2 and B3*

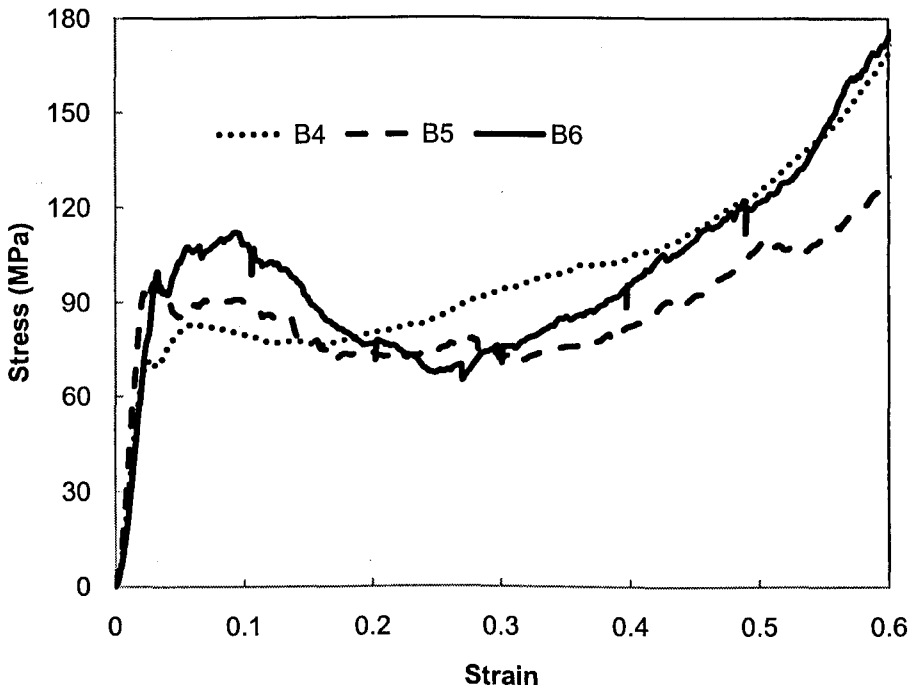

Figure 4.39 *Quasi-static compressive stress-strain curves of syntactic foams B4, B5 and B6*

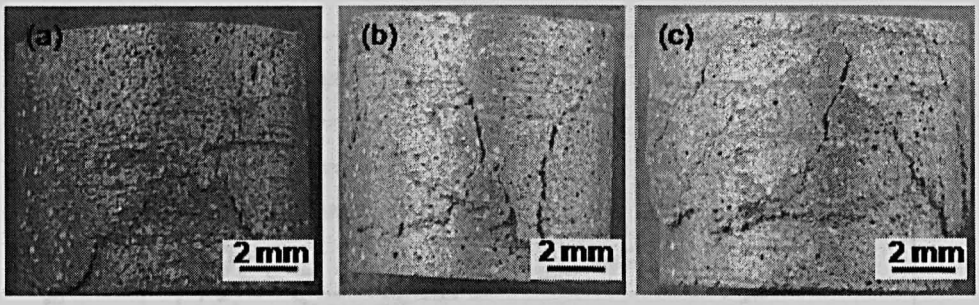

Figure 4.40 *Macrographs of syntactic foams (a) B1, (b) B2 and (B3) compressed to the strain of 0.2*

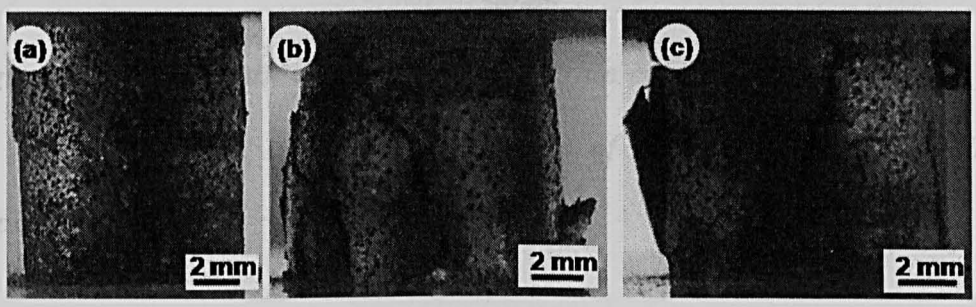

Figure 4.41 *Macrographs of syntactic foams (a) B4, (b) B5 and (c) B6 compressed to the strain of 0.2*

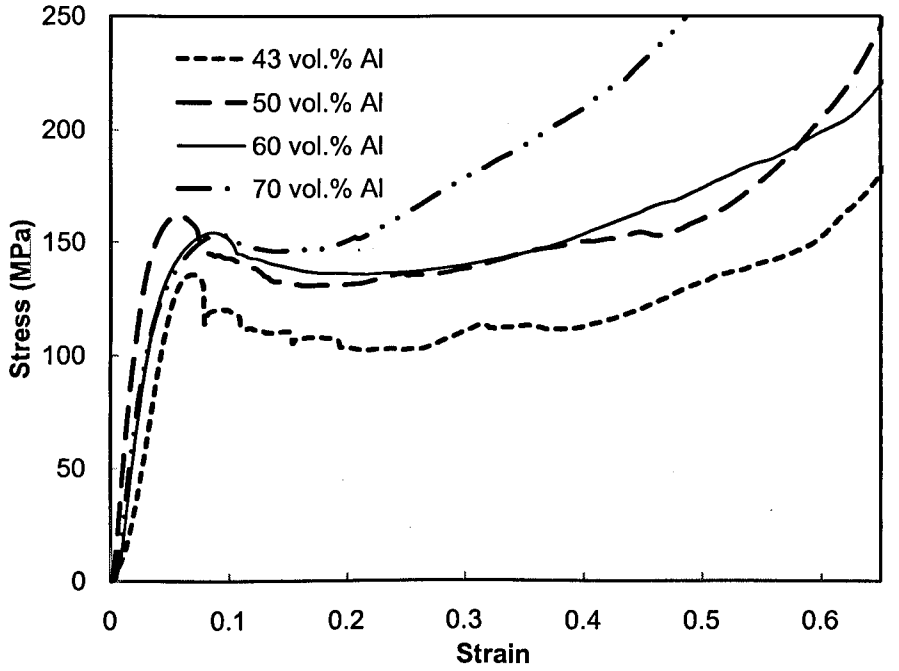

Figure 4.42 *Quasi-static compressive stress-strain curves of syntactic foams T1, T2, T3 and T4 with Al volume percentages of 43%, 50%, 60% and 70%, respectively*

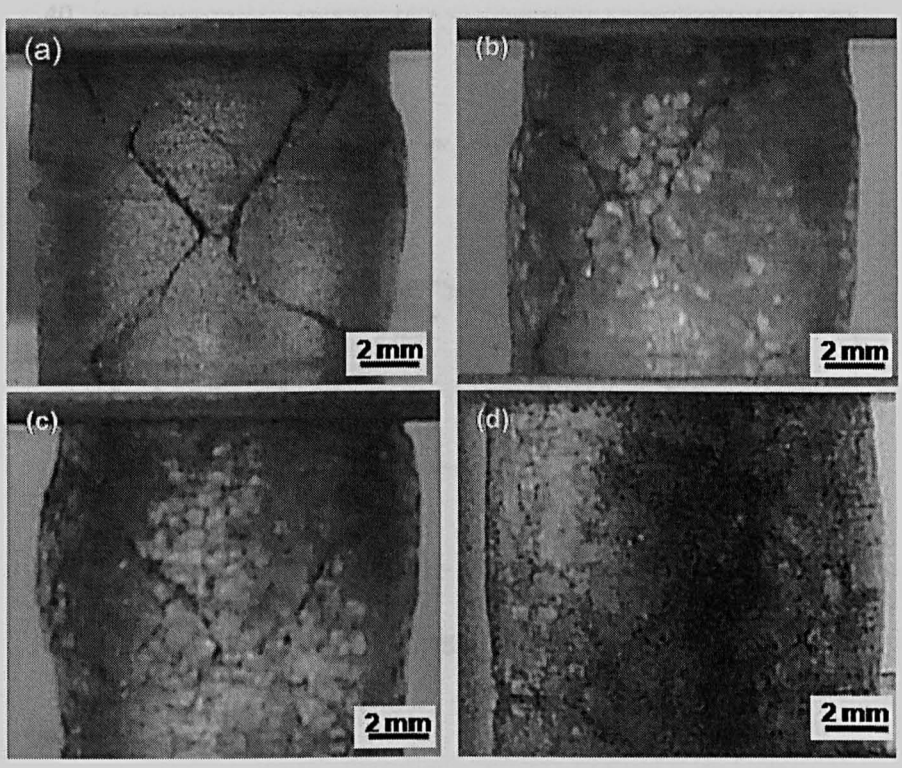

Figure 4.43 *Macrographs of syntactic foams (a) T1, (b) T2, (c) T3 and (d) T4 compressed to a strain of 0.2*

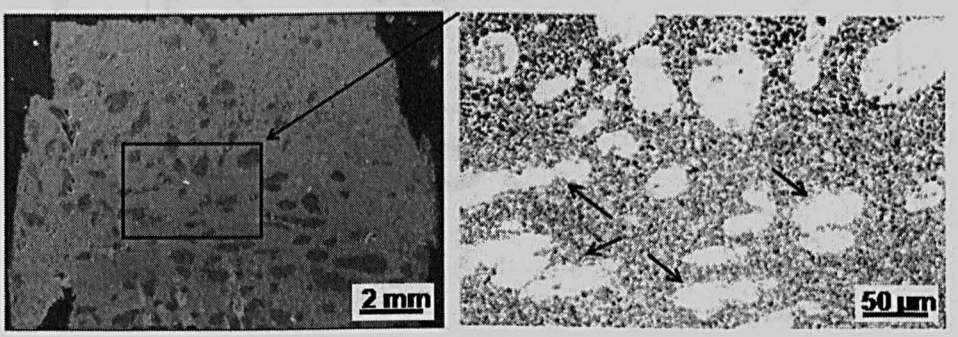

Figure 4.44 *Micrographs of a polished cross section of a deformed Foam T2 sample at the strain of 0.35. Localised plastic deformation of the added Al particles is indicated by arrows*

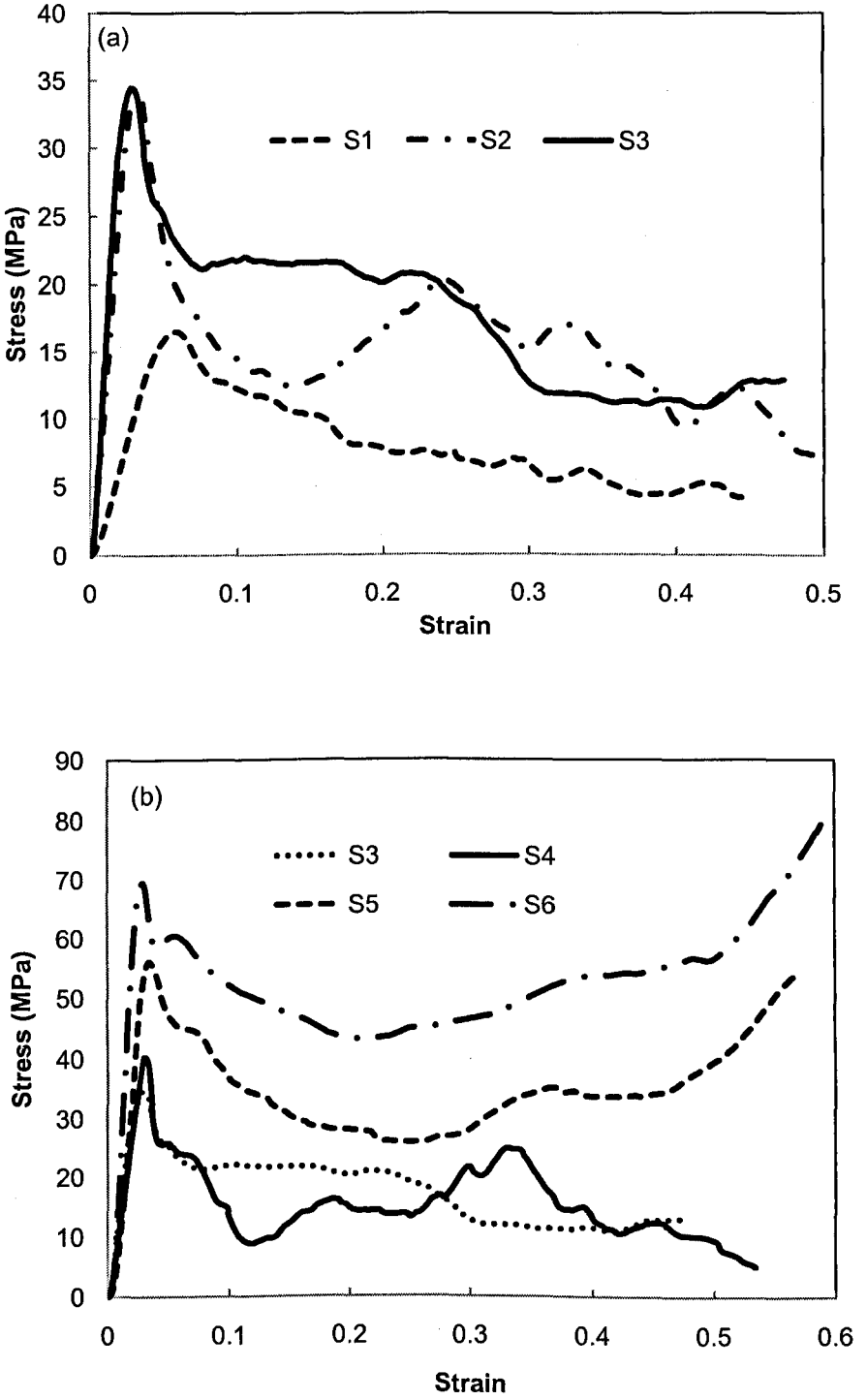

Figure 4.45 *Quasi-static compressive stress-strain curves of syntactic foams fabricated by the liquid sintering method: (a) S1, S2 and S3, and (b) S3, S4, S5 and S6*

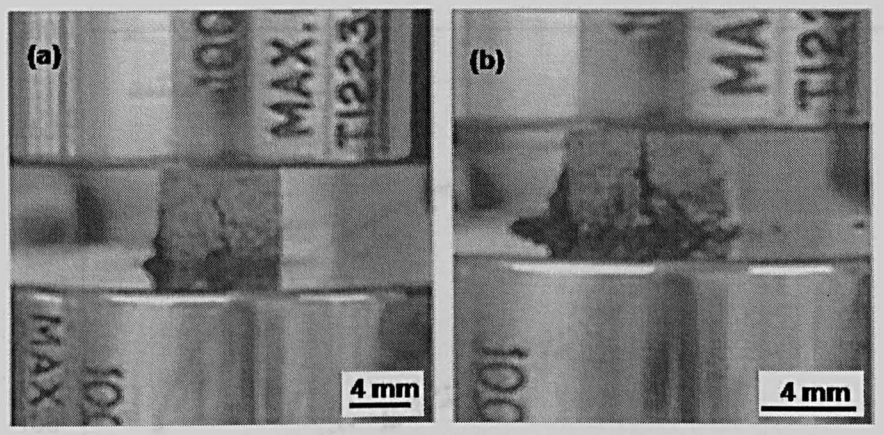

Figure 4.46 *Representative deformation process of a foam sample fabricated by the liquid sintering method under compression at the strains of (a) 0.04 and (b) 0.2*

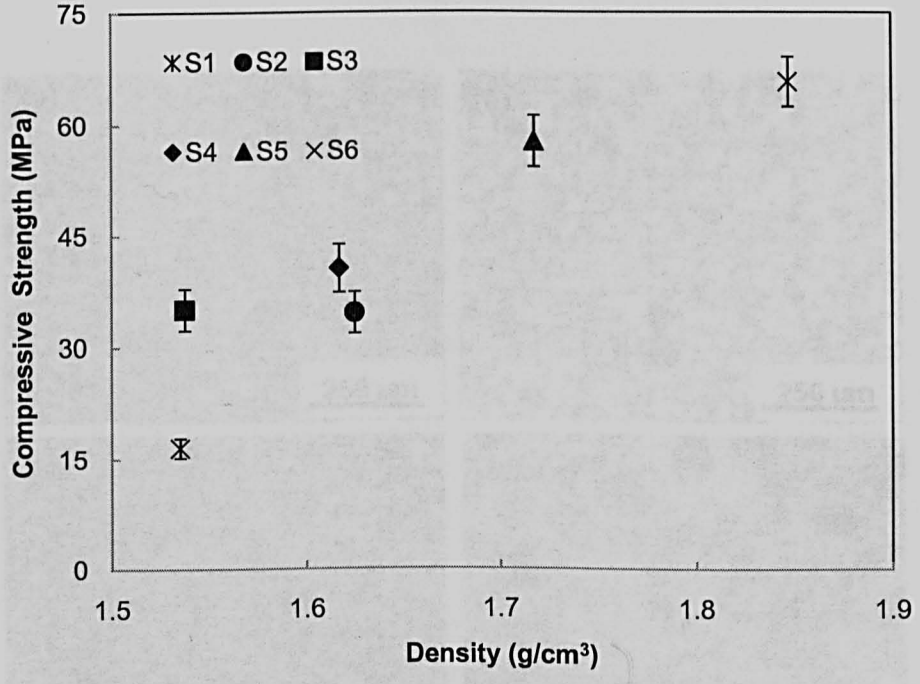

Figure 4.47 *Relationship between compressive collapse strength and foam density* for *Foams* S1-S6

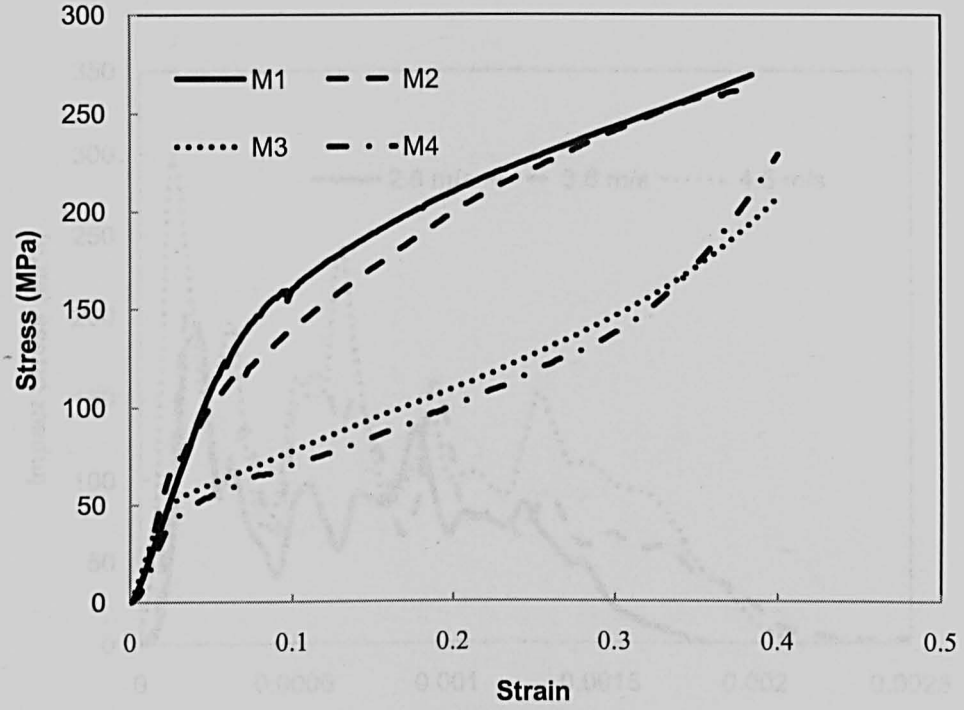

Figure 4.48 *Constrained compression response of Foams M1, M2, M3 and M4*

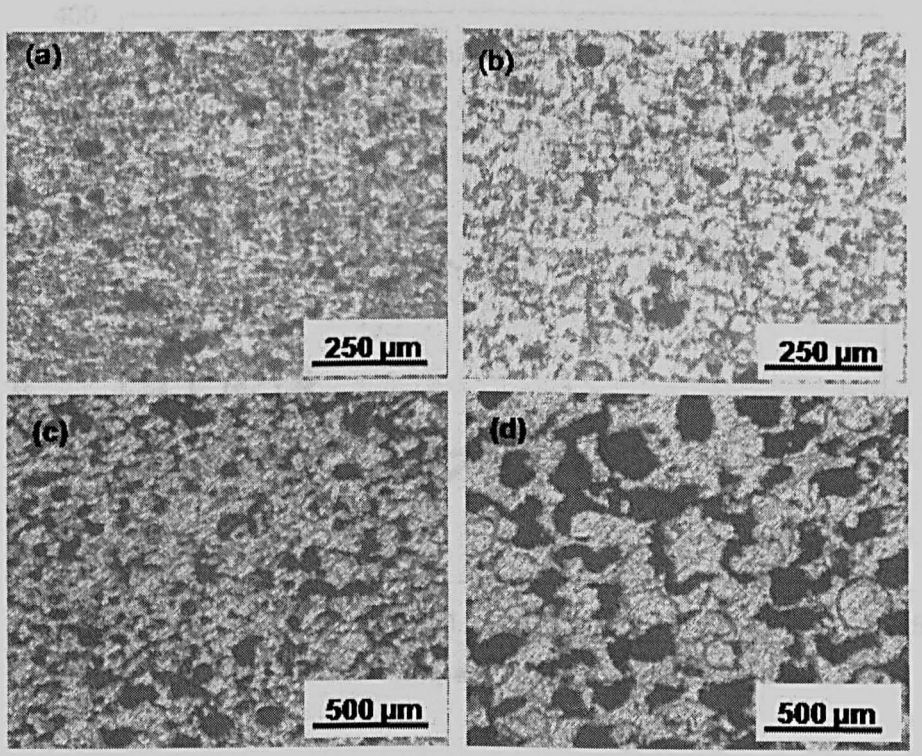

Figure 4.49 *Micrographs of polished cross sections of Foams (a) M1, (b) M2, (c) M3 and (d) M4 at the strain of 0.35 after confined compression*

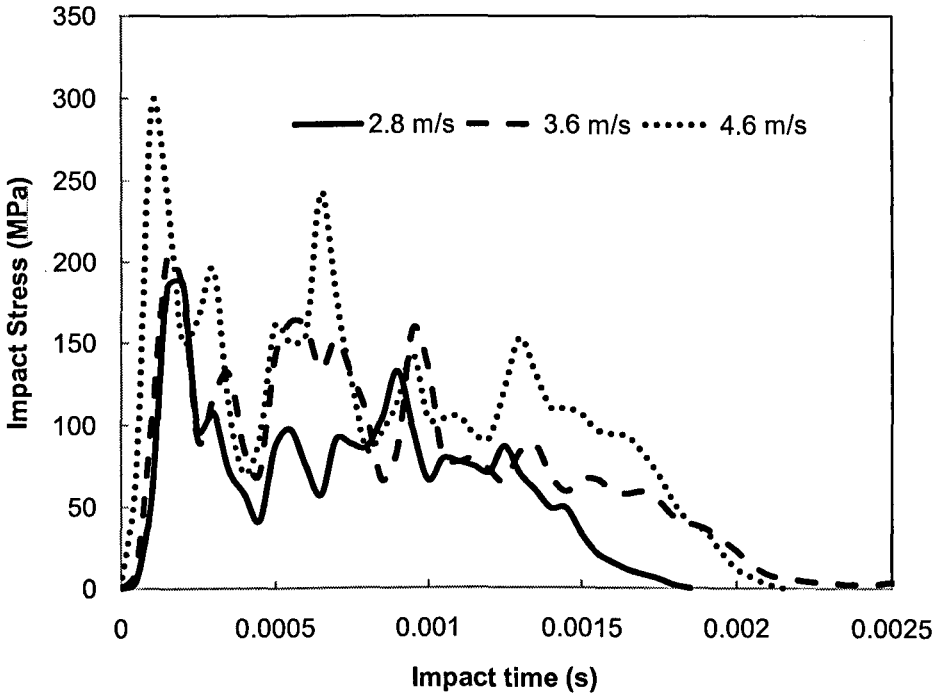

(a)

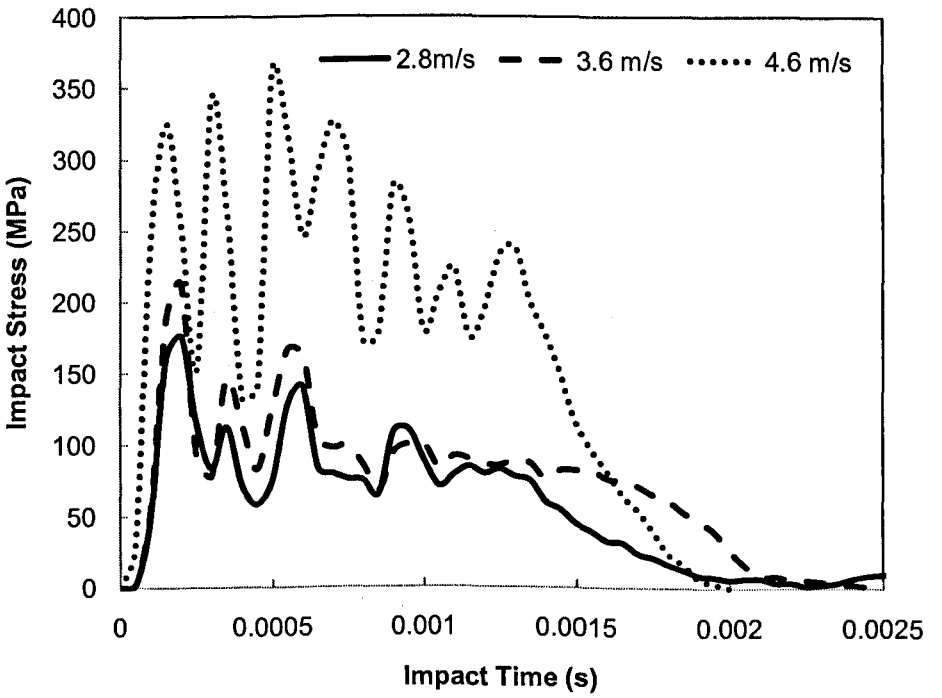

(b)

Figure 4.50 *Stress-time traces of Foams (a) M1, (b) M2, (c) M3 and (d) M4 at three different impactor speeds in drop-weight test (to be continued)*

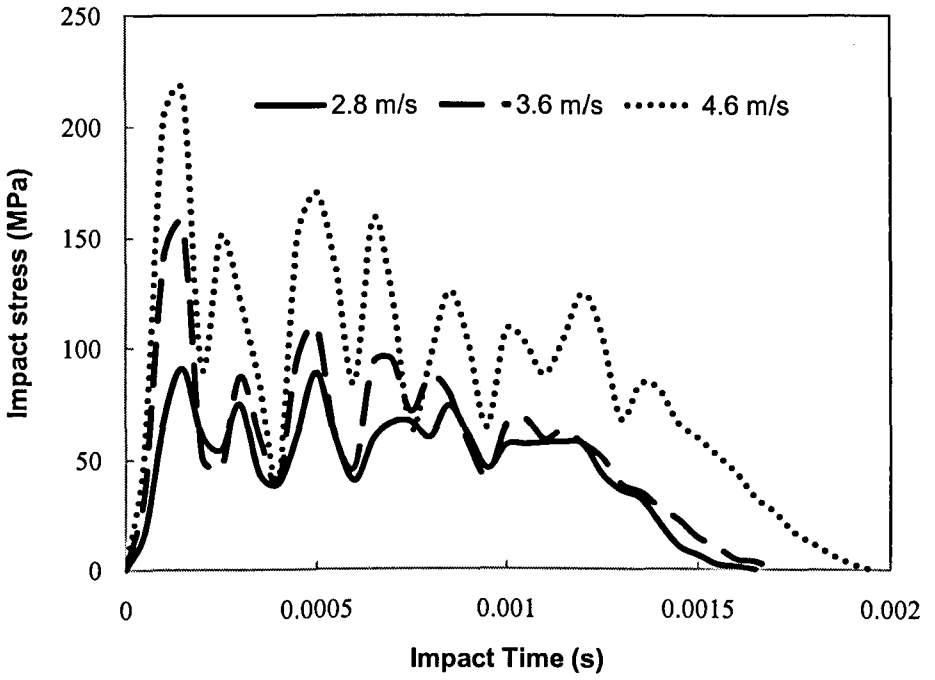

(c)

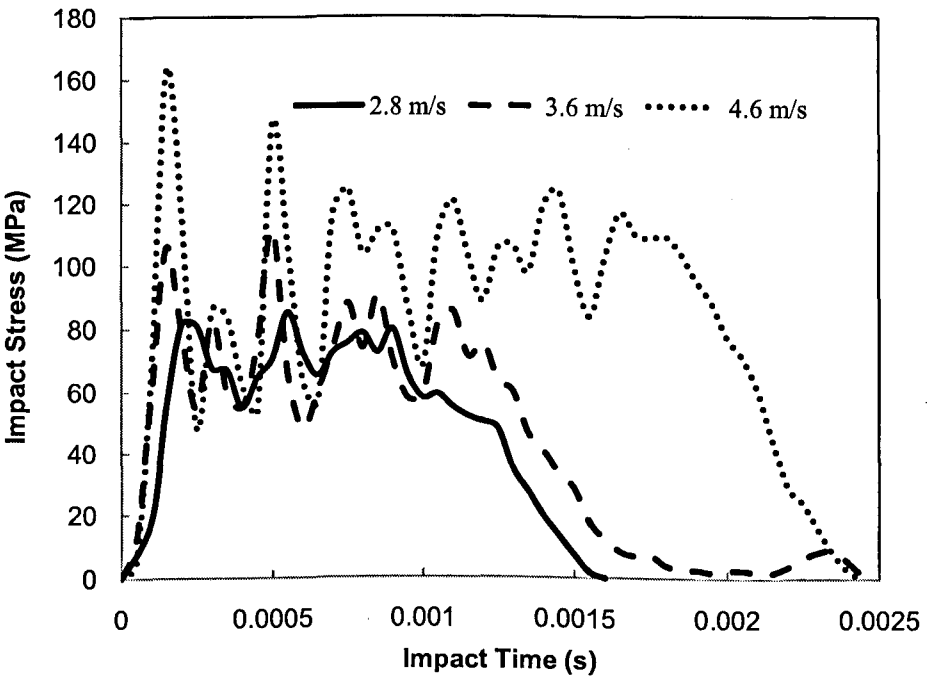

(d)

Figure 4.50 *Stress-time traces of Foams (a) M1, (b) M2, (c) M3 and (d) M4 at three different impactor speeds in drop-weight test (continued)*

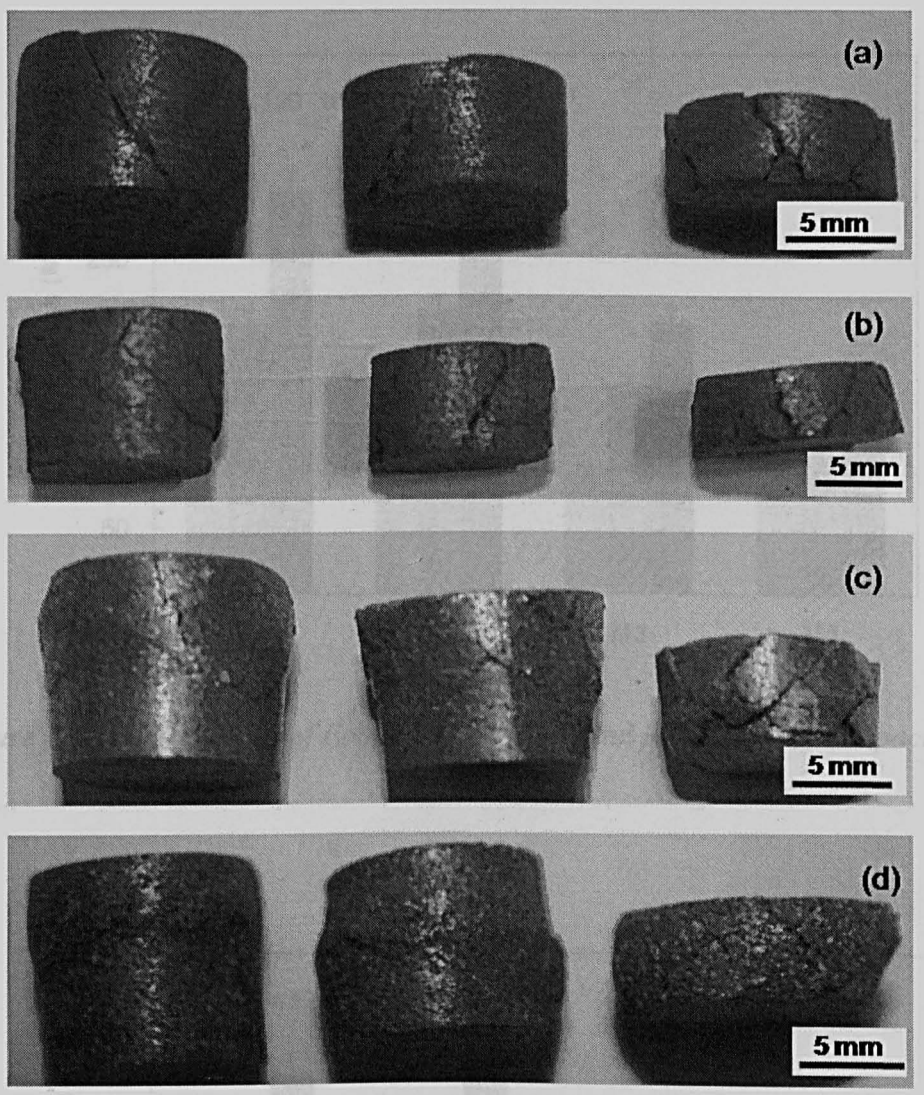

Figure 4.51 *Macrographs of Foams (a) M1, (b) M2, (c) M3 and (d) M4 after impact at different speeds (2.8, 3.6 and 4.6 m/s from left to right)*

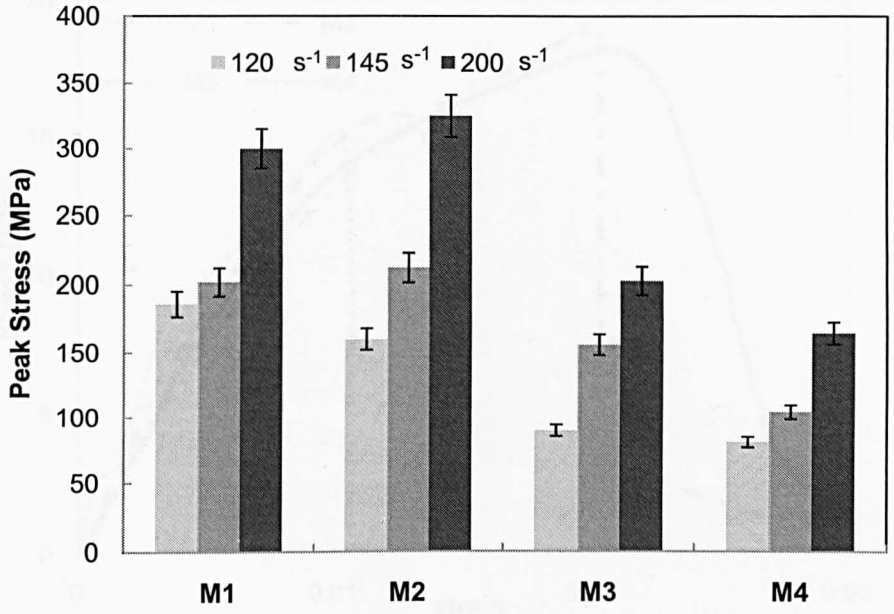

Figure 4.52 *Peak stresses of Foams M1, M2, M3 and M4 at different impact stain rates*

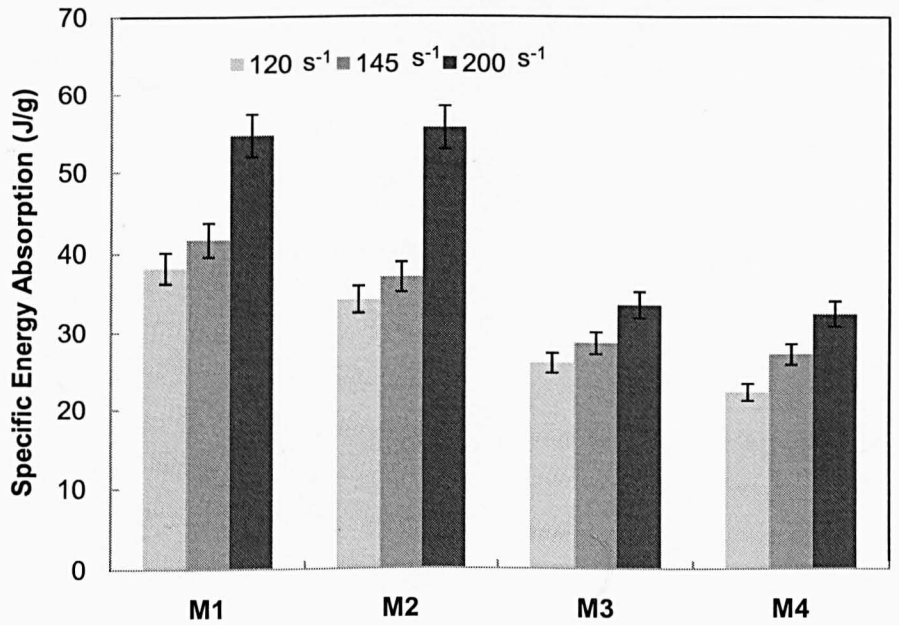

Figure 4.53 *Specific energy absorption of Foams M1, M2, M3 and M4 at different impact stain rates*

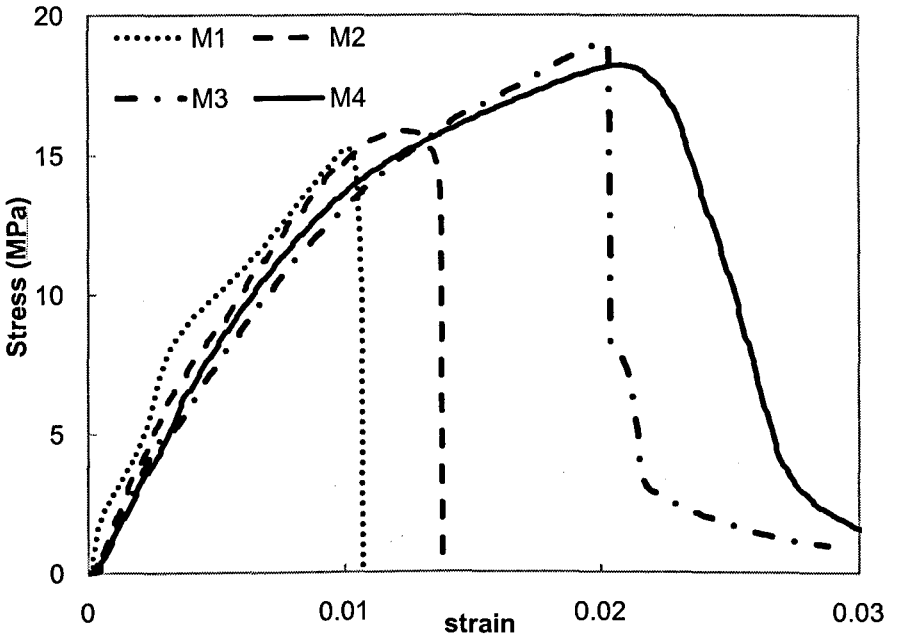

Figure 4.54 *Tensile response of Foams M1, M2, M3and M4*

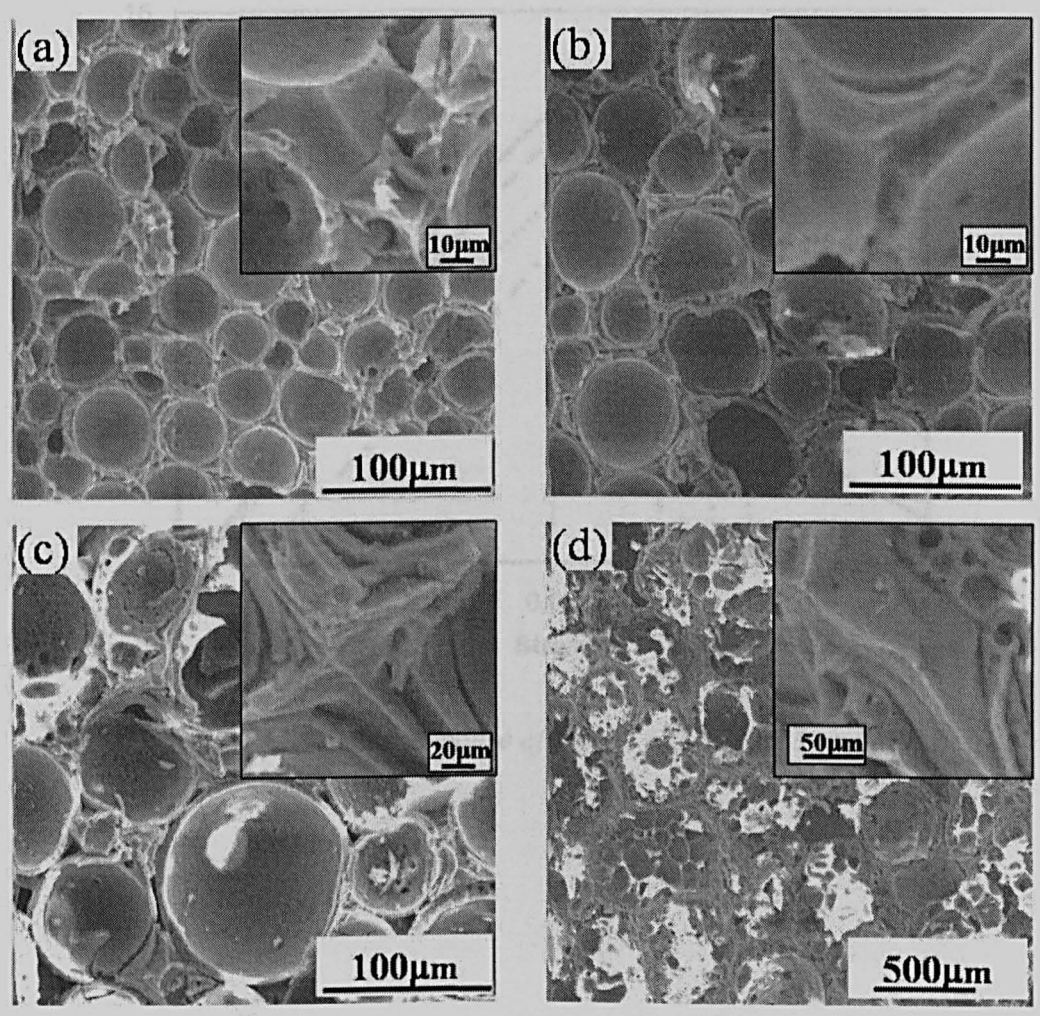

Figure 4.55 *Micrographs of tensile fracture surfaces for Foams (a) M1, (b) M2, (c) M3 and (d) M4. The magnified insets show the fracture surfaces of the Al matrix*

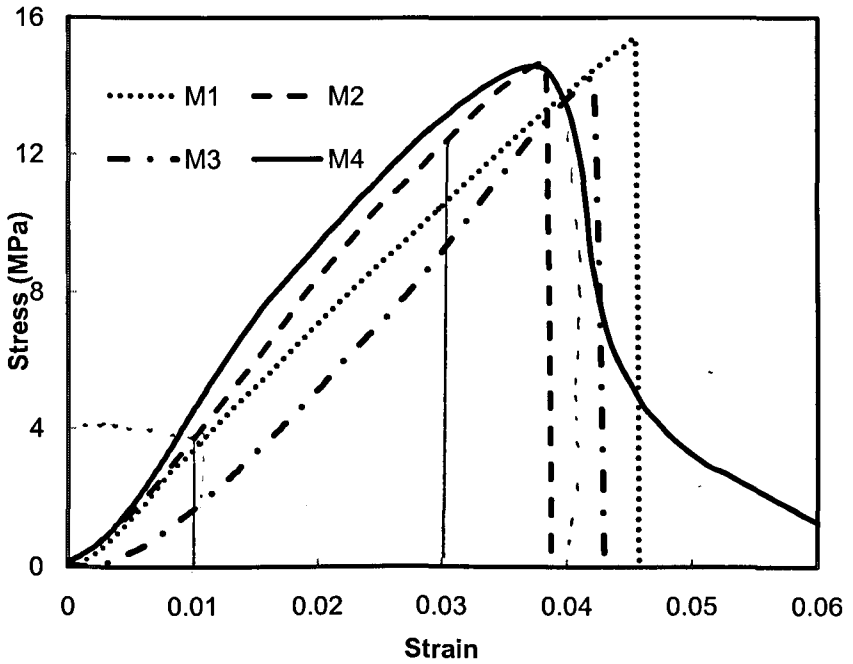

Figure 4.56 Shear response of Foams M1, M2, M3 and M4.

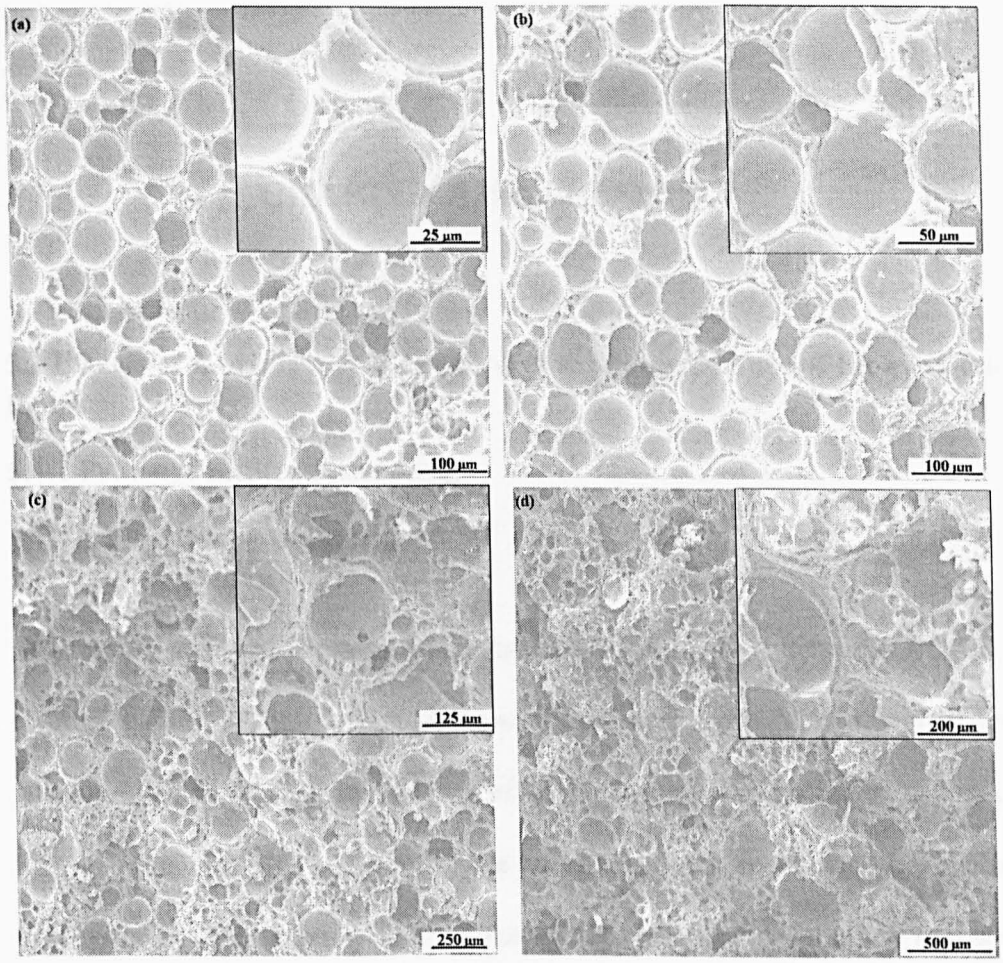

Figure 4.57 *Micrographs of shear fracture surfaces for Foams (a) M1, (b) M2, (c) M3 and (d) M4. The magnified insets show the fracture surfaces of the Al matrix*

CHAPTER 5 DISCUSSIONS

5.1 Effects of fabrication conditions on the microstructure of the syntactic foams

5.1.1 Pressure infiltration casting

5.1.1.1 Flow routes of molten Al

In pressure infiltration casting, the molten Al fills the interstices of the CMs through two flow routes. One is through the interior of CM compact (Route A) and the other is through the surface of CM compact near the inner surface of the tube (Route B). The location where the two routes meet and the infiltration process completes is determined by the relative resistance of the two routes to the flow of the molten Al, as shown schematically in Figure 5.1. In Figure 5.1(a), the resistance of Route A is greater than Route B. The molten Al will first arrive at the bottom of the CM compact through Route B and then flow up through the interior of the CM compact. The flows by Routes A and B will meet inside the lower part of the CM compact. In Figure 5.1(b), the resistance of Route A is less than Route B and the flows will meet at a location near the circumferential surface of the compact.

If the molten Al solidifies before reaching the end of the route, or its fluidity decreases to such an extent that it cannot displace the air trapped inside the CM

compact, or the infiltration pressure is too low to overcome the viscous resistance, then the region where Routes A and B meet cannot be infiltrated, resulting in casting defects. Figure 5.2 shows two typical samples which were not well infiltrated by molten Al, with the casting defects near the surface or in the interior of the samples respectively.

The resistance of the routes in the CM compacts to the molten Al flow depends not only on the local packing of the CMs but also on the temperature variation of the Al flow. The latter is more critical than the former. On the one hand, the interior of the CM compact normally has a lower temperature because of poor thermal conductivity of the CMs. On the other hand, the surface of the compact is subject to more rapid cooling when the Al/CMs/tube assembly is transferred from the furnace to the press for pressure infiltration. Depending on which factor is more dominant, either Route A or Route B may have a higher resistance than the other, resulting in the defects as shown in Figure 5.2. Therefore, proper infiltration pressure and temperature must be maintained throughout the infiltration process to facilitate good flow conditions of the molten Al through both flow routes in order to eliminate casting defects.

5.1.1.2 Heating procedure

In casting, the casting temperature of the molten metal is usually about 100°C above the liquidus temperature of the metal to guarantee its fluidness (Nadler *et al.* 1999). In the fabrication of the syntactic foams with either Al 6082 or 2014 alloy

matrix in this study, the molten Al was kept at 720°C before infiltration. As the liquidus temperatures for Al 6082 and 2014 alloys provided by the suppliers are 650°C and 638°C, the degrees of overheat are less than the recommended value. However, they are proved to be sufficient if the CM compact is pre-heated before the infiltration operation.

Al and CM particles have very different thermal conductivities. To ensure that both the CM compact and the Al block inside the furnace can reach the casting temperature at the point of pressure infiltration, a holding time of half hour was maintained after the furnace reached the set temperature. This operation is to minimise the temperature loss of the molten Al and thus to maintain its fluidity during the infiltration process. Figure 5.3 shows the bottom of two samples fabricated by infiltration with molten Al 6082 at 720°C. The one with the CM compact heated to 720°C and immediately infiltrated has defects. The one with the CM compact heated to 720°C and held for half hour shows no defects.

5.1.1.3 Infiltration pressure

Garcia-Cordovilla *et al.* (1999) proposed a semi-empirical equation to predict the effect of size and volume fraction of packing particles to the minimum infiltration pressure:

$$P_0 = 16\frac{f}{(1-f)D} - 0.09 \qquad (5.1)$$

where P_0 (MPa) is the minimum, or threshold pressure, f is the volume fraction of the particles in the compact and D (μm) is characteristic diameter of the particles. Eq. 5.1 was based on data for particles in the range of 10-100 μm packed to a density of 50-60% and infiltrated with pure aluminum. However, Marchi and Mortensen (2002) considered that the relationship should provide reasonable estimates of the pressure required for infiltration over a broader range of conditions (Mortensen & Cornie 1987, Mortensen & Jin 1992, Garcia-Cordovilla *et al.* 1999).

In this study, the volume fraction of the CMs is largely fixed and is about 0.67. The four CM powders, I, II, III and IV, have size ranges of 20-75 μm, 75-125 μm, 125-250 μm and 250-500 μm. Using the median values of the four size ranges, 47.5 μm, 100 μm, 187.5 μm and 375 μm, the minimum infiltration pressures for the above four types of CMs are estimated by Eq. 5.1 to be 0.59, 0.23, 0.08 and -0.003 MPa, respectively. Clearly, Eq. 5.1 is not applicable for large CM powders. The infiltration pressure needed for sufficient infiltration in this study is found to be higher than the infiltration pressures estimated by Eq. 5.1. This is likely due to the different properties of the ceramic particles used in developing Eq. 5.1 and used in this study, which can lead to very different flow resistance to molten Al.

However, the infiltration process is indeed found to be sensitive to the size range of CMs used. Figure 5.4 shows the samples of Foams M1, M2, M3 and M4 fabricated by infiltration at a pressure of 1 MPa. It is found that the coarser the

CMs in the CM compact, the longer the resultant syntactic foam samples are indicating that the deeper the molten Al can infiltrate.

5.1.2 Liquid sintering

5.1.2.1 Heating procedure

The heating procedure in liquid sintering was different from that used in pressure infiltration casting. In melt infiltration, the Al was in the form of a block. When it was melted, the oxidation of Al was limited because only the top surface was in contact with air. In liquid sintering, the Al was in the form of powder and there existed voids in the powder mixture. The Al particles can be easily oxidized during the heating process. Argon protection was necessary to prevent the Al from extensive oxidation.

5.1.2.2 Pressure

During the fabrication of Al syntactic foams by liquid sintering, a pressure is applied by a piston. The purpose of the application of pressure is different from that in solid powder sintering, where high pressure leads to better sintering because of increased necking between the metal particles. In the randomly packed mixture of CM and Al powders, a large amount of air exists between the particles. The first purpose of pressure application is to expel the air in the mixture by re-locating and densifying the Al and CM particles. The second purpose is to deform

the molten Al particles, which have an alumina skin, so that they are fused to form a continuous Al matrix. Because the average compressive strength of the CMs provided by the supplier is 60 MPa, the pressure in the liquid sintering process is restricted to 50 MPa. This pressure is not high enough to remove all the air in the Al-CM mixture, so there is still porosity in the Al matrix of the samples.

5.2 Microstructure of the syntactic foams

5.2.1 Syntactic foams fabricated by pressure infiltration casting

The microstructure of the syntactic foams fabricated by pressure infiltration casting depends on the inner structure of the CMs. Under the standard infiltration pressure of 3 MPa, a small number of CM particles were found to be infiltrated with Al in all the syntactic foams fabricated by pressure infiltration casting. The infiltrated CMs remained in the original spherical shape, as shown in Figures 4.5 and 4.6. This indicates that the molten Al got into the particles through cracks that were exsiting before the pressure infiltration and were not formed by the compression during the infiltration process. The porous CMs have thin membranes which are more prone to be broken and therefore are more defective than the hollow CMs. As a consequence, the number of infiltrated CM particles increases with increasing the volume fraction of porous CMs.

The number of infiltrated CMs is also affected by the infiltration pressure. When higher infiltration pressures of 4, 7 and 9 MPa were applied, the number of infiltrated CMs in Foam M4 is increased, as shown in Figure 4.6. This is because

a higher pressure will make molten Al pass through narrower cracks that have not been possible at lower pressures.

5.2.2 Syntactic foams fabricated by liquid sintering

The Al/CM particle size ratio has a considerable effect on the structure of the syntactic foam fabricated by liquid sintering. Among Foams S1, S2 and S3, which contain 40% Al with CMs II, III and IV, respectively, Foam S1 has the worst and Foam S3 has the best bonding between the Al particles and CMs. Moreover, the agglomerations of CMs are found in the micrographs of Foams S1 and S2, as shown in Figure 4. 11. The bonding of Al and CMs particles was improving with the increase of CMs size embedded in the Foam. In other words, larger CMs lead to better bonded Al matrix in the syntactic foam. The size effect can be explained by the difference in particle sizes between the Al and CM powders. The average size of Al is 53 μm, which is smaller than the sizes of all the CMs used in this study. If the Al particles are much smaller than the CMs (e.g. Foam S3), the Al particles can fill the spaces between the CM particles well and therefore are in good contact with each other, leading to a good bonding between the Al particles during liquid sintering. If the Al particles are closer to the CMs in size (e.g. Foam S1), some large Al particles cannot fill in the spaces between the CM particles, leading to poor contact between the Al particles in certain locations and therefore weak bonding between the Al particles during subsequent liquid sintering.

With the value above 40%, the volume fraction of Al also has little effect on the structure of the syntactic foam. Foams S3, S4, S5 and S6, which contain 40%, 50%, 60% and 70% Al, respectively, all have roughly uniform distribution of CMs, although Al agglomerations were found S5 and S6 due to the high volume fraction of the matrix. Voids found in all the micrographs of Foams S3, S4, S5 and S6, this is because the low value of compaction pressure to avoid the fracture of the CMs.

5.3 Density and porosity

5.3.1 Monomodal syntactic foams

As reported by Hartmann *et al.* (1999), the volume fraction of air in a compact of randomly packed CMs with a similar size is approximately 63%, which also applies to the monomodal CMs in this study. The volume fractions of the Al matrix of the resultant monomodal syntactic foams, M1-M8, should also be similar. Although the CM powders, I, II, III and IV, embedded in the syntactic foams have different volume ratios of porous and hollow particles, they have a similar density and porosity. As a consequence, Foams M1-M8 should have similar density and porosity.

The experimental values of density showed that the syntactic foams (M3, M4) containing more porous CMs have slightly higher density and lower porosity values than those (M1, M2) with more hollow CMs. The difference is because

porous CMs are more prone to be infiltrated by molten Al, as discussed in Section 5.2.1.

The experimental values of density and porosity are also affected by the infiltration pressure. The density of Foam M4 was increased by more than 30% when the infiltration pressure was increased from 3 to 9 MPa. When the infiltration pressure was higher than the standard value, more CM particles were infiltrated by molten Al, as discussed in Section 5.2.1. Therefore, a higher infiltration pressure can result in a higher density and lower porosity.

5.3.2 Bimodal syntactic foams

The bimodal syntactic foams, B1-B6, have lower densities than the monomodal syntactic foams, M1-M4. Foam B1 has the lowest density, which is about 78% of the density of the monomodal syntactic foam M1. The density of bimodal syntactic foams is found to vary with the volume ratio of the embedded fine and coarse CMs. Foams B1, B2 and B3, which have volume ratios between CM II and IV of 30:70, 50:50 and 30:70, have an increasing trend in their density. The density of Foams B4-B6 firstly decreases and then increases with the volume ratio between CM I and IV increasing from 20:40 to 60:40.

The lower density of bimodal syntactic foams than that of monomodal syntactic foams is due to more CMs in these foams. This can be explained by the effect of

bimodal packing on the volume percentage of CMs in the syntactic foam as illustrated in Figure 5.5. In a syntactic foam embedded with monomodal CMs, the CMs are randomly packed as shown in Figure 5.5(a). The volume percentage of the CMs in the syntactic foams is lower than that of the close packing of monosized spheres (74%) but is more or less fixed (67%). For a stack of monosized coarse CMs, adding fine CMs can increase the overall volume percentage of CMs. As long as the fine CMs are fully accommodated in the interstices between the coarse particles, as illustrated in Figure 5.5(b), the overall volume percentage of CMs increases with increasing amount of fine CMs. When the amount of fine CMs is increased further, however, the coarse CMs are pushed apart and areas of randomly packed fine CMs are formed (Figure 5.5(c)), which is equivalent to monomodal packing. As a consequence, the overall volume percentage of CMs in the syntactic foam starts to decrease.

The different variation trends in density for Foams B1-B3 and B4-B6 are due to different sizes of fine CMs in the two types of bimodal syntactic foams. In Foams B1-B3, when the volume percentage of CM II increases from 30% to 50%, no more fine particles can locate in the inter-particle spaces of the CM IV. The density of Foams B1-B3 thus can have an ascendant trend with the fine CM increasing from 30% to 50%. In Foams B4-B6, when the volume percentage of CM I increases from 20% to 40%, there is still inter-particle spaces in CM IV to fill with CM I due to small particle size of CM I than CM II. The density of the syntactic foam has a descendant trend. When the volume percentage of CM I increase to 60%, the density of the syntactic foam starts to decrease due to the

similar effect in Foams B1-B3. It seems there is an optimum volume ratio for fine and coarse CMs to obtain the lowest density for syntactic foams fabricated with bimodal CMs.

There exist many studies on the relationship between packing density (the volume fraction of the solid particles in the total packing volume) and particle size of particle size distribution and on the optimum particle composition that would yield the maximum packing density (Andreasen & Andersen 1929, Furnas 1931, Westman 1936, Ouchiyama & Tanaka 1981, Ortega *et al.*1999, Liu & Ha 2002). Among these studies, Westman (1936) proposed a simple conical expression for predicting the porosity of bimodal mixtures, which is explicitly written as (Yu, Standish & Mclean 1993):

$$\left(\frac{V-V_L X_L}{V_S}\right)^2 + 2G\left(\frac{V-V_L X_L}{V_S}\right)\left(\frac{V-X_L-V_S X_S}{V_L-1}\right) + \left(\frac{V-X_L-V_S X_S}{V_L-1}\right)^2 = 1 \qquad (5.2)$$

where V is the specific volume of the binary mixture, V_L and V_S are the initial specific volumes of the large and small particles, and X_L and X_S are the volume fractions of the large and small particles (X_L=1- X_S), respectively. The specific volume is defined as the volume occupied by a unit volume of solid particles. The packing parameter G is given by (Yu, Standish & Mclean 1993):

$$\frac{1}{G} = \begin{cases} 1.355r^{1.566} & (r \leq 0.824) \\ 1 & (r > 0.824) \end{cases} \qquad (5.3)$$

where r is the size ratio of the small particle to the large particle. This formula was found to work well for the packing of binary mixtures for both spherical particles and nonspherical particles (Marmur 1985, Yu, Standish & Mclean 1993, Liu & Ha 2002).

All the CMs used in Foams B1-B6 have a random packing density of 0.63. As the specific volume defined in Eq. 5.2 is the reciprocal of packing density, $V_L = V_S = 1/0.63=1.6$ for all CM powders used in this study. The size ratios of small particles to large particles are roughly 0.5 for foams B1-B3 and 0.25 for foams B4-B6 on average, which give the values of G to be 2.18 and 6.47, respectively. Substituting these values into Eq. 5.2 gives the results in a quadratic equation of V and X_S. The packing density of the bimodal mixture, Φ, is the reciprocal of the specific volume of the bimodal mixture ($\Phi = 1/V$) and thus can be determined by this quadratic equation. Figure 5.6 plots Φ as a function of X_S for syntactic foams with binary CM mixtures of II & IV and I & IV. The experimental values of packing density of bimodal CM Foams B1-B6, which are calculated with the average measured density of each foam, average measured value of effective density of the CMs and know density value of Al matrix, are also plotted in Figure 5.6.

The maximum packing volume fractions of bimodal particle mixtures of CMs II & IV and I & IV are to 67% and 70.5%, with the volume fractions of CMs II and I corresponding to 50% and 55%. The experimental data generally agree with the

predictions of the Westman model. Most of the experimental packing volume fractions are lower than the predicted values. The discrepancy can be caused by three deviations from the assumptions. First, the bimodal CM mixture may not be completely uniform. Second, some of the CMs were infiltrated with Al in the fabrication process, which resulted in errors in the calculation in the packing volume fractions. Third, all types of the CMs used in B1-B6 are not monosized.

5.3.3 Syntactic foams toughened with Al particles

The density of syntactic foams fabricated with incorporating additional Al particles can be controlled. As shown in Figure 4.16, the experimental density values of Foams T1-T4 are very close to the theoretical values. The result indicates that it is feasible to fabricate syntactic foams to a design density by embedding additional metal particles, when a high density metallic syntactic foam is desirable.

5.3.4 Syntactic foams fabricated by liquid sintering

The effects of process conditions on the density of the as-fabricated syntactic foams can be studied by examining the experimental density values against the theoretical ones, as displayed in Figure 4.17. The experimental density values can be higher than the theoretical ones, because some CMs are infiltrated with molten Al during liquid sintering. In most cases, however, the measured ones are higher than the theoretical ones because of the existence of voids in the Al matrix.

The density of the syntactic foam fabricated by liquid sintering was found to increase with decreasing Al/CM particle size ratio and with increasing Al volume fraction. This is because the density of the syntactic foam is mainly affected by the amount of voids included in the Al matrix, which in turn decreases with decreasing Al/CM particle size ratio and with increasing Al volume fraction, as discussed in Section 5.2.2.

5.4 Young's modulus

The relationship of relative Young's modulus and relative density for Foams M1, M2, M3 and M4 is displayed in Figure 5.7. The relative Young's modulus is calculated by dividing the measured Young's modulus of the syntactic foam (tested by RFDA) to the Young's modulus of Al 6082, which is 70 GPa. The relative density of the syntactic foam is calculated by dividing the measured density of the syntactic foam to density of Al 6082, which is 2.7 g/cm^3. The Young's modulus of the syntactic foams is found increasing with the increase of sample density. The variation trend indicates that the Young's modulus of the syntactic foam is mainly determined by the volume percentage of the Al matrix. The contribution of the CMs to the Young's modulus of the syntactic foam is limited due to their large porosity (Balch and Dunand 2006). The relationship of relative Young's modulus and relative density for closed cell metal foams (Simone & Gibson 1998b) is also shown in Figure 5.7. For any fixed relative

density, the syntactic foams have a higher relative Young's modulus than that of a metal foam.

5.5 Compressive strength of CMs

The porous and hollow CMs have very different inner structures, as shown in Figure 4.2, and thus different compressive strengths and failure modes. It is difficult to measure the compressive strength of the CM particles due to their small size. When the syntactic foams were under compression, the embedded CMs were subjected to relative uniform compressive stress. With this loading condition, two models may be used to evaluate the compressive strengths of the porous and hollow CMs semi-quantitatively.

For porous ceramic, the following formula for predicting the crushing strength of brittle closed-cell foam (Gibson & Ashby, 1999):

$$\frac{\sigma^*_{cr}}{\sigma_{fs}} = 0.2\left(\emptyset\frac{\rho^*}{\rho_s}\right)^{3/2} + (1-\emptyset)\left(\frac{\rho^*}{\rho_s}\right) \qquad (5.4)$$

where σ^*_{cr}, σ_{fs}, ρ^*, ρ_s are the crushing strength of the brittle foam, flexural strength of the solid material, density of the brittle foam and density of the solid, respectively. The formula separates the solid material distributed in the edge and membrane of the cell and $\emptyset$ is the volume fraction of solid materials on the edge. The porous CMs used this study consist of several cells and the majority of the solid is at the cell edges, as shown in Figure 4.2. The value of $\emptyset$ is estimated to be

in the region of 0.6. With known values of ρ^* and ρ_s of 0.6 and 3.05, the crushing strength of the porous CMs is estimated to be:

$$\sigma_{cr}^* \approx 0.1\sigma_{fs} \tag{5.5}$$

The compressive strength of hollow CMs can be predicted by the theory of spherical vessel under internal or external uniform pressure (Timoshenko & Goodier, 1970). With an external uniform pressure, the compressive strength of the brittle vessel:

$$\sigma_{cr}^* = \frac{2\sigma_s(1-r^3)}{3} \tag{5.6}$$

where r is the ratio of inner diameter to outer diameter of the vessel and σ_s is the yield strength (for ductile material) or flexural strength of solid material of the vessel. The theory is based on elastic deformation of the structure and is therefore suitable for both ductile and brittle materials failing by yielding and fracture, respectively. For hollow CMs, r = 0.9, the compressive strength can be predicted as:

$$\sigma_{cr}^* = 0.18\sigma_{fs} \tag{5.7}$$

Comparing Eq. (5.5) with (5.7) shows that hollow CMs are about twice as strong as porous CMs.

The compressive strength of the four types of CMs was also studied by experiments. The compressive behaviour of all the four types of CMs in the free packed form in Figure 4.29 shows that CM I has a higher crushing strength than

that of CMs II, III and IV, which are similar to each other. However, these results are not sufficient for comparing the compressive strengths of these four CMs, since they are obtained under a point-contact loading condition, which is different from the uniform compression loading of CMs in a syntactic foam.

The results of confined compression tests of syntactic foams M1-M4, as shown in Figure 4.48, may be used to compare the compressive strength of the four CMs quantitatively. In the plastic deformation process of confined compression, with the constraint of the tube, the strain in the transverse direction is very small. The deformation can only proceed in the vertical direction. Therefore, the plastic deformation of the syntactic foam is initiated by the crushing of the CMs. As a consequence, the compressive strength of the confined syntactic foams is mainly determined by the strength of the embedded CMs. The confined compressive strength of foams M1 and M2 is much higher than that of foams M3 and M4, which means the strength of the CMs (mainly hollow structured) embedded in foams M1 and M2 is much higher than that of CMs (mainly hollow structured) in foams M3 and M4. The experimental results agree with the previous predictions that CMs with more hollow particles have higher strength than those with more porous particles.

5.6 Mechanical behaviour in indentation

5.6.1 Indentation load

The indentation collapse load of a syntactic foam is determined to a large extent by its compressive strength (Shaw & Sata 1966, Wilsea *et al.* 1975). The indentation load at any displacement is the sum of the force required to crush the foam beneath the indenter and that required to tear the foam at the perimeter of the indenter (Olurin *et al.* 2000). Because Foams M2, M3 and M4 have a similar volume percentage of Al, they are expected (Zhang and Zhao, 2007) and also measured to have similar shear strength, as shown in Figure 4.57. The collapse load, therefore, largely depends on the maximum force required to crush the foam and is accordingly a function of the compressive plateau strength of the foam. Although the three types of CMs have the same chemical composition, hollow CMs have a higher compressive strength than that of porous CMs, due to different inner structures as discussed in section 5.5. As a consequence, the resultant syntactic foams, Foams M2, M3 and M4, have increasing compressive strengths, leading to increasing indentation collapse loads.

It is worth noting that the Al matrix syntactic foams have a much higher indentation resistance than that of Al foams, although the density of the former is normally much higher than that of the latter. For example, an Alporas closed-cell Al foam with a density of 0.22 g/cm^3 has an indentation yield load of 0.1 kN when tested using an indenter with the same shape and size as the one used in this study

(Olurin *et al.*, 2000). In comparison, the syntactic foams M2, M3 and M4 have a density of about 1.45 g/cm^3 and indentation collapse loads of 2.2, 3.2 and 4.9 kN, respectively.

The use of spreader has a marked effect on the indentation load. For foam M4, the indentation load is gradually increasing with the increase of the thickness of spreader. This is because the deformation of foam M4 is dominated by the layered crush of CMs and Al matrix. Therefore, more load will be shared by the foam with a thicker spreader before the penetration of the spreader. In Foms M2 and M3, the indentation loads do not increase linearly with the increase of spreader thickness. The foams with 0.5 and 1 mm spreaders have a similar indentation load, and so do the foams with 1.5 and 2 mm spreaders. With a thin spreader, most of the load is concentrated in the punch-head area and fractures occur from inside of the indentation hole in the early displacements of the punch. The indentation load is mainly determined by the strength of the spreader, with less load shared by the foam. When the foam is pierced with a thick spreader, more load is shared by the foam before the penetration of the spreader; the indentation load is the combined effect of the foam and the spreader.

5.6.2 Failure modes

The different plastic deformation behaviours between Foam M4 and Foams M2 and M3 are largely because of the different compressive strengths of the foams. The region of the foam outside the indentation hole is subject to an internal

pressure when the sample is subjected to indentation. Foam M4 has relatively low compressive plateau strength. The stress in the region outside the indentation hole may generate a compressive stress higher than the compressive strength of the foam while the shear stress is still below the shear strength of the foam. This region will undergo plastic deformation without brittle fracture. Foams M2 and M3, however, have relatively high compressive strength. The stress in the region outside the indentation hole may generate a shear stress high enough to cause brittle fracture but a compressive stress still below the compressive strength of the foam. As a consequence, cracks are formed. The use of a thick spreader can prevent fracture from occurring because the load is shared by a large volume of the foam. The different sizes of CMs may also affect the ductility in a similar manner as in particulate reinforced metal matrix composites, where the coarser the reinforcement, the more brittle the composite becomes (Smith 2001).

5.7 Compressive behaviour of syntactic foams fabricated by pressure infiltration casting

5.7.1 Compressive strength

5.7.1.1 Effect of Al matrix

The compressive strength of the syntactic foam is sensitive to the strength of the Al matrix. The compressive strength of heat treated M1-M4 is found to be much higher than that of the non-heat treated samples, as displayed in Tables 4.3 and 4.4. This difference is due to the higher compressive strength of the heat treated than the non-heat treated Al 6082 alloy, as displayed in Table 4.2. This result is consistent with the existing studies of metal matrix syntactic foams (Rawal *et*

*al.*1993, Rohatgi *et al.* 1998, Balch & Dunand 2006), where the compressive strength of the syntactic foams was found to increase with increasing compressive strength of the metal matrix. As a consequence, stronger metal matrix results in higher compressive strength of the syntactic foams.

5.7.1.2 Effect of CMs

As discussed in section 5.5, CMs I and II were found to have a higher strength than that of CMs III and IV. With the similar chemical composition, the difference in the strength of the four types is believed to due to their different structures, where hollow structure is stronger than porous structure. With the same Al matrix and a very similar Al/CM ratio, the compressive strength of the syntactic foams increases with increasing volume fraction of hollow CMs in all the embedded CMs. Foam M1 has the highest compressive strength because CM I has the highest volume fraction of hollow CMs. Foam M4 has the lowest compressive strength because CM IV has the lowest volume fraction of hollow CMs. A similar variation trend is found in bimodal foams B1-B3 and B4-B6. For each type of bimodal foams, the compressive strength increases with the volume percentage of the fine CMs, which consist of more hollow CMs. The present finding is in accordance with the existing studies on metal matrix syntactic foams, where the Al_2O_3 spheres with higher wall thickness/radius ratios were reported to result in significantly increased compressive strength of the resultant Al matrix syntactic foams (Rawal *et al.*1993, Kiser *et al.* 1999).

5.7.1.3 Effect of Al/CM ratio

Varying the volume ratio between the metal matrix and the ceramic particles can alter the compressive strength of the syntactic foams. However, the volume fraction of the metal matrix in the metal matrix syntactic foams is difficult to be altered when they are fabricated by the pressure infiltration method. In this study the volume ratio of Al and CMs is varied either by using bimodal CMs or by incorporating Al particles.

The bimodal syntactic foams with higher volume fractions of Al have higher compressive strengths than those with lower volume fractions of Al. Comparing Foams B6 and B5 in terms of the composition of CMs, the former has 60% fine CMs, while the latter has 40% fine CMs. If they had the same Al/CM ratio, B6 would be expect to be stronger than B5 because the fine CMs have a higher strength than the coarse CMs used in this study. In fact, B6 is weaker than B5. This is because Foam B6 has a lower density and a lower volume fraction of Al.

In the syntactic foam toughened with Al particles, the volume percentage of the Al matrix in the syntactic foam can be increased up to 70% from 37%, which is the typical volume percentage of the metal matrix when the syntactic foam is fabricated by pressure infiltration alone. When the volume percentage of Al was increased from 37% to 50%, the compressive strength of the syntactic foam was significantly increased. This can be explained by the lower strength of the CMs

than the Al matrix. When the volume percentage of the Al matrix was increased further from 50% to 70%, however, the compressive strength of the syntactic foam remained nearly unchanged. This is believed due to the compressive strength of the syntactic foam was now largely determined by the compressive strength of the CMs.

5.7.1.4 Load partition of Al and CM

As previously discussed, both the Al matrix and the CMs affect the compressive strength of the foam. However, the compressive strength of the foam seems more sensitive to the strength of the CM than the Al matrix. The hollow structured CMs were predicted to be about twice as strong as the porous CMs. For comparison, the compressive strength of Foam M1 (containing mainly hollow structured CM) is more than twice of Foam M4 (containing mainly porous CM embedded), as shown in Table 4.3. In contrast, although the compressive strength of the heat treated is three times that of the un-heat treated Al, the compressive strength of the foam with heat treated Al matrix was only 10-70% larger than that of the foam with un-heat treated Al matrix, as shown in Tables 4.2 and 4.3.

These results agree with the study of Balch and Dunand (2006), who studied load partition of Al matrix and CMs in Al matrix syntactic foam under uniaxial compression using neutron and synchrotron X-ray diffraction techniques. They reported that the aluminum matrix bears approximately the same stress as it would in a monolithic aluminum sample in the elastic region, while the CMs bear

significantly more stress than the matrix, by a factor of 2 and thus as a reinforcement.

5.7.2 Failure modes

The syntactic foams were found to have very different failure modes during compression. The compressive failure can be either ductile in the form of collapse or crushing of the CMs (e.g. Foam M4, as shown in Figure 4.32), or brittle in the form of shear failure (e.g. Foam T2, as shown in Figure 4.43), or in the form of fracture with cracks at about 30° to the loading direction (e.g. Foams M1 and T1, as shown in Figures 4.32 and 4.43 respectively). The mechanisms and the conditions determining the occurrence of these three failure modes are discussed in this section.

5.7.2.1 Failure mechanisms

Metallic syntactic foams have some structural features in common with each of three very different classes of materials, namely metal matrix composites, porous metals and rocks. The compressive failure modes in metallic syntactic foams can be understood by examining the failure mechanisms existing in these classes of materials.

Metallic syntactic foams and metal matrix composites are similar in that both are composites with ceramic particles embedded in a metal matrix. The theoretical and experimental analyses used for characterising the mechanical behaviour of metal matrix composites are applicable to syntactic foams in the elastic region. Because of the different quantities and different roles of ceramic particles in these two classes of materials, however, the failure mechanisms are usually very different. The solid ceramic particles in metal matrix composites are much stronger than the metal matrix and serve as a reinforcing phase. To maintain reasonable ductility, they normally account for less than 20% in volume. The strength of the composite is therefore sensitive to the weaker phase, i.e., the metal matrix (Kiser *et al.* 1996). As a consequence, metal matrix composites usually behave like solid metals and do not fail by collapse or brittle fracture. In contrast, the ceramic particles in syntactic foams are either hollow or porous. They can be either stronger or weaker than the metal matrix. Furthermore, they often account for up to two thirds of the volume of the syntactic foam. The strength of syntactic foams is therefore more sensitive to the strength of the embedded particles (Kiser *et al.* 1999). The prevailing failure modes are collapsing deformation and brittle fracture. The knowledge accrued for understanding the failure of metal matrix composites has limited application to metallic syntactic foams.

Metallic syntactic foams are porous materials, with the pores being enclosed by ceramic walls of the ceramic particles, which in turn are embedded in a metal matrix. One scenario of compressive loading of a syntactic foam is that the ceramic walls in some of the ceramic particles crumble under the compressive

stress while the metal network retains its integrity. In effect, the metallic syntactic foam becomes a porous metal, with part of the porosity being occupied by intact or broken ceramic particles. In this case, the failure mode of the syntactic foam with a ductile metal matrix is, like porous metals (Gibson and Ashby 1999), gradual collapse by plastic deformation of the metal network through yielding, buckling and stretching (e.g. Foam M4, as shown in Figure 5.8 (a)).

Metallic syntactic foams can be seen as rock like materials when the ceramic particles are in volumetric majority, as is the case for most of the Al matrix syntactic foams in this study. Rocks are aggregates of small grains of minerals and contain many voids and cracks. Metallic syntactic foams with high volume percentages of ceramic particles are in effective aggregates of ceramic particles with the interstices filled with a delicate metal network. Under compression, rocks normally fail by brittle fracture, either due to shear or due to tension failure, and the failure criteria are well known (Jumikis 1983). If the majority of the ceramic microspheres in metallic syntactic foams remain intact during compression, then the syntactic foams are expected to behave like rocks and the failure mechanisms operating in rocks would also be applicable to metallic syntactic foams (e.g. Foam M1, as shown in Figure 5.8 (b)).

From the above discussions, together with examinations of the stress-strain curves and morphological developments in Figures 4.32, 4.40, 4.41 and 4.43, we can ascertain that an Al matrix syntactic foam subjected to compression can fail in one

of three possible failure mechanisms: compressive collapse, shear fracture and tensile fracture. The occurrences of these failure modes can be explained by considering three resolved stresses, namely compressive stress on the ceramic particles, shear stress on a plane with an angle to the loading direction, and tensile stress generated at the tip of a crack, in relation to the compressive, shear and tensile strengths of the metallic syntactic foam or its constituents. When the resolved compressive stress on the ceramic particles exceeds the compressive strength of the particles, the syntactic foam collapses (collapse criterion). When the resolved shear stress on a certain plane exceeds the shear strength of the syntactic foam and overcomes the frictional stress, the syntactic foam fractures by tearing along this plane (Coulomb's criterion). When the resolved tensile stress at the tips of one or more cracks exceeds the local tensile strength of the syntactic foam, the syntactic foam fractures by the growth of the cracks (Griffith's criterion, see Appendix). The mechanism that operates in a particular condition depends on which criterion is met first. These three criteria will be discussed separately in the following sections.

5.7.2.2 Collapse criterion

Confined compression tests provide a direct measurement of the collapse strength of metallic syntactic foams. In an axial-loading compression test of a cylindrical specimen radially confined in a hard jacket, there is only a small amount of deformation in the radial direction due to slack and jacket expansion; the major deformation is limited to the axial direction. The collapse strength of the syntactic foam is simply the stress at which the strain starts to increase rapidly as a result of

progressive collapse of the ceramic microspheres. In a compressive stress-strain curve, the collapse strength corresponds to the transition from the initial elastic region to the plateau region. It can be taken as the interception between the asymptotes of these two regions.

The onset of collapse of the ceramic microspheres takes place when the resolved compressive stress on the ceramic microspheres in the Al matrix syntactic foam exceeds the compressive strength of the ceramic microspheres. According to the study of Balch and Dunand (2006) on similar syntactic foams, the CMs bears approximately twice the applied stress on the syntactic foam in the elastic region. Whether the CMs will collapse or not then becomes a problem of assessing whether the compressive stress exceeds the half the compressive strength of the CMs. The collapse criterion can therefore be expressed as:

$$\sigma_c = \frac{\sigma_{cm}}{2} \tag{5.8}$$

where σ_c is the compressive stress on syntactic foams and σ_{cm} is the compressive strength of the ceramic microspheres.

The compressive strength of the CMs is a critical parameter determining whether the syntactic foam will fail by plastic collapse or by brittle fracture. CMs I and II have higher strengths than CMs III and IV, according to both theoretical prediction and experimental results of confined compression for Foams M1-M4. Therefore, Foams M3 and M4 are more likely to fail by plastic collapse than

Foams M1 and M2. This has been proved by the experimental results, as shown in Figures 4.32-4.34.

However, the collapse mechanism may not take precedence, especially when the strength of the CMs is high. When the strength of the CMs is high (Foams M1 and M2), the syntactic foams fail by brittle fracture. Even in the confined compression, brittle fracture has already happened in Foams M1 and M2 before they collapse, as evidenced by the minor abrupt drops in their stress-strain curves at a stress of 125 MPa for M1 and 75 MPa for M2, as shown in Figure 4.48.

5.7.2.3 Griffith's criterion

In the present work, the cracks developed in Foams M1 and M2 were found to be at a similar angle to the loading direction. The average angle for the twenty cracks found in the samples was 31.6±2.2°. This phenomenon is in accordance with Griffith rupture for brittle solids in which fracture cracks are inclined to propagate at an angle of 30° to the loading direction when the specimen is subjected to uniaxial compression (Griffith 1924, Jayatilaka 1979).

In Griffith's analysis, the compressive stress applied to a brittle solid containing an elliptical crack generates a tensile stress at the tip of the crack. When this tensile stress reaches the tensile strength of the material, rupture occurs. In uniaxial compression, the compressive stress at which the crack starts to propagate

is a function of the tensile strength of the material (obtained when the direction of crack growth is 90° to the loading direction), σ_T, and the angle of the crack to the loading direction, θ, and can be expressed by (Jayatilaka 1979):

$$\sigma = \frac{2\sigma_T}{sin\theta(1-sin\theta)} \tag{5.9}$$

The minimum value of σ occurs when $d\sigma/d\theta = 0$, i.e., $\theta = 30°$. In other words, the crack most likely propagates at an angle of 30° to the loading direction. At this angle, the maximum compressive stress the material can withstand without fracture, i.e., the compressive strength is eight times of its tensile strength. In general, Griffith's criterion can be expressed as:

$$\sigma = 8\sigma_T \tag{5.10}$$

The tensile strengths of Foams M1 and M2 are measured to be 15.2 and 15.8 MPa, respectively. The syntactic foams exhibited very limited elongation during the tensile tests and the fracture direction was perpendicular to the loading direction. The tensile strength values therefore satisfy the applicability condition of Eq. (5.10). The values of the compressive strength of Foams M1 and M2, predicted by Eq. (5.10), would be 121.6 and 126.4 MPa. The predicted values are close to the measured values, which are 128.8 and 123.7 MPa for Foams M1 and M2 respectively. This indicates that Griffith rupture is the most likely failure mechanism in Foams M1 and M2.

Griffith criterion is related to the tensile strength of the syntactic foam, which is largely independent of the mechanical properties of the ceramic microspheres.

Foams M3 and M4 have slightly higher tensile strengths than those of Foams M1 and M2, as shown in Figure 4.53. If Griffith fracture were the predominant failure mechanism in Foams M3 and M4, they would be expected to have slightly higher compressive strengths than Foams M1 and M2. In fact, their compressive strengths are much lower. This is because the ceramic microspheres used in manufacturing Foams M3 and M4, i.e., CMs III and IV, have lower compressive strengths. Under compressive stress, they collapse first before Griffith criterion is met.

5.7.2.4 Coulomb's criterion

Shear fracture is an important failure mechanism in syntactic foams, because they have relatively low shear strength. There are three criteria for shear failure, namely Tresca, Coulomb and Mohr (Jumikis 1983). Tresca's criterion is a special case of Coulomb's criterion and is usually not valid for brittle materials. Mohr's criterion is experimentally established and is therefore difficult to apply for general analysis. While it is more accurate than Coulomb's criterion, it does not have the simplicity required for an insightful mechanistic understanding. Coulomb's criterion is therefore chosen here for shear analysis, because it is simple to apply and in the same time captures the important characteristics of rock-like materials.

Coulomb's criterion takes into account not only the shear stress but also the friction along the crack faces. Under an applied compressive stress σ, a crack with

an orientation angle θ to the loading direction is subject to a resolved shear stress along the crack plane, $\frac{\sigma}{2}sin2\theta$, and a resolved compressive stress normal to the crack plane, $\frac{\sigma}{2}(1-cos2\theta)$. The normal stress component results in a friction along the crack plane and in effect reduces the shear stress component. The effective shear stress along the crack plane is therefore (Jaeger *et al.* 2007):

$$\tau_e = \frac{\sigma}{2}sin2\theta - \mu\frac{\sigma}{2}(1-cos2\theta) \tag{5.11}$$

where μ is the coefficient of friction. For a fixed friction coefficient μ, the maximum effective shear stress occurs when $d\tau_e/d\theta = 0$, i.e., at $\theta = \text{arcctg}(\mu)/2$, and its value is

$$\tau_{em} = \frac{\sigma}{2}\left(\sqrt{1+\mu^2}-\mu\right) \tag{5.12}$$

When this maximum effective shear stress exceeds the shear strength of the material, shear fracture occurs at an angle of $\text{arcctg}(\mu)/2$ to the loading direction. Coulomb's criterion can therefore be written as:

$$\sigma = \frac{2\sigma_s}{\sqrt{1+\mu^2}-\mu} \tag{5.13}$$

where σ_s is the shear strength of the material.

In shear fracture, the friction coefficient of the material apparently has a decisive influence on the magnitude of the maximum shear stress and the angle of the fracture plane. Unfortunately, the values of friction coefficient of metallic syntactic foams are not readily available and may not be obtainable by

experimental measurements. However, Coulomb's criterion, Eq. (5.13), can still provide some valuable insight into the occurrence of shear fracture.

The shear tests have shown that Foams M1 and M2 have similar shear strengths (15.4 and 15.8 MPa) and compressive strengths (128.8 and 123.7 MPa). Substituting these values into Eq. (5.13) would give friction coefficient values $\mu >$ 1.3 and fracture plane angles $\theta < 19°$. The measured fracture plane angles, however, are in the range of 29 ~ 34°, and are much higher than the predictions based on Coulomb's criterion. This further confirms that the fracture of Foams M1 and M2 under unconfined compression was not a result of shear failure.

The fact that shear fracture was not predominant in Foams M1 and M2 implies that the values of friction coefficient are greater than 1.3. The predicted values seem very high, but are not considered to be unrealistic. The syntactic foams contain relatively large ceramic particles interlocked together. The interfacial paths between the ceramic particles and the metal matrix, or the neighbouring particles, can be considered as existing cracks. These cracks are extremely rough, giving rise to significant resistance to sliding, i.e. a high friction coefficient in effect.

5.7.2.5 Effects of foam structure

In essence, the failure mode of a syntactic foam is determined by the relative load bearing capabilities of the two constituent phases, i.e. the metal matrix and the ceramic microspheres. For any given metal-ceramic system, the load bearing capabilities of the two phases are largely determined by two key structural parameters: the volume fraction of the metal matrix and the microstructure of the ceramic microspheres.

The microstructure of the ceramic microspheres determines their strength, which in turn determines whether the syntactic foam fails by plastic collapse or brittle fracture. For the same density or porosity, hollow ceramic microspheres are stronger than porous ones. Syntactic foams manufactured with hollow ceramic microspheres have higher compressive strengths but are more prone to brittle fracture failure. They are more suitable for applications requiring low weight and high stiffness or strength, e.g. lightweight panels. In contrast, syntactic foams manufactured with porous ceramic microspheres are less prone to fracture and thus have a better structural integrity. They can produce a large amount of volume reduction under compression before complete failure and therefore are more suitable for energy absorption applications.

5.8 Compressive behaviour of syntactic foams fabricated by liquid sintering

5.8.1 Compressive strength

5.8.1.1 Effect of Al/CM particle size ratio

The compressive strength of the syntactic foam fabricated by the liquid sintering method can be affected by the size ratio of the Al and CM particles used. Foams S1, S2 and S3, which were fabricated with 40% Al but different CMs, I, II and III, show different compressive strengths in Figure 4.45(a). Foams S2 and S3 have a similar compressive strength, which is much higher than that of Foam S1. This is because the spatial distribution of the powder mixture for syntactic foams S1, S2 and S3 can be affected by the size ratio of Al and CM powders. Because the Al particles used in this study are finer than the CM particles, with larger CMs, Al particles are located between the CM particles. In Foam S1, the size of the CMs is comparable to that of the Al particles. Due to the low volume fraction of Al, some Al particles may be separated and do not form good contact, leading to weaker bonding during sintering.

5.8.1.2 Effect of volume fraction of Al particles

The compressive strength of Foams S3, S4, S5 and S6 is found to increase with increasing Al volume percentage in the syntactic foam. This is mainly because the Al matrix has a higher strength than the CMs, as discussed in Section 5.7.1.3. Another reason is pertinent to the spatial distribution of the Al particles as discussed in Section 5.8.1.1. With more Al, the Al particles have higher chances of good contact with each other, leading to better bonding during sintering.

5.8.1.3 Effect of oxide

With a similar volume percentage of Al, the compressive strength of the syntactic foams fabricated by liquid sintering is lower than that fabricated by pressure infiltration casting, e.g. Foam S3 vs M4. The difference is due to the existence of a large amount of oxide at the surface of the Al particles. This oxide impedes the formation of strong bonding between the Al particles during the sintering process.

5.8.2 Failure mode

The syntactic foams fabricated by liquid sintering, S1-S6, are more brittle than those fabricated by pressure infiltration. Foams S1, S2, S3 and S4 show no or a low and short plateau region in their compressive strength-strain curves. When the volume percentages of Al are increased to 60% and 70% (Foams S5 and S6), large stress drops are still present in the plateau regions, as shown in Figure 4.45(b). The plateau strengths of S5 and S6 are even much lower than that of M4, which has a lower Al volume percentage of 40%.

The brittle failure mode of Foams S1-S6 is largely due to the existence of voids and oxide in the syntactic foams. Under static compression, cracks can form at and propagate through the oxide and voids. This failure mode is similar to the static compressive failure of the epoxy resin matrix syntactic foam fabricated by

the mix stirring method, where a certain amount of voids are embedded in the foam (Gupta & Ricci 2006).

5.9 Energy absorption in compression

The capability of metal matrix syntactic foams in energy absorption can be characterised by two parameters: plateau strength and onset strain of densification. The former is dependent upon the strengths of the metal matrix and the ceramic particles, as well as upon the volume ratio between the two. The densification strain is mainly dependent upon the level of porosity in the syntactic foam.

In this study, two approaches are adopted to increase the energy absorption. One is using bimodal ceramic particles and the other is introducing Al particles. The monomodal Al matrix syntactic foams manufactured by conventional pressure infiltration, M1-M4, have specific energy absorption values of 20-33 J/g. By using bimodal CM, the specific energy absorption of Foams B4-B6 is increased to 30-35 J/g. The capability of energy absorption of bimodal syntactic foams is clearly higher than that of the monomodal syntactic foams. However, the difference is not marked. On the one hand, the higher porosity of Foams B4-B6 can lead to higher onset strain of densification than monomodal syntactic foams. On the other hand, the decreased volume percentage of Al in the bimodal syntactic foams can lead to a decrease in their plateau strength. It indicates that bimodal foams are a good approach to increase the porosity but not an efficient method to increase energy absorption capability.

By introducing Al particles into the syntactic foams, the specific energy absorption of Foams T1-T4 is significantly increased to 43-50 J/g. With 13% more Al compared with M2, the density of Foam T1 is not significantly increased but a high and stable plateau strength is obtained in the static compression, leading to a marked increase in specific energy absorption of the syntactic foam. The Al toughening seems an effective method to increase the specific energy absorption of Al syntactic foams.

The energy absorption of syntactic foams fabricated by liquid sintering is much lower than that of syntactic foams manufactured by melt infiltration casting. Foam S1, S2, S3 S4 is not suitable for energy absorption due to their relative low compressive strength and brittle plastic deformation. The values of specific energy absorption for Foams S5 and S6 are 9.2 and 13.6 J/g.

5.10 Impact response

5.10.1 Peak stress

The syntactic foams had a much higher peak stress in the low speed impact than in static compression, where the strain rate was about 2×10^{-3} s^{-1}. The higher peak stress in the impact of Foams M1, M2, M3 and M4 is due to micro-inertial hardening which is related to lateral and rotational inertia of rapidly displacing cell walls of CMs within and ahead of the localized deformation band. Under very

low strain rates, as in the static compression, micro-inertia has very little effect and the deformation of Foams M1-M4 is dominated either by brittle fracture or collapse of CMs and crushing of the Al/CM network. At high strain rates, the micro-inertia effect becomes important and the resistance to the fracture or collapse of CMs is increased, leading to an increased peak stress. Klintworth and Stronge (1988) found that the micro-inertial effect becomes significant at ~10 s^{-1} for honeycomb. Paul and Ramamurty (2000) found that the micro-inertial effect becomes significant at 0.01 s^{-1} for a low density metal foam (relative density of about 0.1). The critical strain rate at which micro-inertial effect becomes significant in metal matrix syntactic foams is much higher, because they are much denser and stronger than the metal foams.

In this study, the peak stress of Foams M1, M2, M3 and M4 at a strain rate of 120 s^{-1} is 25-40% higher than their static compressive strength. When the strain rate is increased from 120 s^{-1} to 200 s^{-1}, the peak stress increases more significantly, doubled in three of the four foams. Similar results were reported by Zhang and Zhao (2007). They found that the compressive strength of Al matrix syntactic foam was doubled at a strain rate of about 100 s^{-1} in comparison with static compression.

5.10.2 Failure mode

Although the failure mode of Foams M1-M4 in impact is similar to that in static compression in most cases, the impact speed has some influence on the failure

mode, as shown in Figure 4.53. At strain rates of 120 s^{-1} and 145 s^{-1}, Foams M1 and M2 failed in the same manner as in static compression, i.e., brittle fracture with an angle about 30°C to the loading direction. After large deformation in impact at a strain rate of 200 s^{-1}, however, Foams M1 and M2 were still in one piece without fracturing into pieces.

5.10.3 Specific impact energy absorption

The capability of energy absorption in low speed impact increases with strain rate, due to the increased strength. The specific energy absorption at a strain rate of 200 s^{-1} is nearly double that in static compression. It is indicated that metal matrix syntactic foam has potential for energy absorption applications in low speed impact.

5.11 Tensile and shear properties

5.11.1 Strength

The monomodal syntactic foams, M1, M2, M3 and M4, which are embedded with a similar volume fraction of CMs, were found to have a similar tensile and shear strength. The tensile and shear strengths of metallic syntactic foams are mainly determined by the strength and volume fraction of the metal matrix, largely independent of the characteristics of the ceramic microspheres. For the same metal or alloy, a high volume fraction of the metal matrix results in high tensile and shear strengths of the syntactic foam. The syntactic foam is consequently less prone to brittle fracture. This result agrees with the studies on tensile and shear

behaviour of polymeric syntactic foams and particulate reinforced MMCs. Kiser *et al.* (1996) found that Al-Si-Mg alloy matrix MMCs have a higher tensile strength when reinforced with 10% Si than reinforced with 20% Si and the tensile strength for both MMCs is lower than the tensile strength of the pure matrix. The shear strength of polymeric syntactic foams was also found to decrease with increasing volume fraction of microballoons (Kishore *et al.* 2005).

The syntactic foams manufactured by the melt infiltration method, however, have a more or less fixed volume fraction of the metal matrix. To increase this volume fraction, one method is to blend a certain amount of metal particles into the ceramic microspheres before melt infiltration and another is to use the conventional stir casting, where the ceramic microspheres are dispersed in the molten metal before casting. When the metal matrix becomes the dominant phase, the syntactic foam would behave more like a metal matrix composite.

5.11.2 Fracture mode

The tensile and shear fracture cracks of monomodal syntactic foams M1, M2, M3 and M4 were found to propagate right through the Al network and CM particles instead of at the interface between Al and CMs. These syntactic foams have the same shear fracture behaviour as polymeric syntactic foams (Kishore *et al.* 2005), where the shear fracture occurs along a path across the foam, irrespective of encountering resin or ceramic microspheres. However, their tensile fracture behaviour is different from that of polymeric syntactic foams (Wouterson *et al.*

2005, Pawlak & Galeski 2003). In polymeric syntactic foams, some glass microspheres were found to be intact in tensile fracture due to the presence of debonding between the resin and glass microspheres, although many glass microspheres on the fracture surface were found to be fractured. The different fracture behaviour is likely because there is certain amount of void in polymeric syntactic foams (Wouterson *et al.* 2005), which can lead to the debonding of the matrix and cellular spheres. Very little void was found in the metal matrix syntactic foams fabricated by pressure infiltration in this study.

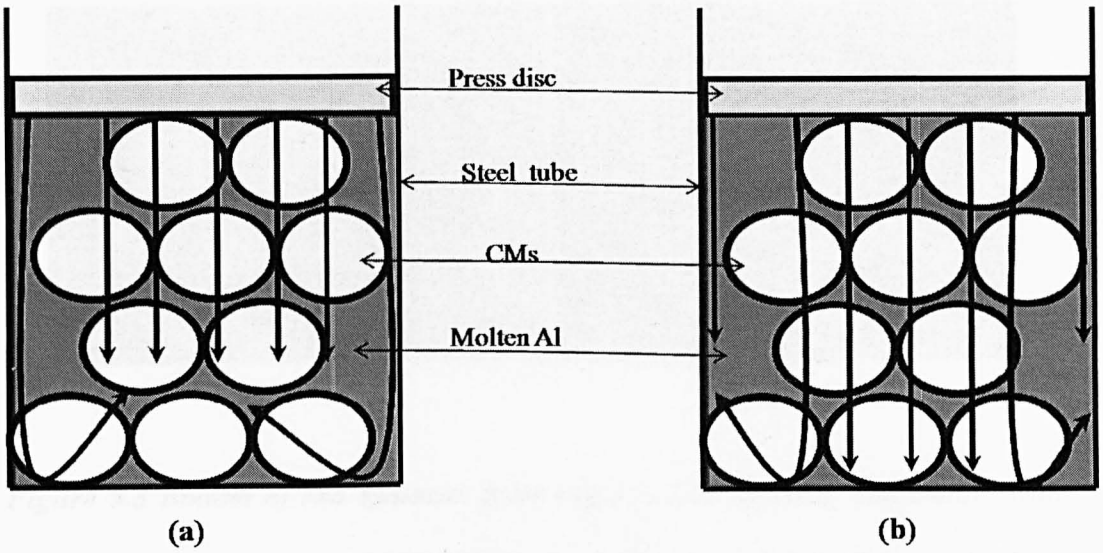

Figure 5.1 *Schematic diagrams showing the two flow routes of the molten Al ending at two different locations of the sample: (a) interior and (b) surface*

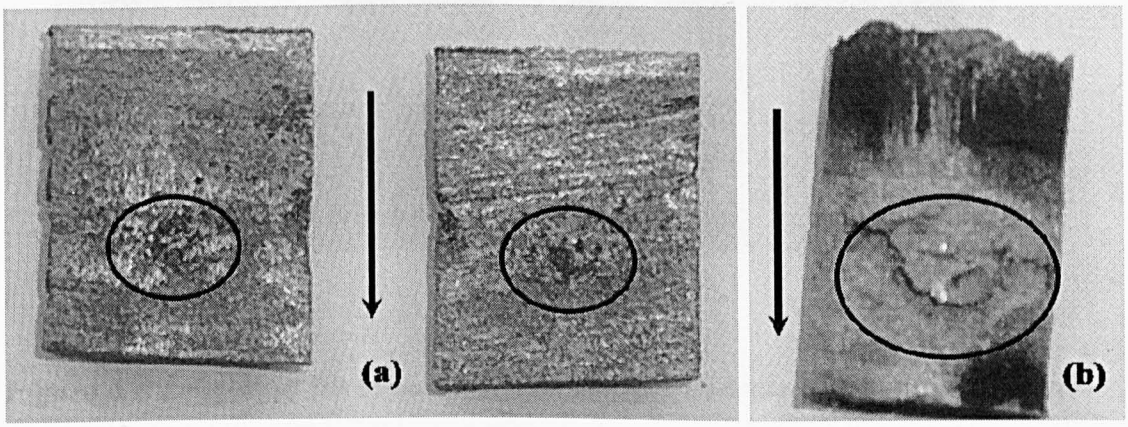

Figure 5.2 *Locations of typical casting defects in syntactic foam samples fabricated by pressure infiltration casting: (a) interior and (b) surface. The flow direction is indicated by arrows and the defects are circled*

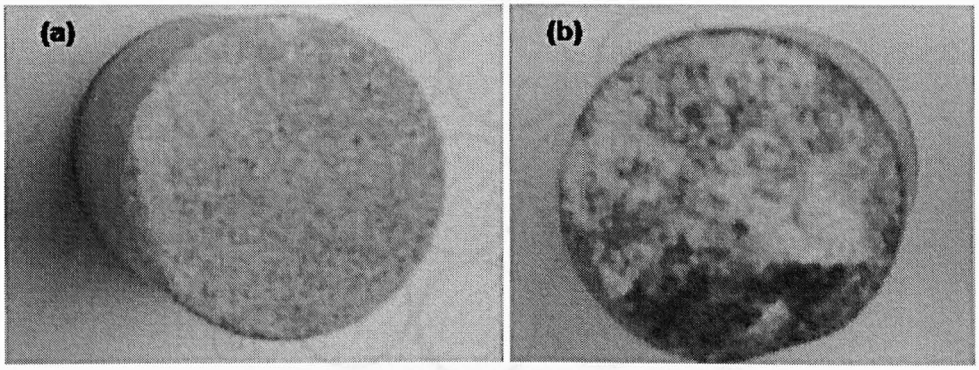

Figure 5.3 *Bottom of two syntactic foam samples fabricated by infiltration with molten Al 6082 at 720°C after the CM compact was heated to 720°C and (a) held for half hour and (b) without any holding time*

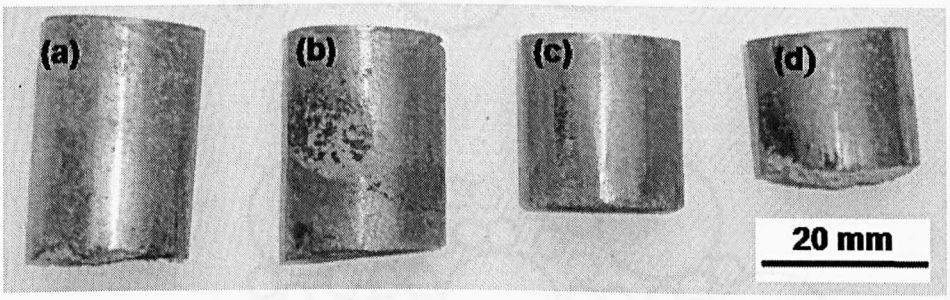

Figure 5.4 *Lengths of the syntactic foam samples fabricated by infiltration at a pressure of 1 MPa: (a) M1-H1, (b) M2-H1, (C) M3-H1 and (d) M4-H1*

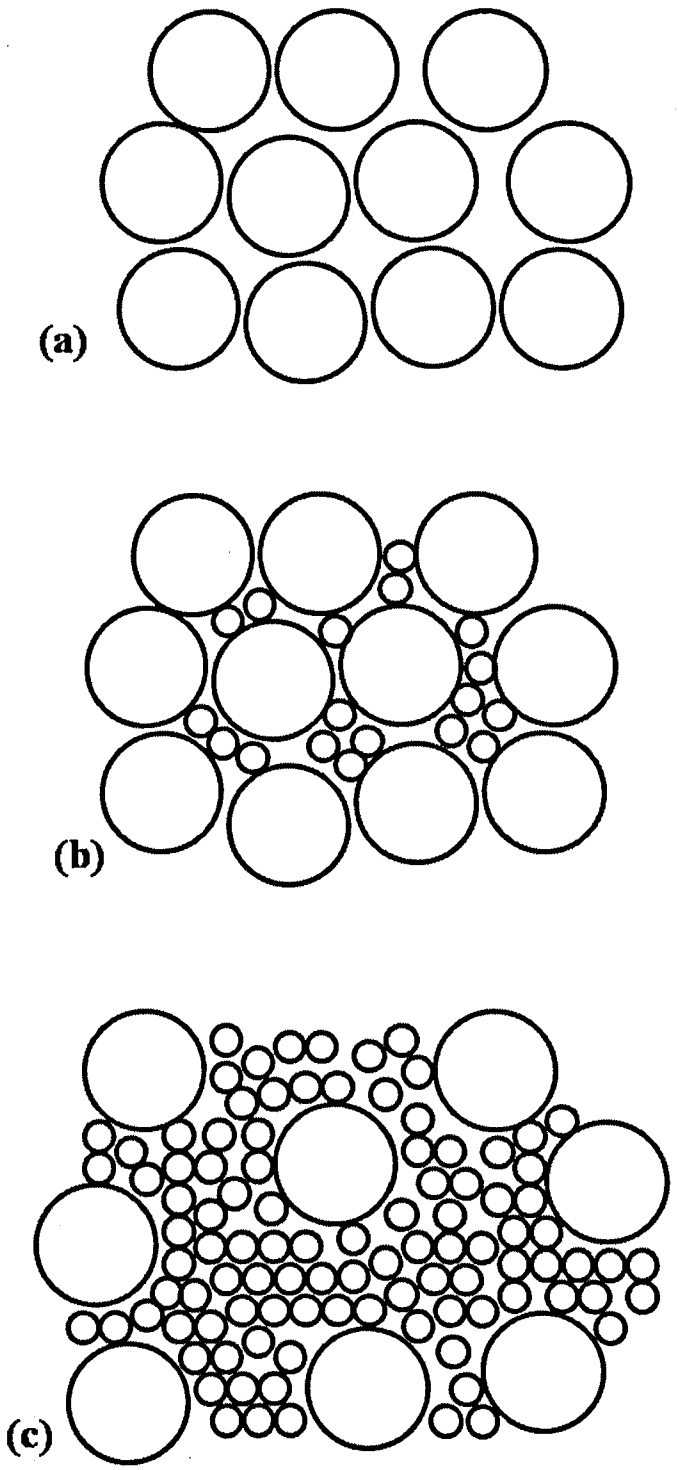

Figure 5.5 *Schematic representative packing of CMs: (a) monomodal, (b) bimodal with fine particles completely contained within the interstices between coarse particles, and (c) bimodal with more fine particles than in (b)*

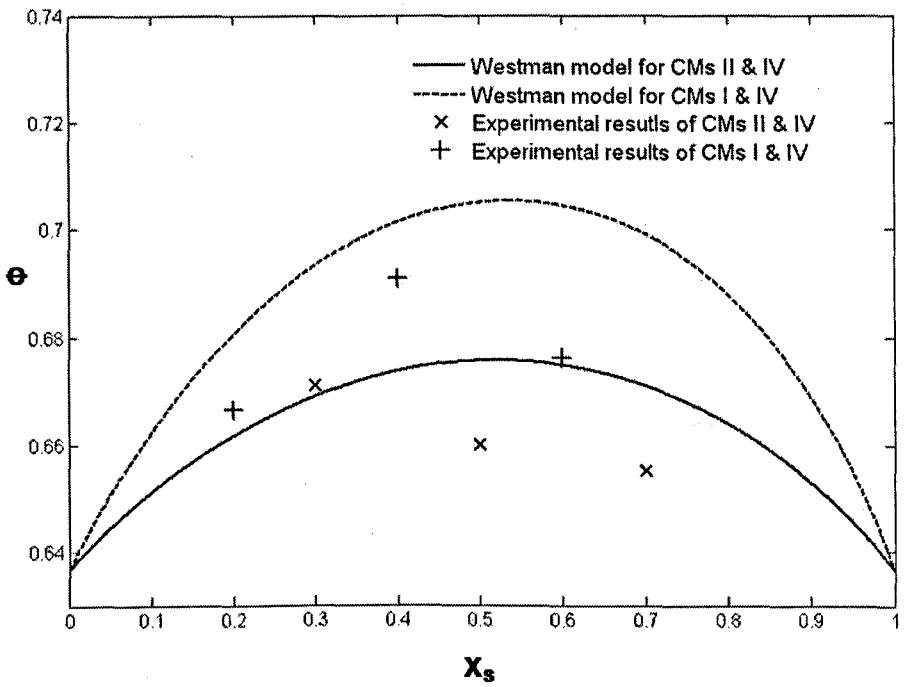

Figure 5.6 *Relationship between theoretical and experimental packing volume fraction, Φ and volume fraction of small particles, X_S for bimodal mixtures of CMs II & IV and CMs I & IV*

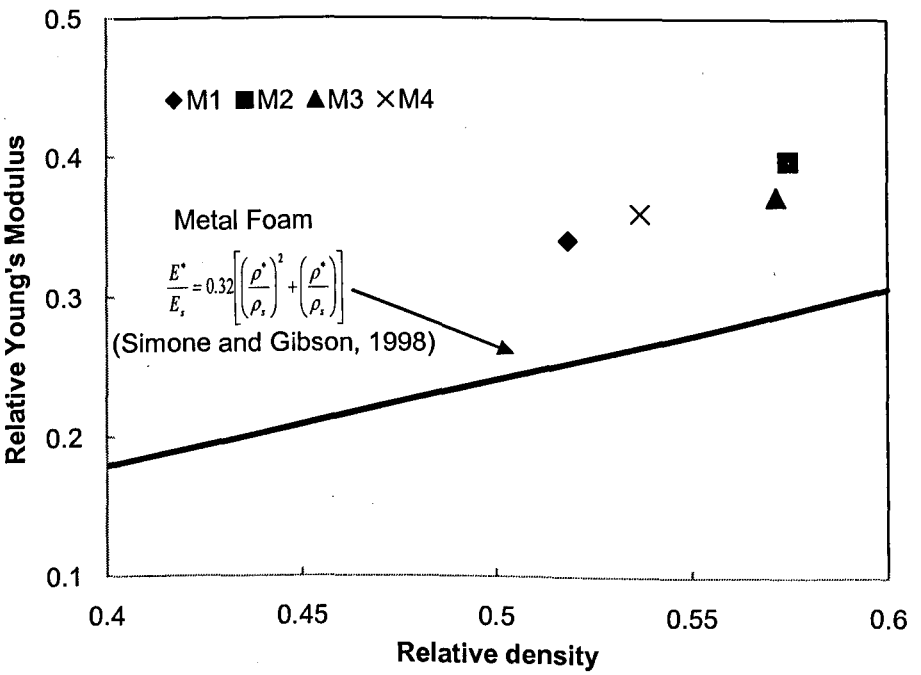

Figure 5.7 *Relationships between relative Young's modulus and relative density for syntactic foams and metal foams*

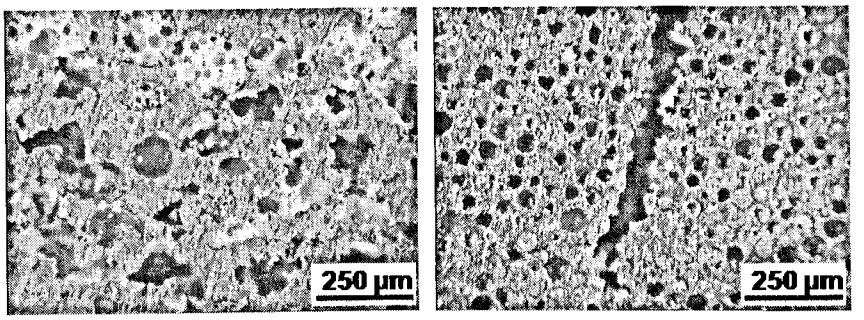

Figure 5.8 *Micrographs of cross-sections of syntactic foam specimen in static compression at a strain of 0.1, loaded vertically, showing: (a) ductile, localized, layered collapse of CMs and Al matrix in Foam M4 and (b) initiation and propagation of brittle fracture in Foam M1*

CHAPTER 6 CONCLUSIONS AND FUTURE WORK

6.1 Conclusions

6.1.1 Fabrication of Al matrix syntactic foams

6.1.1.1 Pressure infiltration process

Syntactic foams with monomodal or bimodal CMs or additional Al particles were fabricated by the pressure infiltration process. Syntactic foams with monomodal CMs, which have a similar porosity but different particle sizes and structures, had a nearly fixed volume fraction of CMs of about 63%. Syntactic foams with bimodal CMs had a volume fraction of CMs up to 6% higher than those with monomodal CMs, and had a lower density and a higher porosity. The volume fraction of Al was increased by adding different amounts of Al particles into the CM preforms. The microstructure of the as-fabricated foams exhibited the CMs well bonded to and uniformly distributed in the Al matrix. Syntactic foams with coarse CMs were found more prone to be infiltrated by molten Al during fabrication due to their porous structure and thinner membranes than the fine CMs.

6.1.1.2 Liquid sintering process

Syntactic foams with different volume fractions of Al were fabricated by liquid sintering of Al/CM powder mixtures. There were voids trapped in the syntactic foams which adversely affected the structural integrity. The amount of voids

increased with increasing Al/CM particle size ratio and increasing volume fraction of Al.

6.1.2 Young's modulus

The monomodal syntactic foams measured by RFDA had a much higher young's modulus than metal foams. The specific Young's modulus increased with the specific density of the syntactic foam, with a similar variation trend as in metal foams. The Young's modulus of metal matrix syntactic foam was mainly determined by the volume fraction of the metal matrix, whereas contribution of the CMs was very limited due to their low Young's modulus.

6.1.3 Indentation behaviour

Indentation loads of the syntactic foams were largely determined by their compressive strengths, which in turn depended on the compressive strengths of the CMs. In indentation, syntactic foams with hollow CMs were brittle and those with porous CMs were ductile. Using a disc spreader increased the indentation collapse load significantly. A combination of ductile syntactic foam and a thick disc is a good choice for indentation resistance.

6.1.4. Compressive behaviour

6.1.4.1 Compressive strength

The compressive strength of the syntactic foams was affected by the strengths of the Al matrix and the CMs and also by the volume ratio of the two components. The compressive strength of heat-treated, monomodal syntactic foams was higher than that of the non-heat treated ones. Monomodal syntactic foams with hollow CMs had higher compressive strength than the ones with porous CMs, because hollow CMs were stronger than porous CMs. The compressive strength of most bimodal syntactic foams was sensitive to the volume fraction of the fine CMs. Syntactic foams with high volume fractions of Al, resulting either from large number of infiltrated CMs or from Al particle toughening or from high volume fraction of Al in liquid sintering, generally had higher strengths than the monomodal syntactic foams. The compressive strength of syntactic foams toughened with Al particles with high volume fractions of Al, however, did not increase with increasing Al volume fraction, because the compressive strength was mainly determined by the strength of the CMs.

6.1.4.2 Failure mode

The syntactic foams fabricated by pressure infiltration showed different failure modes under the compression. Three criteria, collapse, Griffith and Coulomb, were developed to explain the different failure modes. The failure mode depends

on which criterion is met first and is determined by the Al/CM volume ratio and the relative strengths of the Al and CMs, the latter of which depends on the structure of the CMs. The brittle failure of syntactic foams fabricated by liquid sintering was due to the large amounts of voids and oxide incorporated in the foams.

6.1.5 Energy absorption

The energy absorption of syntactic foams is mainly determined by plateau strength and onset strain of densification. The former is related to the compressive strength and mode of plastic deformation, while the latter is largely determined by the porosity of the syntactic foam. The capability of energy absorption for different types of syntactic foams was compared. Syntactic foams toughened with Al particles had the highest specific energy absorption due to higher volume percentages of Al, and specific energy absorption increased with increasing volume percentages of Al. The monomodal syntactic foams had lower specific energy absorption either due to lower compressive strength or due to brittle fracture. The bimodal syntactic foams had a moderate specific energy absorption because of their higher porosity and thus greater onset strain of densification.

6.1.6 Tensile and shear behaviour

The tensile and shear strengths of the monomodal syntactic foams were similar; they were not affected by the different structures and sizes of the embedded CMs. The foams failed by brittle fracture with the cracks developing across the Al matrix and the CMs rather than at the interface between the Al matrix and CMs.

6.1.7 Low speed impact behaviour

Both peak stress and energy absorption of the monomodal syntactic foams were found to be sensitive to the impact speed and were higher than in static compression. However, the failure modes were the same as in static compression.

6.2 Future work

6.2.1 Syntactic foams with bimodal CMs

Further work is needed in the study on manufacturing syntactic foams with bimodal CMs to obtain maximum porosity. Syntactic foams with bimodal CMs were found to have lower density and higher porosity due to larger packing density of the CM mixture. However, with the limited size ratios of small particles to large particles (0.25 and 0.5) studied in this thesis the changes were limited (6%). According to Westman model, the packing density of the mixture increases with decreasing size ratio of small particle to large particle. The study of Liu and Ha (2002) showed that a size ratio value of 0.09 can give the packing density of

bimodal particles as high as 79%. Further studies are needed on the fabrication of syntactic foam with lower size ratios to maximize the packing volume fraction of the CM mixture and thus to maximum the porosity in the syntactic foam.

Further work are also needed to optimise the energy absorption capability of syntactic foams by combining effects of lower size ratio of bimodal CMs and of Al particle addition. The former will lead to high porosity and the latter will improve the ductility and energy absorption of the syntactic foam (e.g., Foams B1 and B2).

6.2.2 Liquid sintering

Further work is needed to optimise the fabrication conditions of liquid sintering. In comparison to the pressure infiltration method, the liquid sintering process has the advantage of a simpler operation procedure and easier control of volume ratio between the matrix and the CMs. Only preliminary work was carried out on the liquid sintering process in this study and the as-fabricated syntactic foams showed poor microstructure and mechanical properties. The bonding of Al particles were found to be improved by increasing the Al/CM size ratio (from 2 to 7). More work is needed to find the optimum Al/CM size ratio to obtain the strongest bonding of Al particles. The compaction pressure used in this study was limited to 50 MPa due to the low strength of CMs. The low pressure led to a considerable number of voids located within the particle mixture. It is suggested that stronger CMs be used to minimise the number of voids.

6.2.3 High speed impact of syntactic foam

The syntactic foams showed higher strength and energy absorption in low speed impact (up to 4 m/s) than that in static compression. There is a need to study the mechanical properties and energy absorption of syntactic foams impact of much higher speeds (up to 50 m/s). The study, if successful, may lead to applications of the syntactic foams in vehicles as an energy absorber to protect people in the circumstances of crash. The syntactic foams with a relatively thick disc cover showed good resistance to the indentation. Further work is needed on the behaviour of this structure in the high speed bullet impact (300-800 m/s) behaviour of this structure, which may be of interest in the application of this structure in bullet-proof armour.

REFERENCES

Andreasen, A.H.M. & Andersen, J. 1929, "Relation between grain size and interstitial space in products of unconsolidated granules", *Kolloid-Zeitschrift & Zeitschrift für Polymere,* vol. 50, pp. 217-228.

Andrews, E., Sanders, W. & Gibson, L.J. 1999, "Compressive and tensile behaviour of aluminum foams", *Materials Science and Engineering A: Structural Materials: Properties, Microstructure and Processing,* vol. 270, no. 2, pp. 113-124.

Arsenault, R.J. 1984, "Strengthening of aluminum alloy 6061 by fiber and silicon", *Materials science and engineering,* vol. 64, no. 2, pp. 171-181.

Arsenault, R.J. & Flom, Y. 1986, "Role of interfaces in SiC/Al composites", Proceedings of a Symposium 'Phase Boundary Effects on Deformation,pp. 261-279.

Ashby, M., Evans, T., Fleck, N.A., Gibson, L.J., Hutchinson, J.W. & Wadley, H.N.G. 2000, Metal Foams: A Design Guide, Elsevier Butterworth-Heinemann.

ASTM E 1876-01 2001, "Standard test method for dynamic young's modulus, shear modulus, and poisson's ratio by impulse excitation of vibration", Annual Book of ASTM Standards, West Conshohocken, PA, United State

ASTM E9-89a 1989, "Standard methods of compression testing of metallic materials at room temperature", Annual Book of ASTM Standards, West Conshohocken, PA, United State.

ASM Handbook 1991, "Heat treating of nonferrous alloys", ASM International, Ohio, United State.

Avalle, M., Belingardi, G. & Montanini, R. 2001, "Characterization of polymeric structural foams under compressive impact loading by means of energy-absorption diagram", *International Journal of Impact Engineering,* vol. 25, no. 5, pp. 455-472.

Balch, D.K., O'Dwyer, J.G., Davis, G.R., Cady, C.M., Gray III, G.T. & Dunand, D.C. 2005, "Plasticity and damage in aluminum syntactic foams deformed under dynamic and quasi-static conditions", *Materials Science and Engineering A,* vol. 391, no. 1-2, pp. 408-417.

Balch, D.K. & Dunand, D.C., 2006, "Load partitioning in aluminum syntactic foams containing ceramic microspheres", Acta Materialia vol.54, pp. 1501-1511.

Banerji, A., Rohatgi, P.K. & Reif, W. 1984, "Role of wettability in the preparation of metal-matrix composites (A review)", *Metall,* vol. 38, no. 7, pp. 656-661.

Banhart, J. & Brinkers, W. 1999, "Fatigue behavior of aluminum foams", *Journal of Materials Science Letters,* vol. 18, no. 8, pp. 617-619.

Banhart, J. 2001, "Manufacture, characterisation and application of cellular metals and metal foams", *Progress in Materials Science,* vol. 46, no. 6, pp. 559-632.

Bunn, P. & Mottram, J.T. 1993, "Manufacture and compression properties of syntactic foams", *Composites,* vol. 24, no. 7, pp. 565-571.

Cvitkovich, M.K. & Jackson, W.C. 1999, "Compressive failure mechanisms in composite sandwich structures", *Journal of the American Helicopter Society,* vol. 44, no. 4, pp. 260-268.

D'Almeida, J.R.M. 1999, "An analysis of the effect of the diameters of glass microspheres on the mechanical behavior of glass-microsphere/epoxy-matrix composites", *Composites Science and Technology,* vol. 59, no. 14, pp. 2087-2091.

Daoud, A. 2007, "Synthesis and characterization of novel ZnAl22 syntactic foam composites via casting", *Materials Science and Engineering A,* vol. 488, no. 1-2, pp. 281-295.

Davies, G.J. & Zhen, S. 1983, "Metallic foams: their production, properties and applications", *Journal of Materials Science,* vol. 18, no. 7, pp. 1899-1911.

Divecha, A.P. & Fishman, S.G. 1980, "Mechanical properties of silicon carbide reinforced aluminum", *Proceedings - Computer Networking Symposium,* vol. 3, pp. 351-361.

Divecha, A.P., Fishman, S.G. & Karmarkar, S.D. 1981, "Silicon carbide reinforced aluminum", *Journal of Metals,* vol. 33, no. 9, pp. 12-17.

Doel, T.J.A. & Bowen, P. 1996, "Tensile properties of particulate-reinforced metal matrix composites", *Composites Part A: Applied Science and Manufacturing,* vol. 27, no. 8, pp. 655-665.

Dou, Z.Y. , Jiang, L.T., Wu, G.H., Zhang, Q., Xiu, Z.Y. & Chen, G.Q. 2007, "High strain rate compression of cenosphere-pure aluminum syntactic foams", Scripta Materialia, vol.57,pp. 945–948.

El-Mahallawy, N., Taha, M.A., Pokora, E. & Klein, F. 1998, "On the influence of process variables on the thermal conditions and properties of high pressure

die-cast magnesium alloys", *Journal of Materials Processing Technology,* vol. 73, no. 1-3, pp. 125-138.

Edwin, R. & Daniel, B.S.S. 2007, "Aluminum melt foam processing for light-weight structures", *Materials and Manufacturing Processes*, vol. 22, no. 4, pp. 525-530.

Fishman, S.G.B., Ahmed, M. & Potter, D.I. 1986, "Compouds and microstructures of silicon-implanted nickel", *Materials science and engineering,* vol. 90, pp. 135-142.

Flom, Y. & Arsenault, R.J. 1989, "Effect of particle size on fracture toughness of SiC/Al composite material", *Acta Metallurgica,* vol. 37, no. 9, pp. 2413-2423.

Flom, Y. & Arsenault, R.J. 1986, "Deformation of SiC/Al composites", *Journal of Metals,* vol. 38, no. 7, pp. 31-34.

Flom, Y. & Arsenault, R.J. 1986, "Interfacial bond strength in an aluminium alloy 6061 — SiC composite", *Materials Science and Engineering,* vol. 77, pp. 191-197.

Flom, Y. & Arsenault, R.J. 1986, "Interfacial bond strength in an aluminum alloy 6061-SiC composite", *Materials science and engineering,* vol. 77, pp. 191-197.

Furnas, C.C. 1931, "Grading aggregates: I. Mathematical relations for beds of broken solid of maximum density", *Industrial and Engineering Chemistry,* vol. 23, pp. 1052-1058.

Garcia-Cordovilla, C., Louis, E. & Narciso, J. 1999, "Pressure infiltration of packed ceramic particulates by liquid metals", *Acta Materialia,* vol. 47, no. 18, pp. 4461-4479.

Gibson, L.J. & Ashby, M. 1999, *Cellular Solids: Structure and properties,* 2nd edn, New York :Cambridge University Press, Cambridge.

Gnjidic, Z., Bozic, D. & Mitkov, M. 2001, "The influence of SiC particles on the compressive properties of metal matrix composites", *Materials Characterization,* vol. 47, no. 2, pp. 129-138.

Goldsmith, W. & Sackman, J. 1992, "Experimental study of energy absorption in impact on sandwich plates", *International Journal of Impact Engineering,* vol. 12, no. 2, pp. 241-262.

Griffith A.A. 1924, "The theory of rupture", Proceedings of first International congress of applied mechanics, Delft, pp. 55-63.

Gupta, N., Karthikeyan, C.S., Sankaran, S. & Kishore 1999, "Correlation of processing Methodology to the Physical and Mechanical Properties of Syntactic Foams With and Without Fibers", Materials Characterization vol.43, no. 4, pp. 271-277.

Gupta, N. & Nagorny, R. 2005, "Tensile Strength of Glass Microballoon-Epoxy ResinSyntactic Foams", *Proceedings of the American Society for Composites—TwentiethTechnical Conference*Philadelphia, PA.

Gupta, N., Kishore, Woldesenbet, E. & Sankaran, S. 2001, "Studies on compressive failure features in syntactic foam material", *Journal of Materials Science,* vol. 36, no. 18, pp. 4485-4491.

Gupta, N., Priya, S., Islam, R. & Ricci, W. 2006, "Characterization of mechanical and electrical properties of epoxy-glass microballoon syntactic composites", Taylor and Francis Inc, pp. 1.

Gupta, N. & Ricci, W. 2006, "Comparison of compressive properties of layered syntactic foams having gradient in microballoon volume fraction and wall thickness", *Materials Science and Engineering A,* vol. 427, no. 1-2, pp. 331-342.

Gupta, N. & Woldesenbet, E. 2002, "Microscopic studies of syntactic foams tested under three-point bending conditions", *2002 Engineering Technology Conference On Energy ETCE 2002, Febrary 4, 2002 - Febrary 5*American Society of Mechanical Engineers, Houston, TX, United states, pp. 147.

Gupta, N., Woldesenbet, E. & Mensah, P. 2004, "Compression properties of syntactic foams: Effect of cenosphere radius ratio and specimen aspect ratio", *Composites Part A: Applied Science and Manufacturing,* vol. 35, no. 1, pp. 103-111.

Hall, I.W., Guden, M. & Yu, C.-. 2000, "Crushing of aluminum closed cell foams: density and strain rate effects", *Scripta Materialia,* vol. 43, no. 6, pp. 515-521.

Hall, J.N., Wayne Jones, J. & Sachdev, A.K. 1994, "Particle size, volume fraction and matrix strength effects on fatigue behavior and particle fracture in 2124 aluminum-SiCp composites", *Materials Science and Engineering: A,* vol. 183, no. 1-2, pp. 69-80.

Hanumanth, G.S. & Irons, G.A. 1993, "Particle incorporation by melt stirring for the production of metal-matrix composites", *Journal of Materials Science,* vol. 28, no. 9, pp. 2459-2465.

Hartmann, M., Croβman, I., Reindel, K. & Singer, R.F. 1999, "Behaviour of Composites structures" in *Metal Foams and Porous Structures*, eds. J. Banhart, M.F. Ashby & N.A. Fleck, 1st edn, Verlag MIT, Bremen, pp. 331-336.

Hiel, C., Dittman, D. & Ishai, O. 1993, "Composite sandwich construction with syntactic foam core: A practical assessment of post-impact damage and residual strength", *Composites,* vol. 24, no. 5, pp. 447-450.

Hinves, J.B. & Douglas, C.D. 1993, "Development of a hybrid advanced composite-syntactic foam structural component for use in undersea vehicles", *Part 3 (of 3), October 18, 1993 - October 21*Publ by IEEE, Victoria, BC, Can, pp. 468.

Ibrahim, I.A., Mohamed, F.A. & Lavernia, E.J. 1991, "Particulate reinforced metal matrix composites -a review", *Journal of materials Science,* vol. 26, pp. 1137-1156.

Jaeger, J.C., Cook, N.G.W. & Zimmerman, R.W. 2007, *Fundamentals of Rock Mechanics,* 4th edn, Blackwell Publishing, Oxford, UK.

Jayatilaka, A.S. 1979, *Fracture of Engineering Brittle Materials,* 1st edn, Applied Science Publishers Ltd, Barking, England.

Jize, N.N., Hiel, C. & Ishai, O. 1996, "Mechanical performance of composite sandwich beams with syntactic foam cores", *Proceedings of the 1994 Symposium on Composite Materials: Testing and Design (Twelfth Volume), May 16, 1994 - May 17*ASTM, Montreal, Can, pp. 125.

Jones, H. 1982, *Rapid Solidification of Metals and Alloys,* 1st edn, Ashgate Publishing.

Jumikis, A.R. 1983, Rock mechanics, 2nd edn, Trans Tech Publications, Germany.

Kamat, S.V., Hirth, J.P. & Mehrabian, R. 1989, "Mechanical properties of particulate-reinforced aluminum-matrix composites", *Acta Metallurgica,* vol. 37, no. 9, pp. 2395-2402.

Karthikeyan, C.S., Kishore & Sankaran, S. 2000, "Comparison of compressive properties of fiber-free and fiber-bearing syntactic foams", *Journal of Reinforced Plastics and Composites,* vol. 19, no. 9, pp. 732-742.

Kim, H.S. & Oh, H.H. 2000, "Manufacturing and Impact Behavior of Syntactic Foam", *Journal of Applied Polymer Science,* vol. 76, pp. 1324-1328.

Kim, H.S. & Khamis, M.A. 2001, "Fracture and impact behaviours of hollow micro-sphere/epoxy resin composites", *Composites - Part A: Applied Science and Manufacturing,* vol. 32, no. 9, pp. 1311-1317.

Kim, H.S. & Khamis, M.A. 2001, "Fracture and impact behaviours of hollow micro-sphere/epoxy resin composites", *Composites - Part A: Applied Science and Manufacturing,* vol. 32, no. 9, pp. 1311-1317.

Kim, H.S. & Plubrai, P. 2004, "Manufacturing and failure mechanisms of syntactic foam under compression", *Composites Part A: Applied Science and Manufacturing,* vol. 35, no. 9, pp. 1009-1015.

Kiser, M., He, M.Y. & Zok, F.W. 1999, "Mechanical response of ceramic microballoon reinforced aluminum matrix composites under compressive loading", *Acta Materialia,* vol. 47, no. 9, pp. 2685-2694.

Kiser, M.T., Zok, F.W. & Wilkinson, D.S. 1996, "Plastic flow and fracture of a particulate metal matrix composite", *Acta Materialia,* vol. 44, no. 9, pp. 3465-3476.

Kishore, Shankar, R. & Sankaran, S. 2005, "Short-beam three-point bend tests in syntactic foams. Part II: Effect of microballoons content on shear strength", *Journal of Applied Polymer Science,* vol. 98, no. 2, pp. 680-686.

Klier, E.M., Mortensen, A., Cornie, J.A. & Flemings, M.C. 1991, *Journal of Materials Science,* vol. 26, pp. 2519-2526.

Klintworth, J.W. & Stronge, W.J. 1988, "Elasto-plastic yield limits and deformation laws for transversely crushed honeycombs", *International Journal of Mechanical Sciences,* vol. 30, no. 3-4, pp. 273-292.

Kok, M. 2005, "Production and mechanical properties of Al_2O_3 particle-reinforced 2024 aluminium alloy composites", *Journal of Materials Processing Technology,* vol. 161, no. 3, pp. 381-387.

Li, Q.M., Magkiriadis, I. & Harrigan, J.J. 2006, "Compressive strain at the onset of densification of cellular solids", *Journal of Cellular Plastics,* vol. 42, no. 5, pp. 371-392.

Liu, S. & Ha, Z. 2002, "Prediction of random packing limit for multimodal particle mixtures", *Powder Technology,* vol. 126, pp. 283-296.

Lopatnikov, S.L. & Cheng, A.H.-. 2002, "Variational formulation of fluid infiltrated porous material in thermal and mechanical equilibrium", *Mechanics of Materials,* vol. 34, no. 11, pp. 685-704.

Manoharan, M. & Lewandowski, J.J. 1992, "Effect of reinforcement size and matrix microstructure on the fracture properties of an aluminum metal matrix composite", *Materials Science and Engineering: A,* vol. 150, no. 2, pp. 179-186.

Manoharan, M. & Lewandowski, J.J. 1992, "Effect of reinforcement size and matrix microstructure on the fracture properties of an aluminum metal matrix composite", *Materials Science and Engineering A,* vol. A150, no. 2, pp. 179-186.

Marchi, C.S. & Mortensen, A. 2002, "Infiltration and Replication Process for Producing Metal Sponges" in *Handbook of Cellular Metals*, eds. H. Degischer & B. Kriszt, WILEY-VCH, Weinheim, Germany, pp. 43-56.

Marmur, A. 1985, "A thermodynamic approach to the packing of particle mixtures", *Powder Technology,* vol. 44, no. 3, pp. 249-253.

Mazen, A.A. & Emara, M.M. 2004, "Effect of Particle Cracking on the Strength and Ductility of Al-SiCp Powder Metallurgy Metal Matrix Composites", *Journal of Materials Engineering and Performance,* vol. 13, no. 1, pp. 39-46.

Miyoshi, T., Itoh, M., Mukai, T., Kanahashi, H., Kohzu, H., Tanabe,S. & Higashi, K. 1999, "Enhancement of energy absorption in a closed-cell aluminum by the modification of cellular structures", *Scripta Materialia,* vol. 41, no. 10, pp. 1055-1060.

Mortensen, A. & Jin, I. 1992, "Solidification processing of metal matrix composites", *International Materials Reviews,* vol. 37, no. 3, pp. 101-128.

Mortensen, A. & Cornie, J.A. 1987, "On the infiltration of metal matrix composites", *Metallurgical transactions A, Physical metallurgy and materials science,* vol. 18 A, no. 6, pp. 1160-1163.

Motz, C. & Pippan, R. 2001, "Deformation behaviour of closed-cell aluminium foams in tension", *Acta Materialia,* vol. 49, no. 13, pp. 2463-2470.

Mukai, T., Kanahashi, H., Miyoshi, T., Mabuchi, M., Nieh, T.G. & Higashi, K. 1999, "Experimental study of energy absorption in a close-celled aluminum foam under dynamic loading", *Scripta Materialia,* vol. 40, no. 8, pp. 921-927.

Nadler, J.H., Hurysz, K.M., Clark, J.L., Cochran, J.K., Lee, K.J. & Sanders, J. 1999, "Sintering Methods" in , eds. J. Banhart, M.F. Ashby & N.A. Fleck, 1st edn, Verlag MIT, Bremen, pp. 179-182.

Nair, S.V., Tien, J.K. & Bates, R.C. 1985, "SiC-Reinforced Aluminum metal matrix composites", *International metals reviews,* vol. 30, no. 6, pp. 275-290.

Nardone, V.C. & Prewo, K.M. 1986, "On the strength of discontinuous silicon carbide reinforced Aluminum", *Scripta metallurgica,* vol. 20, no. 1, pp. 43-48.

Olurin, O.B., Fleck, N.A. & Ashby, M.F. 2000, "Indentation resistance of an aluminium foam", *Scripta Materialia,* vol. 43, no. 11, pp. 983-989.

Ortega, F.S., Pileggi, R.G., Sepulveda, P. & Pandolfelli, V.C. 1999, "Optimizing particle packing in powder consolidation", *American Ceramic Society Bulletin,* vol. 78, no. 8, pp. 106-111.

Ouchiyama, N. & Tanaka, T. 1981, "The porosity of a mass of solid particles having a range of sizes", *Industrial and Engineering Chemistry fundamentals,* vol. 20, pp. 66-71.

Ouellet, S., Cronin, D. & Worswick, M. 2006, "Compressive response of polymeric foams under quasi-static, medium and high strain rate conditions", *Polymer Testing,* vol. 25, no. 6, pp. 731-743.

Palmer, R.A., Gao, K., Doan, T.M., Green, L. & Cavallaro, G. 2007, "Pressure infiltrated syntactic foams-Process development and mechanical properties", *Materials Science and Engineering A,* vol. 464, no. 1-2, pp. 85-92.

Palumbo, M., Donzella, G., Tempesti, E. & Ferruti, P. 1996, "On the compressive elasticity of epoxy resins filled with hollow glass microspheres", *Journal of Applied Polymer Science,* vol. 60, no. 1, pp. 47-53.

Park, C. & Nutt, S.R. 2002, "Strain rate sensitivity and defects in steel foam", *Materials Science and Engineering A,* vol. 323, no. 1-2, pp. 358-366.

Paul, A. & Ramamurty, U. 2000, "Strain rate sensitivity of a closed-cell aluminum foam", *Materials Science and Engineering A,* vol. 281, no. 1, pp. 1-7.

Pawlak, A. & Galeski, A. 2002, "Determination of stresses around beads in stressed epoxy resin by photoelasticity", *Journal of Applied Polymer Science,* vol. 86, no. 6, pp. 1436-1444.

Polmear, I.J. 1989, *Light Alloys,* 2nd edn, Edward Arnold, Great Britain.

Rack, H.J. 1988, "Fabrication of high performance powder-metallurgy aluminum matrix composites", *Advanced materials and manufacturing processes,* vol. 3, no. 3, pp. 327-358.

Radford, D.D., Deshpande, V.S. & Fleck, N.A. 2005, "The use of metal foam projectiles to simulate shock loading on a structure", *International Journal of Impact Engineering,* vol. 31, no. 9, pp. 1152-1171.

Raj, R.E. & Daniel, B.S.S. 2007, "Aluminum melt foam processing for light-weight structures", Taylor and Francis Inc, 325 Chestnut St, Suite 800, Philadelphia PA, PA 19106, United States, pp. 525.

Rawal, S.P., Lanning, B.R. & Misra, M.S. 1993, "Design and Mechanical Properties of Microballoon-aluminum Composite-core Laminates", *Metal Matrix Composites, Proceeding of 9th International Conference on* Composite Materials, ed. A. Miravete, ICCM, Madrid, pp. 203-10.

Rodelheimer, M.T. & D'Almeida, 2001, "Analysis of the use of an industrial waste as reinforecement in Epoxy composites", *Macromol Symposium*, vol. 169, pp. 229-35.

Rohatgi, P.K., Guo, R.Q., Iksan, H., Borchelt, E.J. & Asthana, R. 1998, "Pressure infiltration technique for synthesis of aluminum-fly ash particulate composite", Materials Science Engineering A, vol. A244, no. 1, pp. 22-30.

Rohatgi, P.K., Daoud, A., Schultz, B.F. & Puri, T. 2009, "Microstructure and mechanical behavior of die casting AZ91D-Fly ash cenosphere composites", *Composites Part A: Applied Science and Manufacturing,* vol. 40, no. 6-7, pp. 883-896.

Rohatgi, P.K., Gupta, N., Weiss, D. & Miracle, D. 2006, "Synthesis and applications of cast metal matrix composites and syntactic foams", *38th SAMPE Fall Technical Conference: Global Advances in Materials and Process Engineering, November 6, 2006 - November 9*Soc. for the Advancement of Material and Process Engineering, Dallas, TX, United states.

Schott, N.R. & Bhattacharjee, T.K. 1993, "New Syntactic Foams with Polystyrene", *Journal of Cellular Plastics,* vol. 29, no. 6, pp. 556-568.

Seamark, M.J. 1991, "Use of syntactic foams for subsea buoyancy", *Cellular Polymers,* vol. 10, no. 4, pp. 308-321.

Seo, Y. & Kang, C. 1995, "Effect of applied pressure on particle-dispersion characteristics and mechanical properties in melt-stirring squeeze-cast SiCp/Al composites", *Journal of Materials Processing Technology,* vol. 55, no. 3-4, pp. 370-379.

Shaw, M.C. & Sata, T. 1966, "The plastic behavior of cellular materials", *International Journal of Mechanical Sciences,* vol. 8, no. 7, pp. 469-472, IN1-IN2, 473-478.

Simone, A.E. & Gibson, L.J. 1998, "Aluminum foams produced by liquid-state processes", *Acta Materialia,* vol. 46, no. 9, pp. 3109-3123.

Simone, A.E. & Gibson, L.J. 1998, "Effects of solid distribution on the stiffness and strength of metallic foams", *Acta Materialia,* vol. 46, no. 6, pp. 2139-2150.

Slipenyuk, A., Kuprin, V., Milman, Y., Spowart, J.E. & Miracle, D.B. 2006, "The effect of matrix to reinforcement particle size ratio (PSR) on the microstructure and mechanical properties of a P/M processed AlCuMn/SiCp MMC", *Materials Science and Engineering A,* vol. 381, no. 1-2, pp. 165-170.

Smith, D.J. 2001, "Materials Science and Engineering B. Solid-State Materials for Advanced Technology: Preface", *Materials Science and Engineering B: Solid-State Materials for Advanced Technology,* vol. 87, no. 3, pp 203.

Sugimura, Y., Meyer, J., He, M.Y., Bart-Smith, H., Grenstedt, J. & Evans, A.G. 1997, "On the mechanical performance of closed cell Al alloy foams", *Acta Materialia,* vol. 45, no. 12, pp. 5245-5259.

Taha, M.A. & El-Mahallawy, N. 1998, "Metal-matrix composites fabricated by pressure-assisted infiltration of loose ceramic powder", *Journal of Materials Processing Technology,* vol. 73, no. 1-3, pp. 139-146.

Tan, P.J., Reid, S.R., Harrigan, J.J., Zou, Z. & Li, S. 2005, "Dynamic compressive strength properties of aluminium foams. Part i - Experimental data and observations", *Journal of the Mechanics and Physics of Solids,* vol. 53, no. 10, pp. 2174-2205.

Timoshenko, S.P. & Goodier, J.N. 1970, *Theory of Elasticity,* 3rd edn, McGraw-Hill, New York.

Tjong, S.C. & Ma, Z.Y. 2000, "Microstructural and mechanical characteristics of in situ metal matrix composites", *Materials Science and Engineering R: Reports,* vol. 29, no. 3, pp. 49-113.

Tsai, S.W. & Hahn, H.T. 1980, "Role of interface in the strength of composite materials", *Polymer Science and Technology,* vol. 12 B, pp. 463-472.

Varma, V.K., Kamat, S.V., Mahajan, Y.R. & Kutumbarao, V.V. 2001, "Effect of reinforcement size on low strain yielding behaviour in Al–Cu–Mg/SiCP composites", *Materials Science and Engineering A,* vol. 318, no. 1-2, pp. 57-64.

Vendra, L.J. & Rabiei, A. 2007, "A study on aluminum-steel composite metal foam processed by casting", *Materials Science and Engineering A,* vol. 465, no. 1-2, pp. 59-67.

Viot, P., Bernard, D. & Plougonven, E. 2007, "Polymeric foam deformation under dynamic loading by the use of the microtomographic technique", *Journal of Materials Science,* vol. 42, no. 17, pp. 7202-7213.

Watkins, L. 1988, "Syntactic foam buoyancy for production", *OMAE 1988 Houston*ASME, Houston, TX, USA, pp. 403.

Westman, A.E.R. 1936, "The packing of particles: empirical equations for intermediate diameter ratios", *Journal of American Ceramic Society,* vol. 19, pp. 127-129.

Wilsea, M., Johnson, K.L. & Ashby, M.F. 1975, "Indentation of foamed plastics", *International Journal of Mechanical Sciences,* vol. 17, no. 7, pp. 457-460, IN5-IN6.

Woldesenbet, E., Gupta, N. & Jadhav, A. 2005, "Effects of density and strain rate on properties of syntactic foams", *Journal of Materials Science,* vol. 40, no. 15, pp. 4009-4017.

Wouterson, E.M., Boey, F.Y.C., Hu, X. & Wong, S. 2005, "Specific properties and fracture toughness of syntactic foam: Effect of foam microstructures", *Composites Science and Technology,* vol. 65, no. 11-12, pp. 1840-1850.

Wu, G.H., Dou, Z.Y., Sun, D.L., Jiang, L.T., Ding, B.S. & He, B.F. 2007, "Compression behaviors of cenosphere-pure aluminum syntactic foams", *Scripta Materialia,* vol. 56, no. 3, pp. 221-224.

Yu, A.B., Standish, N. & Mclean, A. 1993, "Porosity calculation of binary mixtures of nonspherical particles", *Journal of American Ceramic Society,* vol. 76, pp. 2813-2816.

zhang, Q., Lee, P.D., Singh, R., Wu, G.H. & Lindley, T.C. 2009, "Micro-CT characterization of Structural Features and Deformation Behavior of Fly Ash/Aluminum Syntactic Foam", *Acta Materialia,* vol. 57, pp. 3303-3311.

Zhang, H., Ramesh, K.T. & Chin, E.S.C. 2004, "High strain rate response of aluminum 6092/B4C composites", *Materials Science and Engineering A,* vol. 384, no. 1-2, pp. 26-34.

Zhang, L.P. & Zhao, Y.Y. 2007, "Mechanical response of Al matrix syntactic foams produced by pressure infiltration casting", *Journal of Composite Materials,* vol. 41, no. 17, pp. 2105-2117.

APPENDIX GRIFFITH'S THEORY OF RUPTURE

(Reproduced from *Fracture of Engineering Brittle Materials,* Jayatlaka, A.S. 1st edn, Applied Science Publishers Ltd, Barking, England, 1979, pp. 90-95)

4.3. GRIFFITH'S THEORY OF RUPTURE—MAXIMUM STRESS CRITERION FOR AN ELLIPTICAL CRACK

Concept

Griffith[1] in 1924 proposed a theory of rupture for brittle solids subjected to complex loading systems (biaxial, uniaxial tension and uniaxial compression). He used an elliptical crack (very slender elliptical hole) for his analysis. In this section we shall concentrate only on the analysis of a single elliptical crack subjected to biaxial stresses as shown in Fig. 4.8. Griffith's theory is based on the fact that the rupture occurs when the stress at any point on the surface of the crack reaches a specific tensile stress. In other words, *fracture commences when the maximum stressed point on the surface reaches a specific tensile stress* (usually the crack tip

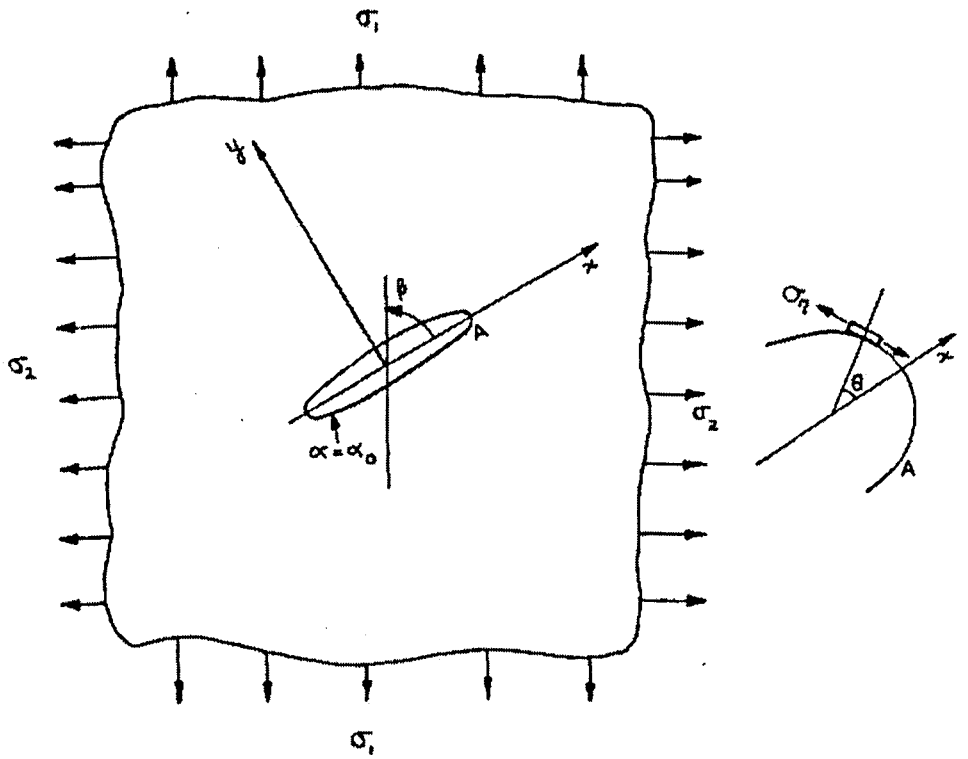

FIG. 4.8. A slender elliptical crack subjected to biaxial stresses σ_1 and σ_2.

stress under a uniaxial tensile stress, i.e. Mode I). Hence it is possible to determine the direction of crack growth. This criterion is similar to Rankine's criterion, described in the previous section relating to ductile materials.

Application of Inglis' Solutions

Let us recall (see Section 2.7.2) the expressions given by Inglis[2] for the tangential stress, σ_η, at the boundary of an inclined elliptical crack subjected to a uniform stress, σ.

$$\sigma_\eta = \sigma \frac{\sinh 2\alpha_0 + \cos 2\beta - \exp(2\alpha_0)\cos 2(\beta - \eta)}{\cosh 2\alpha_0 - \cos 2\eta} \tag{4.10}$$

α and η are elliptical co-ordinates as defined in Section 2.7. That is,

$$\begin{aligned} x &= c \cosh \alpha \cos \eta \\ y &= c \sinh \alpha \sin \eta \end{aligned} \tag{4.11}$$

α_0 describes the surface of the slender elliptical slit while η describes the position along the length of the ellipse. $x = \pm c$ are the foci of the ellipse. Hence we have

$$c \cosh \alpha_0 = a, c \sinh \alpha_0 = b \text{ and } a^2 - b^2 = c^2 \tag{4.12}$$

From expression (4.11) we have

$$\begin{aligned} \frac{dx}{d\eta} &= -c \cosh \alpha \sin \eta \\ \frac{dy}{d\eta} &= c \sinh \alpha \cos \eta \end{aligned} \tag{4.13}$$

Therefore,

$$\frac{dx}{dy} = -\frac{\cosh \alpha}{\sinh \alpha} \tan \eta \tag{4.14}$$

For the slender slit $\alpha = \alpha_0$ where α_0 is small ($\alpha_0 \ll 1$).
Therefore,

$$\tan \eta = -\alpha_0 \frac{dx}{dy} \tag{4.15}$$

$\frac{dy}{dx}$ in the above expression is the *local slope* of the elliptical slit. If θ_0 is defined as the angle of crack propagation (see Fig. 4.8) then it is given by

the *normal* to the local slope. Therefore we have

$$\tan\eta = -\alpha_0(-\tan\theta_0) = \alpha_0\tan\theta_0 \tag{4.16a}$$

In the case of a very slender elliptical slit, crack propagation occurs in the vicinity of the crack tip, and consequently η is very small. Therefore $\tan\eta \to \eta$ and we have

$$\eta = \alpha_0\tan\theta_0 \tag{4.16b}$$

If we now apply expression (4.10) to the biaxial stress system, shown in Fig. 4.12, the tangential stress (σ_η) due to σ_1 and σ_2 becomes

$$\sigma_\eta = \frac{(\sigma_1+\sigma_2)\sinh 2\alpha_0 - (\sigma_1-\sigma_2)[\exp(2\alpha_0)\cos 2(\eta-\beta) - \cos 2\beta]}{\cosh 2\alpha_0 - \cos 2\eta}. \tag{4.17}$$

Condition of Crack Propagation

According to Griffith's theory, crack propagation occurs when the tangential stress at the point on the surface reaches a maximum value (which is the specific tensile stress referred to previously). For a given crack angle, β, $\dfrac{d\sigma_\eta}{d\eta} = 0$ and this gives the condition for the direction of crack propagation. That is, one can determine the critical value of η and therefore obtain the critical value of the tangential stress, σ_η, in terms of the stresses and angle, β. It must be emphasised that fracture occurs only when the critical value of σ_η reaches a specific tensile stress. Therefore we have, on simplification,

$$\left[\frac{d\sigma_\eta}{d\eta} = 0\right]$$

$$\exp(2\alpha_0)\sin 2\beta(1-\cos 2\eta\cosh 2\alpha_0) + \sin 2\eta\cos 2\beta[\exp(2\alpha_0)-1] - \frac{\sigma_1+\sigma_2}{\sigma_1-\sigma_2}\sinh 2\alpha_0\sin 2\eta = 0 \tag{4.18}$$

Since α_0 and η are small for a slender elliptical slit,

$$\exp(2\alpha_0) \simeq 1+2\alpha_0,\ \cosh 2\alpha_0 \simeq 1+2\alpha_0^2,\ \sinh 2\alpha_0 \simeq 2\alpha_0,$$
$$\cos 2\eta \simeq 1-(2\eta)^2,\ \sin 2\eta \simeq 2\eta$$

Using the above approximations, the expression (4.18), on simplification, takes the form

$$\eta^2(\sigma_1-\sigma_2)\sin\beta\cos\beta - \eta\,2\alpha_0(\sigma_1\sin^2\beta + \sigma_2\cos^2\beta) - \alpha_0^2(\sigma_1-\sigma_2) \times \sin\beta\cos\beta = 0 \tag{4.19}$$

That is,

$$\sigma_{crit} = \alpha_0^{-1} \sigma_C \sin\beta(1 - \sin\beta) \tag{4.28}$$

Note that σ_{crit} cannot be a negative value. For the *uniaxial tension case*, $\sigma_1 = \sigma_T$, expression (4.21) becomes

$$\sigma_{crit} = \alpha_0^{-1} \sigma_T \sin\beta(1 + \sin\beta) \tag{4.29}$$

It must be reiterated that for a *given slender ellipse* (fixed α_0) σ_{crit} is the *same for both tensile and compressive cases or for any other loading case.* σ_{crit} has been defined previously as a specific tensile stress and it is *convenient* to relate this stress to the Mode I uniaxial tensile stress, σ_I, (a crack normal to the applied tensile stress). σ_I is also the minimum value of σ_T when $\beta = \pi/2$. Expression (4.29) then takes the form

$$\sigma_I = (\alpha_0 \sigma_{crit})/2 \tag{4.30}$$

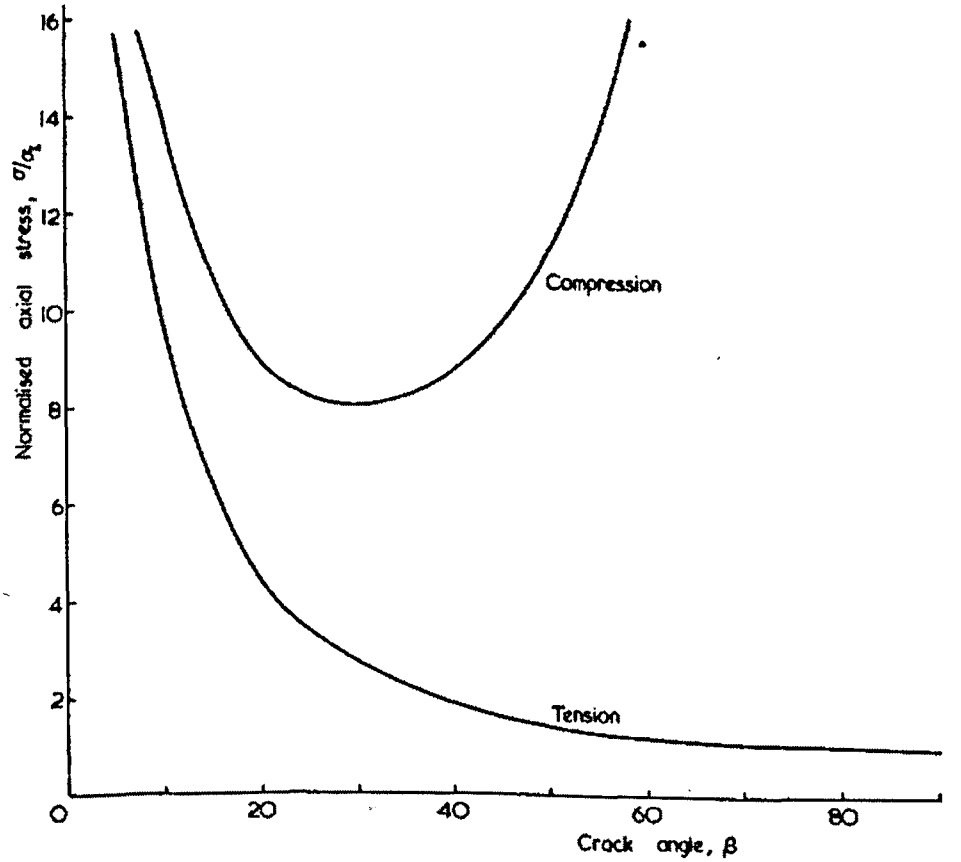

FIG. 4.9. Stress required to propagate an inclined crack according to Griffith's theory.

Hence expressions (4.28) and (4.29) can written in the form

$$\sigma_C = 2\sigma_I/\sin\beta(1-\sin\beta) \tag{4.31}$$

$$\sigma_T = 2\sigma_I/\sin\beta(1+\sin\beta) \tag{4.32}$$

Figure 4.9 shows the form of the two curves for σ_C and σ_T.

From expression (4.12) it can easily be shown that for a very slender ellipse

$$\alpha_0 = b/a \tag{4.33}$$

or in terms of the radius of curvature, ρ, $\alpha_0 = \sqrt{\rho/a}$ (see Section 2.7). It has also been shown previously that when an elliptical crack is normal to the applied stress (σ_I), the crack tip stress, σ_{tip}, is given by

$$\sigma_{tip} = \sigma_I\left[1+2\left(\frac{a}{b}\right)\right] \simeq \sigma_I.2\left(\frac{a}{b}\right) = \frac{2}{\alpha_0}\sigma_I$$

That is,

$$\sigma_I = \alpha_0\sigma_{tip}/2 \tag{4.34}$$

The above result confirms expression (4.30) where $\sigma_{tip} = \sigma_{crit}$.

The *minimum value of* σ_C occurs when $\frac{d\sigma_C}{d\beta} = 0$, that is

$$\cos\beta - 2\sin\beta\cos\beta = 0$$

Therefore, $\beta = \pi/6$ (4.35)

The minimum value of σ_C is therefore obtained by making $\beta = \pi/6$ in eqn (4.28), and is equal to $4\alpha_0\sigma_{crit}$. Therefore the *ratio of minimum values of compressive stress to tensile stress is* 8.

References cited in the original work:

Griffith A.A. 1924, "The theory of rupture", *Proceedings of first International congress of applied mechanics*, Delft, pp. 55-63.

Inglis, C.E. 1913, Stresses in a plate due to the presence of cracks and sharp corners, *Transactions of the Institution of Naval Architects*, vol. 55, pp. 219–230.